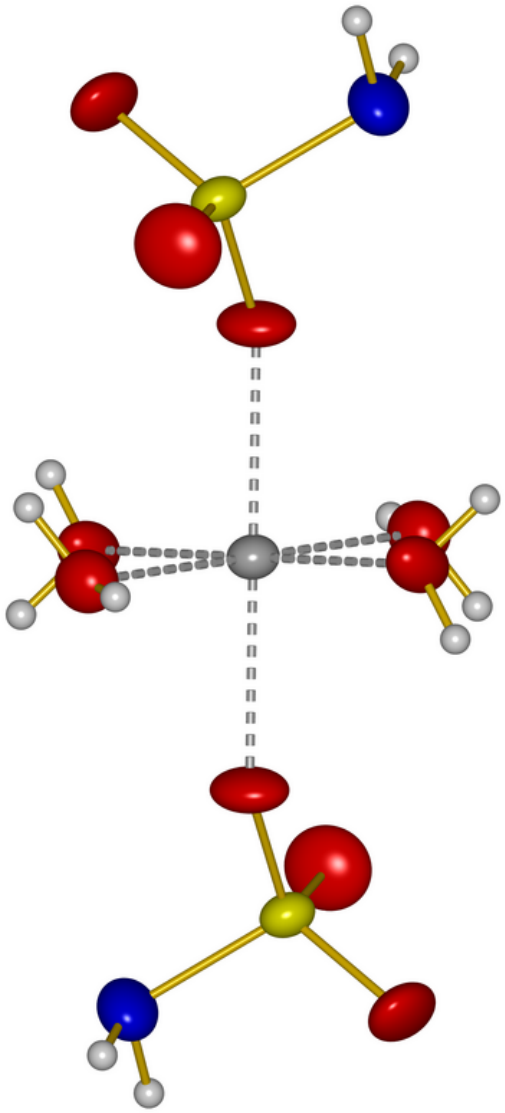

Figure S1: Coordination environment of Mg^{2+} in $Mg(NH_2SO_3)_2 \cdot 4\,H_2O$ (H atoms in white, N atoms in blue, O atoms in red, S atoms in yellow, Mg atom in grey, covalent bonds as yellow sticks and coordinate bonds as grey broken lines; displacement ellipsoids for all atoms but hydrogen correspond to 70% probability level).

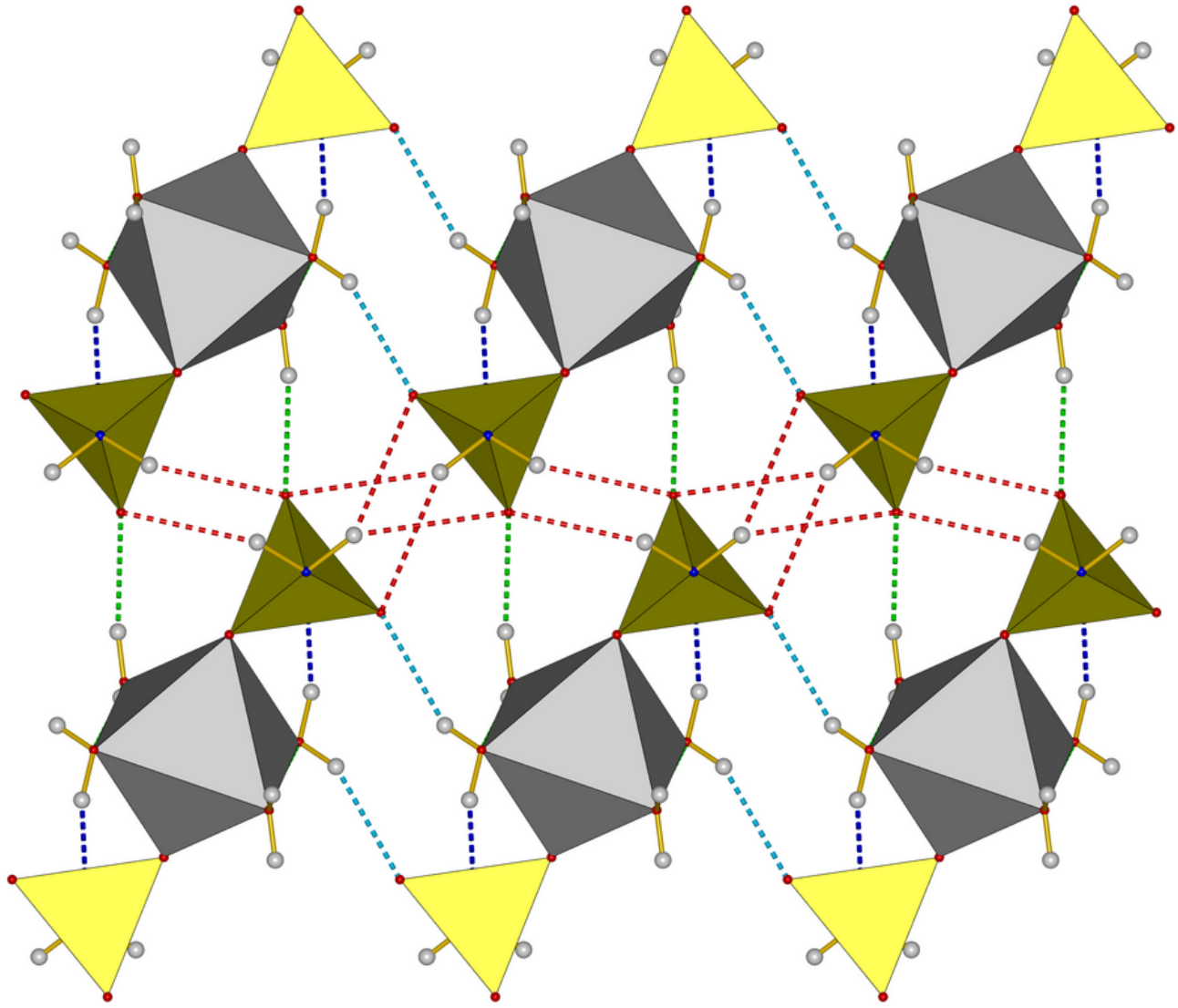

Figure S2: Hydrogen bonding pattern of $Mg(NH_2SO_3)_2 \cdot 4\,H_2O$ viewed along [0 1 0] (H atoms in white, N atoms in blue, O atoms in red, MgO8 octahedra in grey, SO_3N tetrahedra in yellow). Hydrogen bonds are displayed as broken lines with colour coding as follows: N-H$\cdots$O$_{as}$ in red, O-H$\cdots$O$_{as}$ in violett, O-H$\cdots$O$_w$ in light green, O-H$\cdots$N in dark blue.

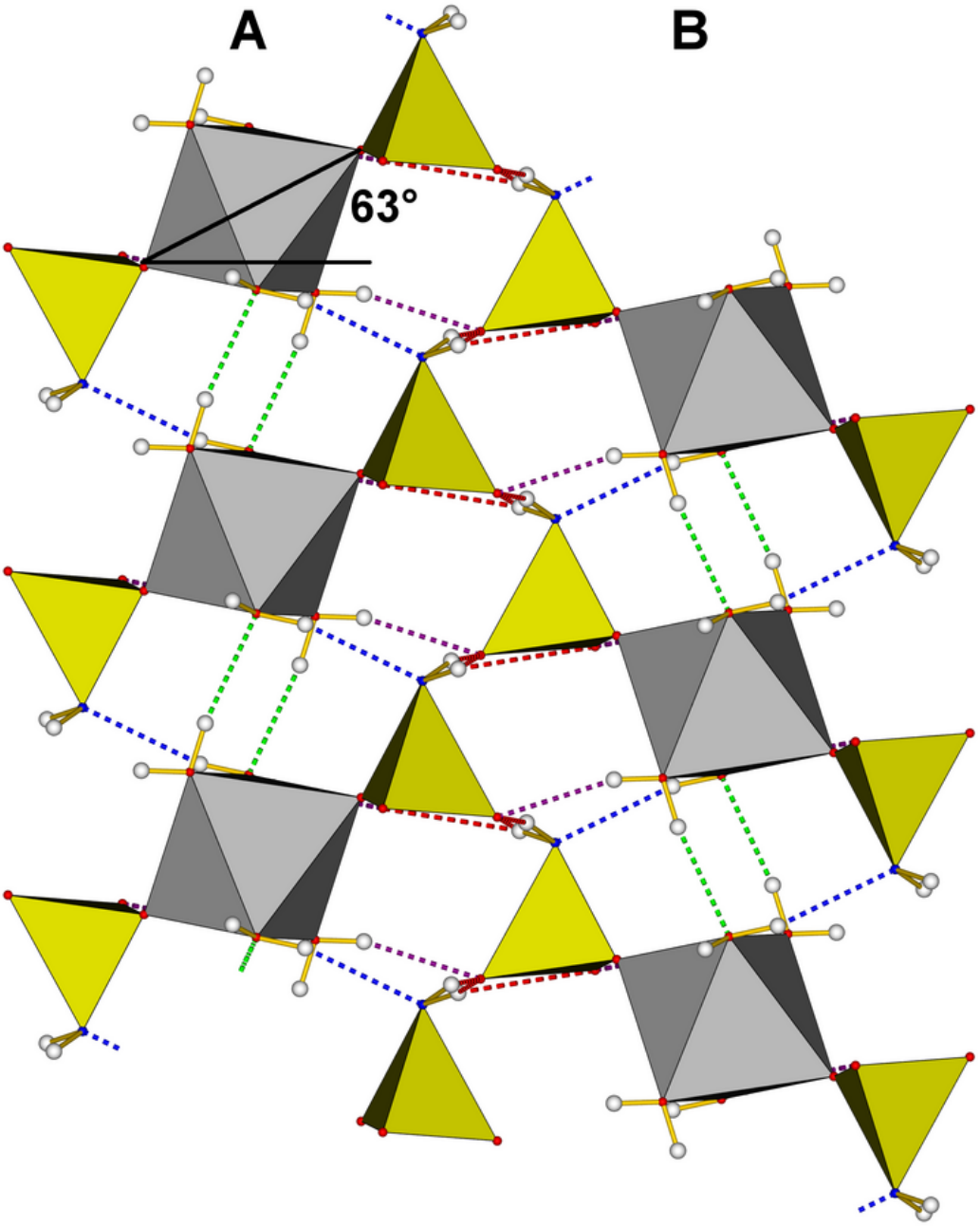

Figure S3: Hydrogen bonding pattern of $Mg(NH_2SO_3)_2 \cdot 4\,H_2O$ viewed along [1 0 0] (H atoms in white, N atoms in blue, O atoms in red, MgO8 octahedra in grey, SO_3N tetrahedra in yellow). Hydrogen bonds are displayed as broken lines with colour coding as follows: N-H$\cdots$O$_{as}$ in red, O-H$\cdots$O$_{as}$ in violett, O-H$\cdots$O$_w$ in light green, O-H$\cdots$N in dark blue.

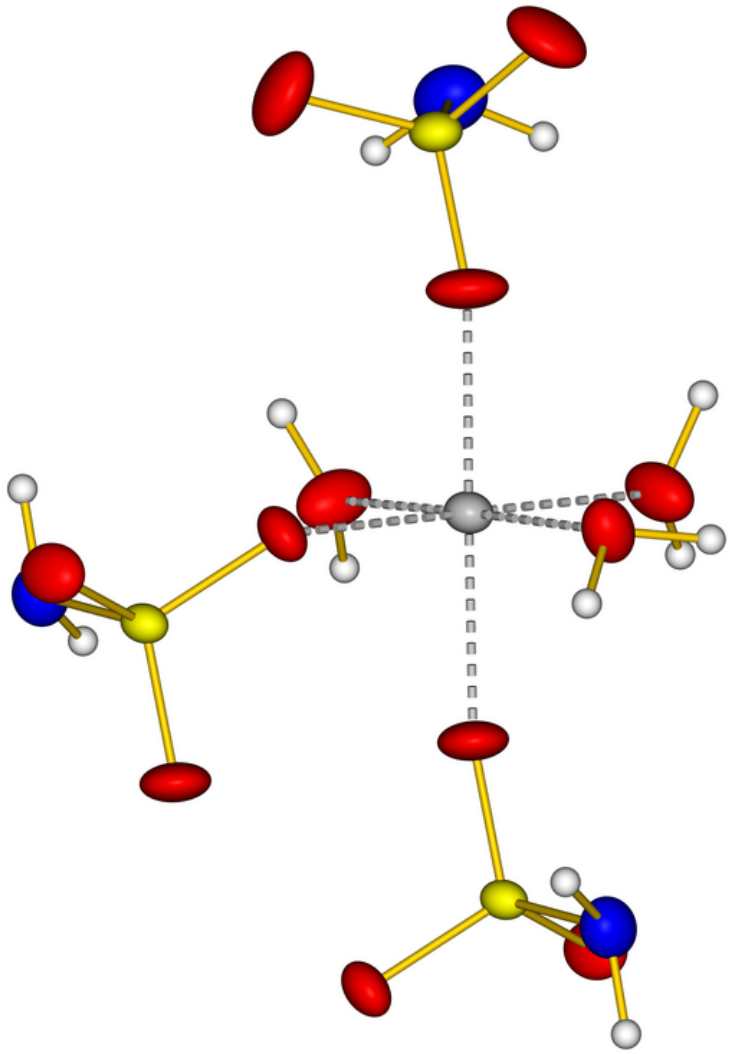

Figure S4: Coordination environment of Mg^{2+} in $Mg(NH_2SO_3)_2 \cdot 3\,H_2O$ (H atoms in white, N atoms in blue, O atoms in red, S atoms in yellow, Mg atom in grey, covalent bonds as yellow sticks and coordinate bonds as grey broken lines; displacement ellipsoids for all atoms but hydrogen correspond to 70% probability level).

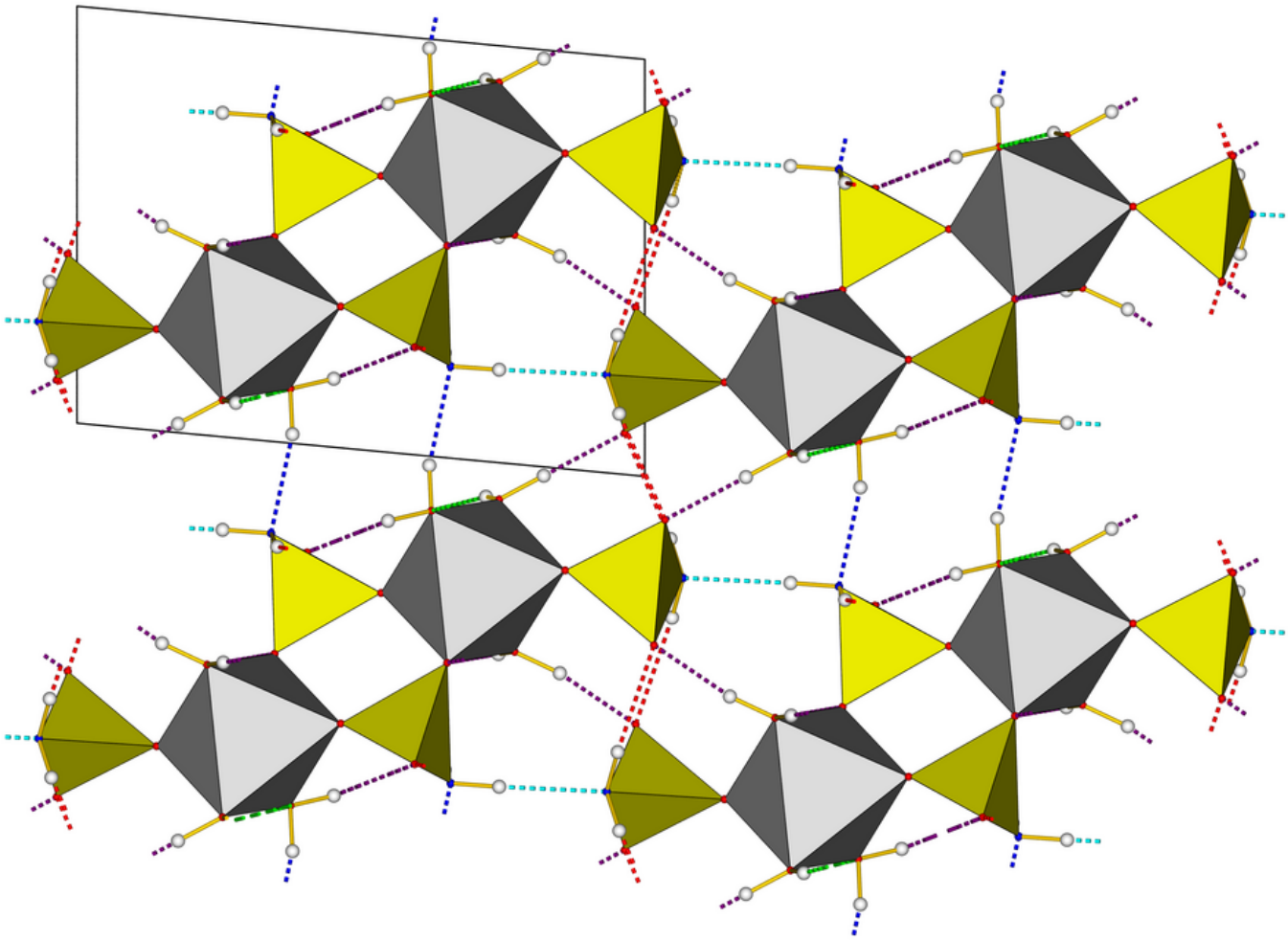

Figure S5: Hydrogen bonding pattern of $Mg(NH_2SO_3)_2 \cdot 4\,H_2O$ viewed along [1 0 0] (H atoms in white, N atoms in blue, O atoms in red, MgO8 octahedra in grey, SO_3N tetrahedra in yellow). Hydrogen bonds are displayed as broken lines with colour coding as follows: N-H$\cdots$O$_{as}$ in red, N-H$\cdots$N in light blue, O-H$\cdots$O$_{as}$ in violett, O-H$\cdots$O$_w$ in light green, O-H$\cdots$N in dark blue.

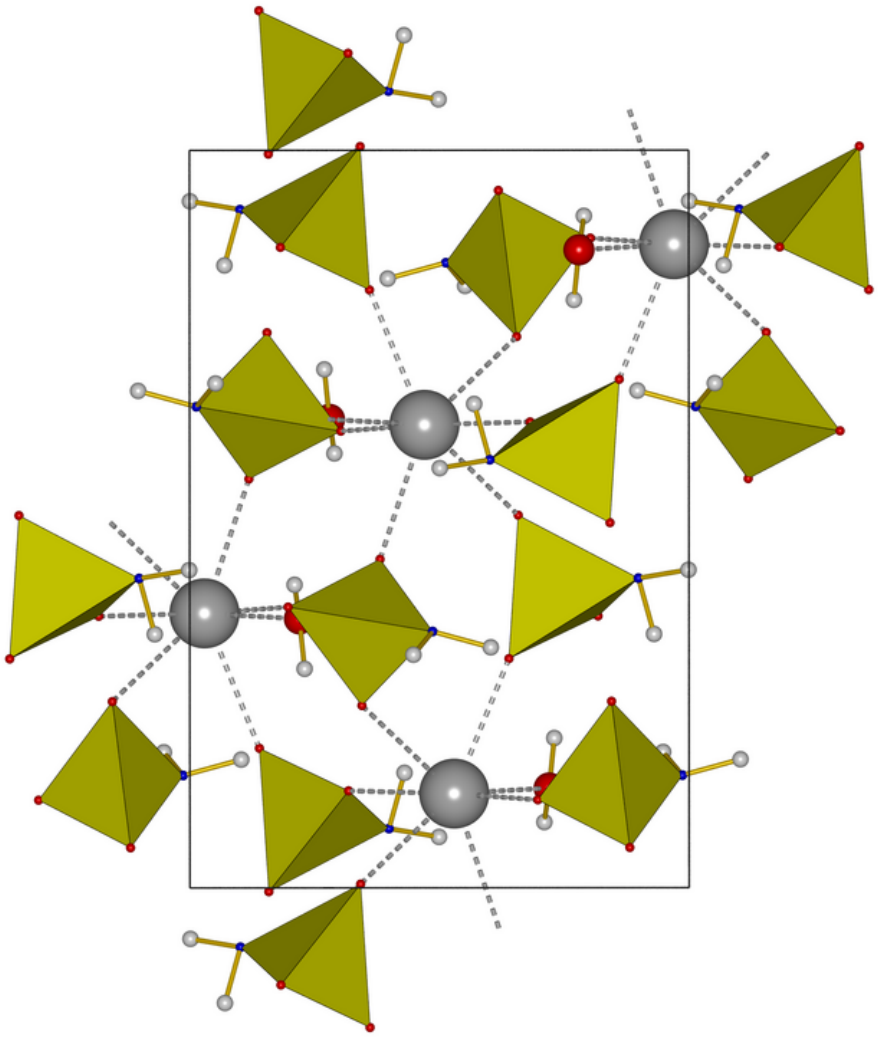

Figure S6: The unit cell of $Ca(NH_2SO_3)_2 \cdot H_2O$ viewed along [1 0 0] (H atoms in white, N atoms in blue, O atoms in red, SO_3N tetrahedra in yellow, Ca atoms in grey, covalent bonds as yellow sticks and coordinate bonds as grey broken lines).

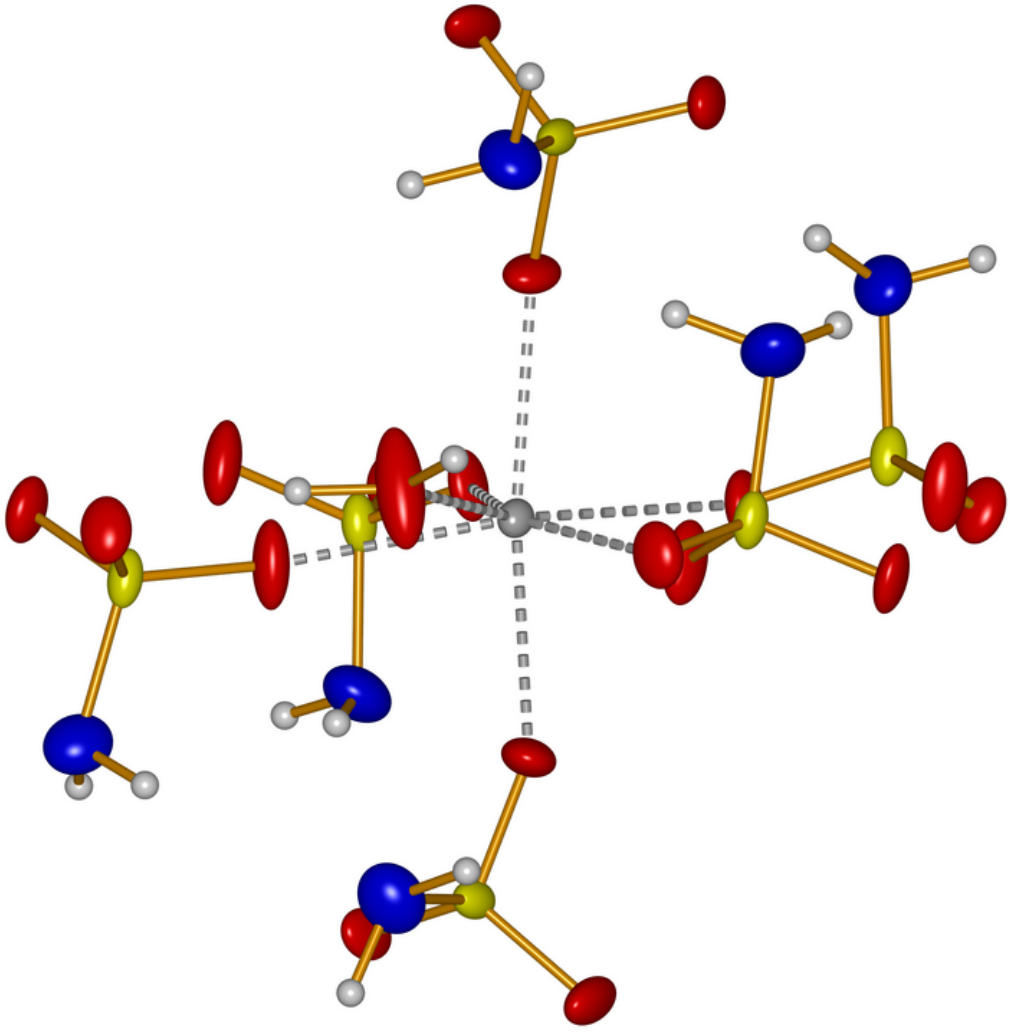

Figure S7: Coordination environment of Ca^{2+} in $Ca(NH_2SO_3)_2 \cdot H_2O$ (H atoms in white, N atoms in blue, O atoms in red, S atoms in yellow, Ca atom in grey, covalent bonds as yellow sticks and coordinate bonds as grey broken lines; displacement ellipsoids for all atoms but hydrogen correspond to 70% probability level).

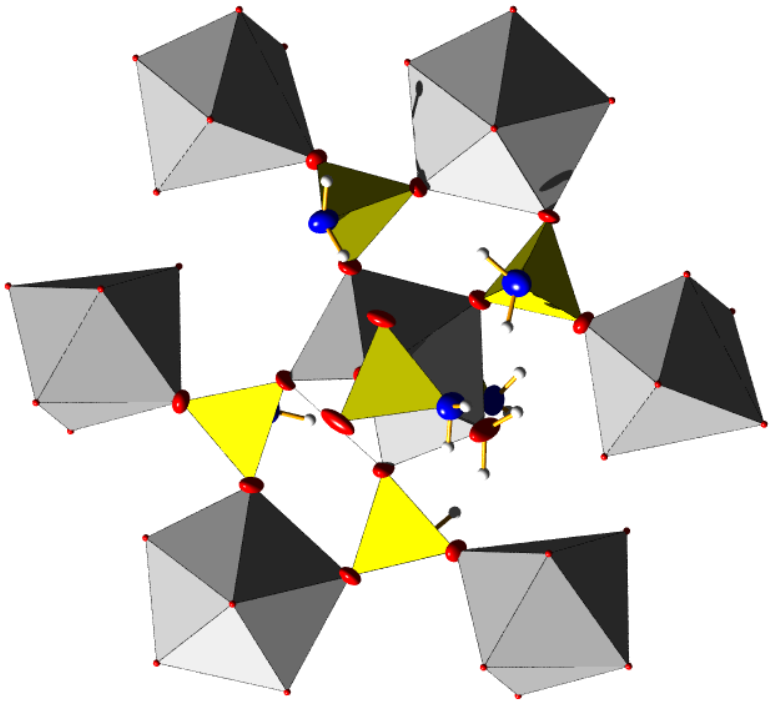

Figure S8: Hexagonal packing of CaO_9 pentagonal bipyramids (shown in grey) bridged via SO_3N tetrahedra (shown in yellow).

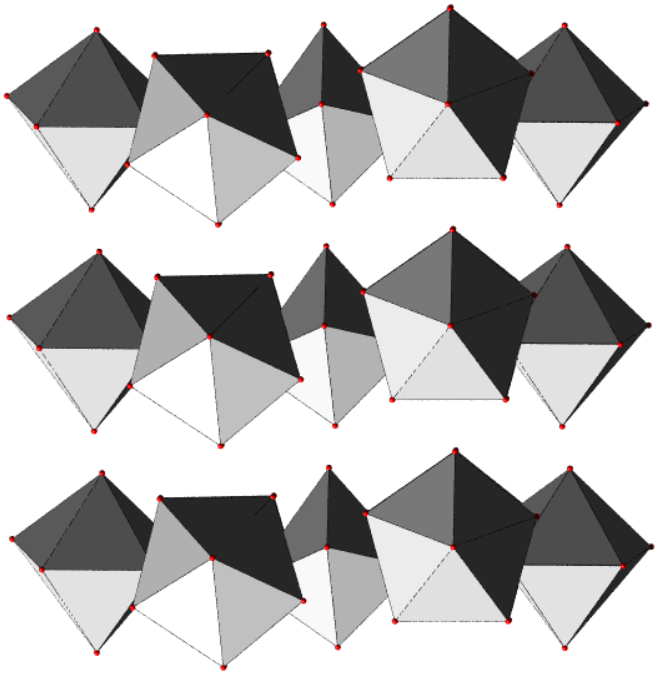

Figure S9: AA layered dense packing of CaO_7 bipyramids (shown in grey).

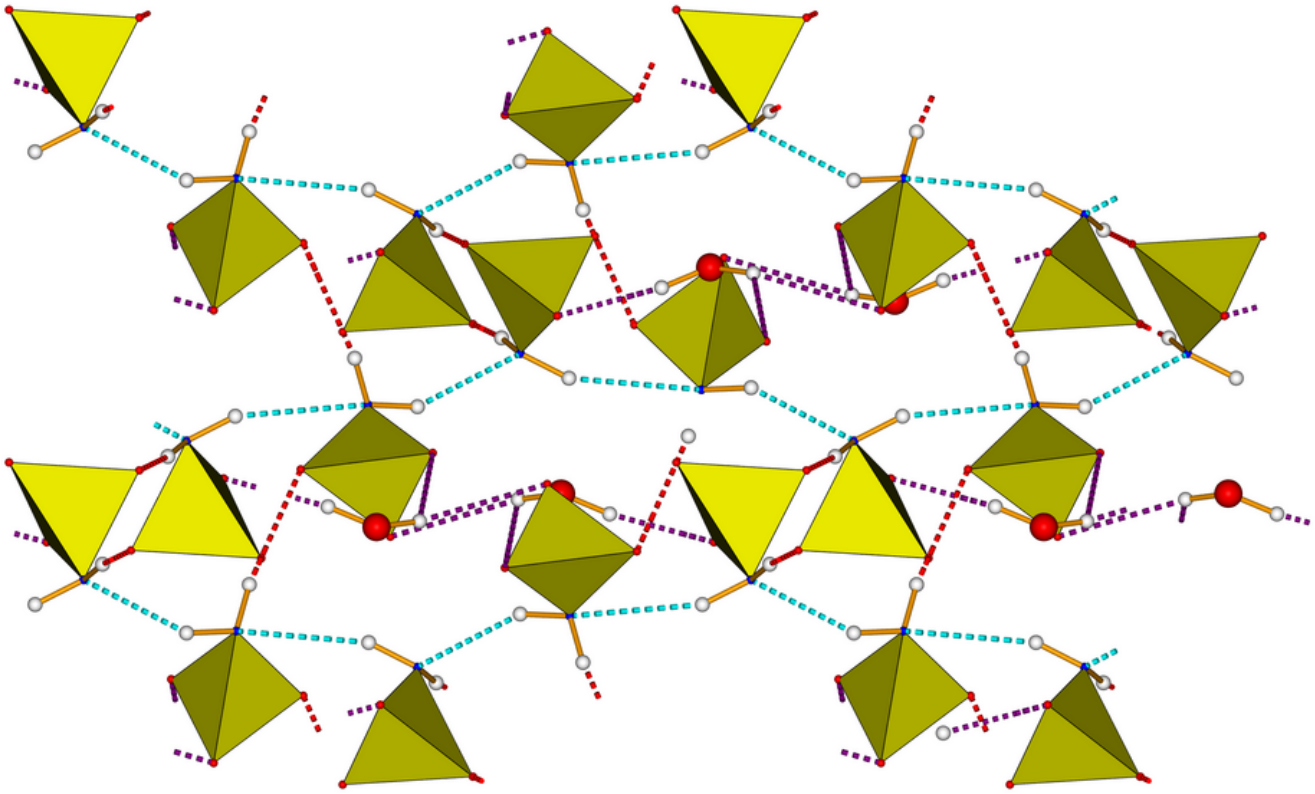

Figure S10: Hydrogen bonding pattern of $Ca(NH_2SO_3)_2 \cdot H_2O$ viewed along [1 0 0] (H atoms in white, N atoms in blue, O atoms in red, SO_3N tetrahedra in yellow). Hydrogen bonds are displayed as broken lines with colour coding as follows: N-H$\cdots$O$_{as}$ in red, N-H$\cdots$N in light blue, O-H$\cdots$O$_{as}$ in violett.

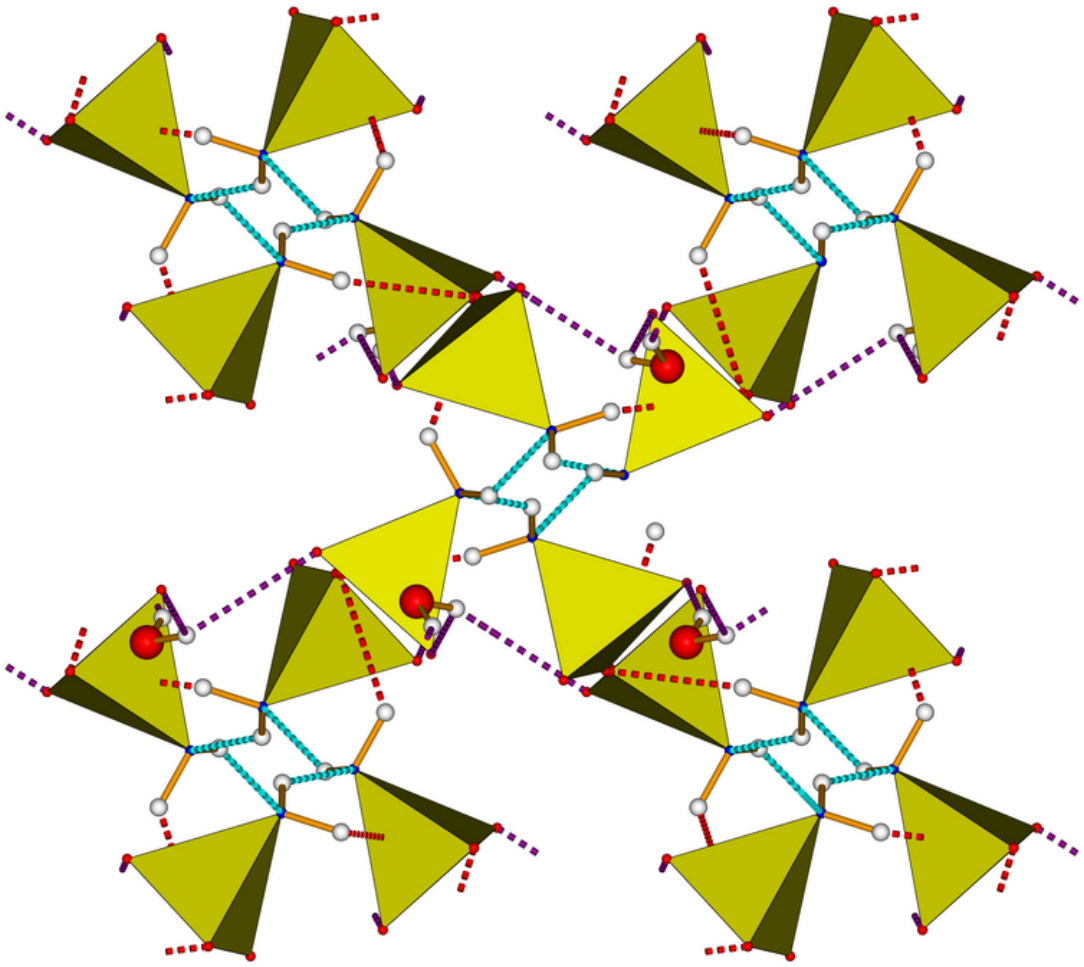

Figure S11: Hydrogen bonding pattern of $Ca(NH_2SO_3)_2 \cdot H_2O$ viewed along [0 0 1] (H atoms in white, N atoms in blue, O atoms in red, SO_3N tetrahedra in yellow). Hydrogen bonds are displayed as broken lines with colour coding as follows: N-H$\cdots$O$_{as}$ in red, N-H$\cdots$N in light blue, O-H$\cdots$O$_{as}$ in violett.

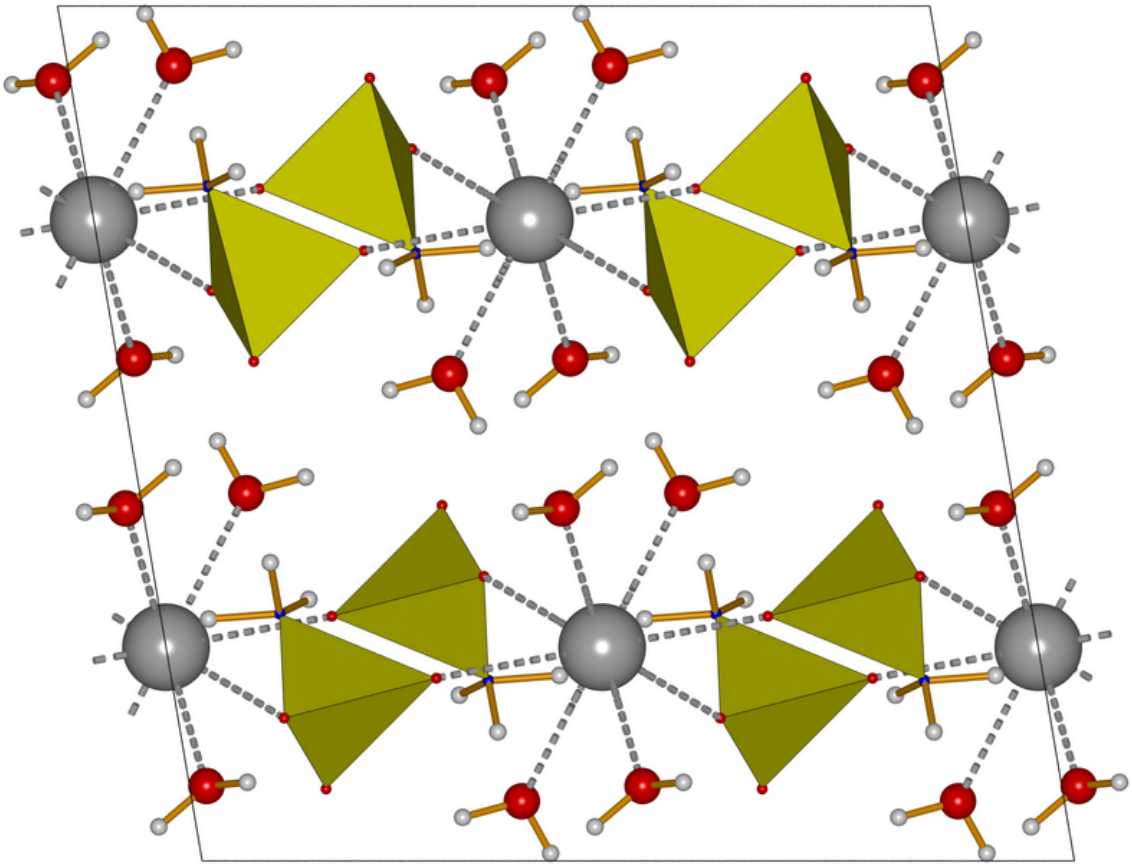

Figure S12: The unit cell of $Sr(NH_2SO_3)_2 \cdot 4\,H_2O$ viewed along [0 1 0] (H atoms in white, N atoms in blue, O atoms in red, SO_3N tetrahedra in yellow, Sr atoms in grey, covalent bonds as yellow sticks and coordinate bonds as grey broken lines).

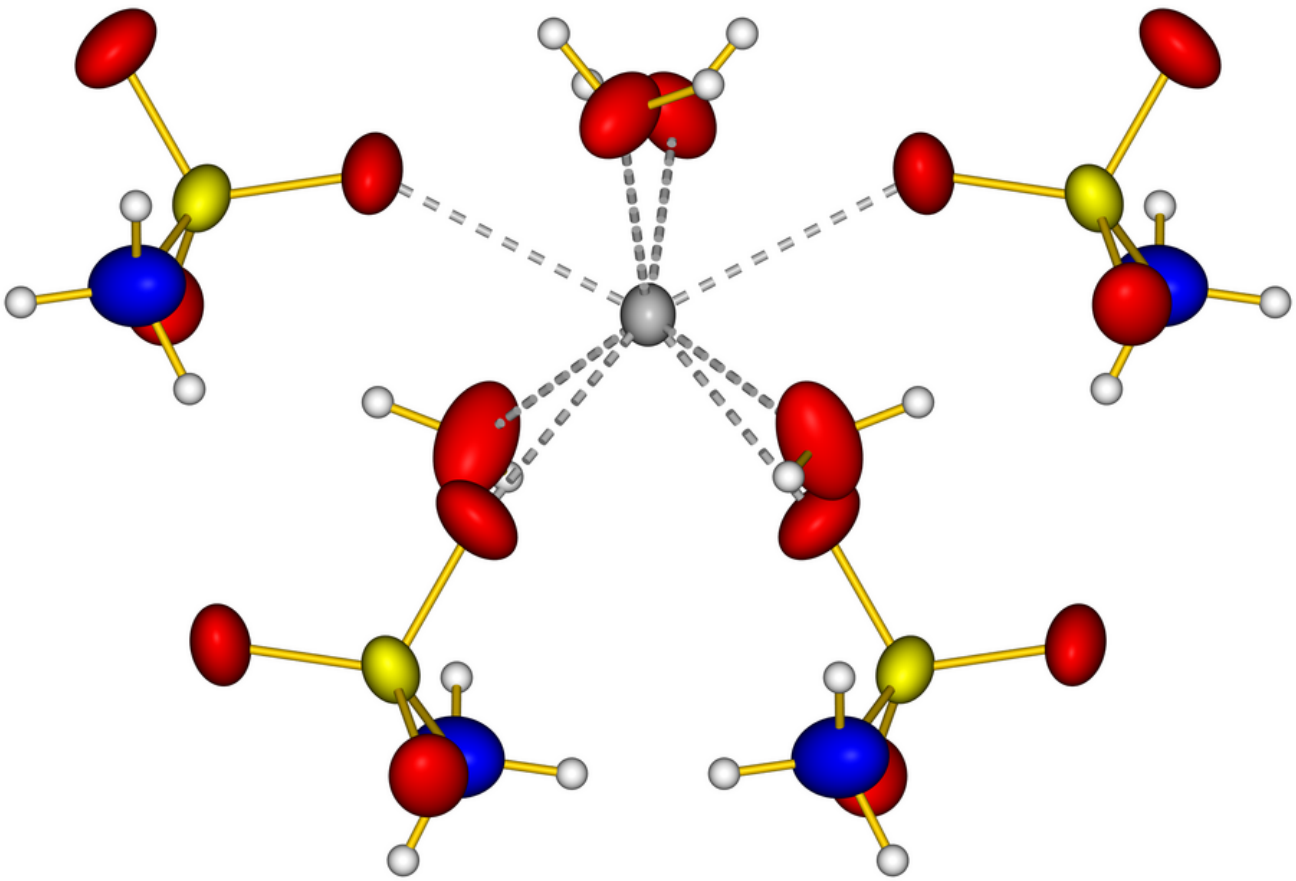

Figure S13: Coordination environment of Sr^{2+} in $Sr(NH_2SO_3)_2 \cdot 4\,H_2O$ (H atoms in white, N atoms in blue, O atoms in red, S atoms in yellow, Sr atom in grey, covalent bonds as yellow sticks and coordinate bonds as grey broken lines; displacement ellipsoids for all atoms but hydrogen correspond to 70% probability level)

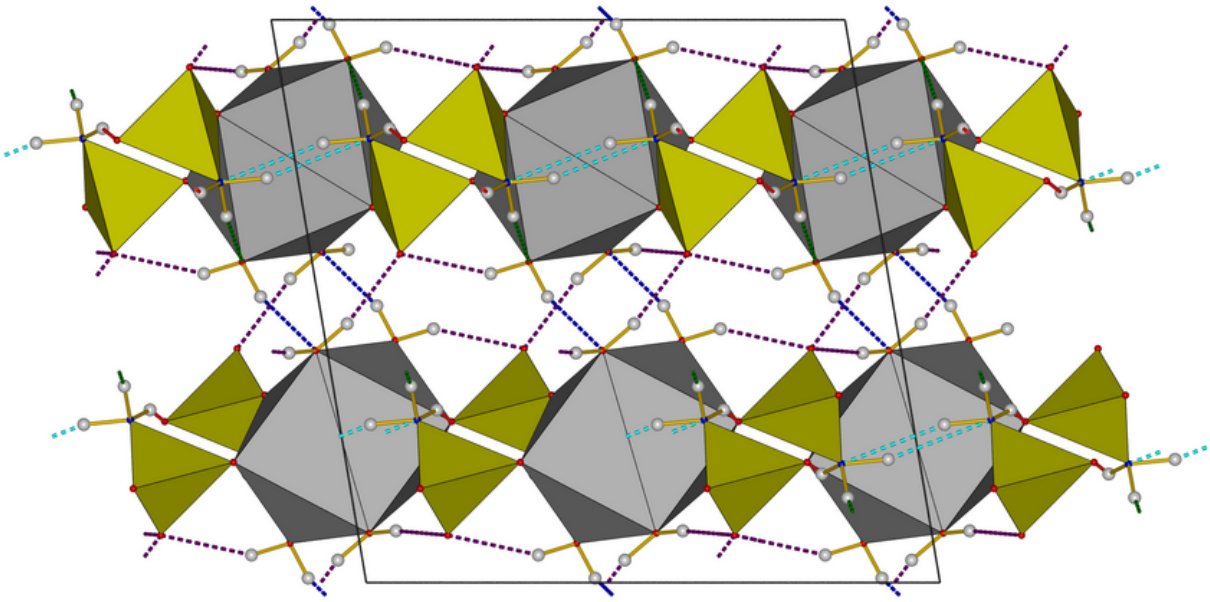

Figure S14: Hydrogen bonding pattern of $Sr(NH_2SO_3)_2 \cdot 4\,H_2O$ viewed along [0 1 0] (H atoms in white, N atoms in blue, O atoms in red, SO_3N tetrahedra in yellow and SrO_8 antiprisms in grey). Hydrogen bonds are displayed as broken lines with colour coding as follows: N-H$\cdots$O$_{as}$ in red, N-H$\cdots$O$_w$ in dark green, N-H$\cdots$N in light blue, O-H$\cdots$O$_{as}$ in violett, O-H$\cdots$N in dark blue.

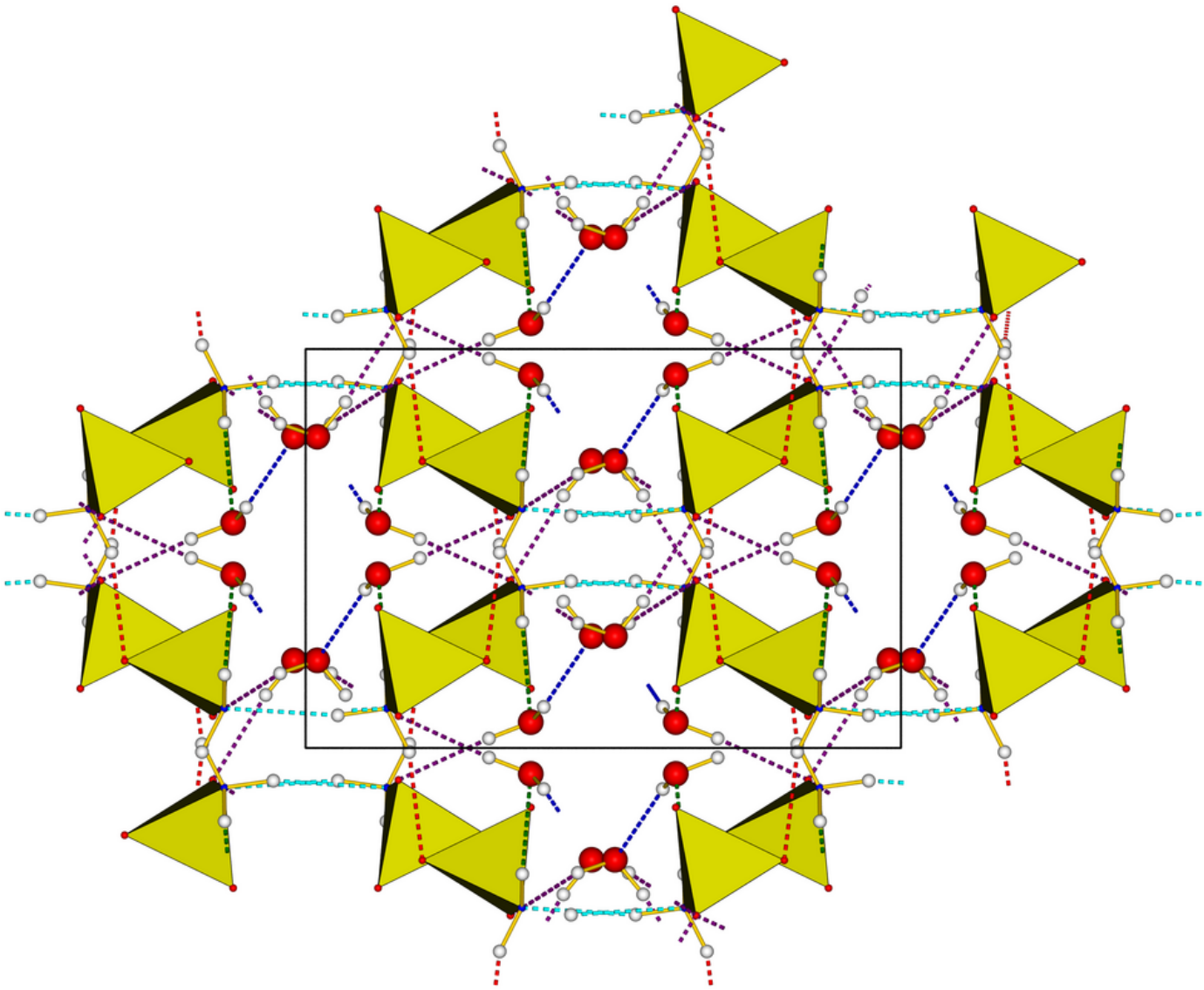

Figure S15: Hydrogen bonding pattern of $Sr(NH_2SO_3)_2 \cdot 4\,H_2O$ viewed along [0 0 1] (H atoms in white, N atoms in blue, O atoms in red, SO_3N tetrahedra in yellow). Hydrogen bonds are displayed as broken lines with colour coding as follows: N-H$\cdots$O$_{as}$ in red, N-H$\cdots$O$_w$ in dark green, N-H$\cdots$N in light blue, O-H$\cdots$O$_{as}$ in violett, O-H$\cdots$N in dark blue.

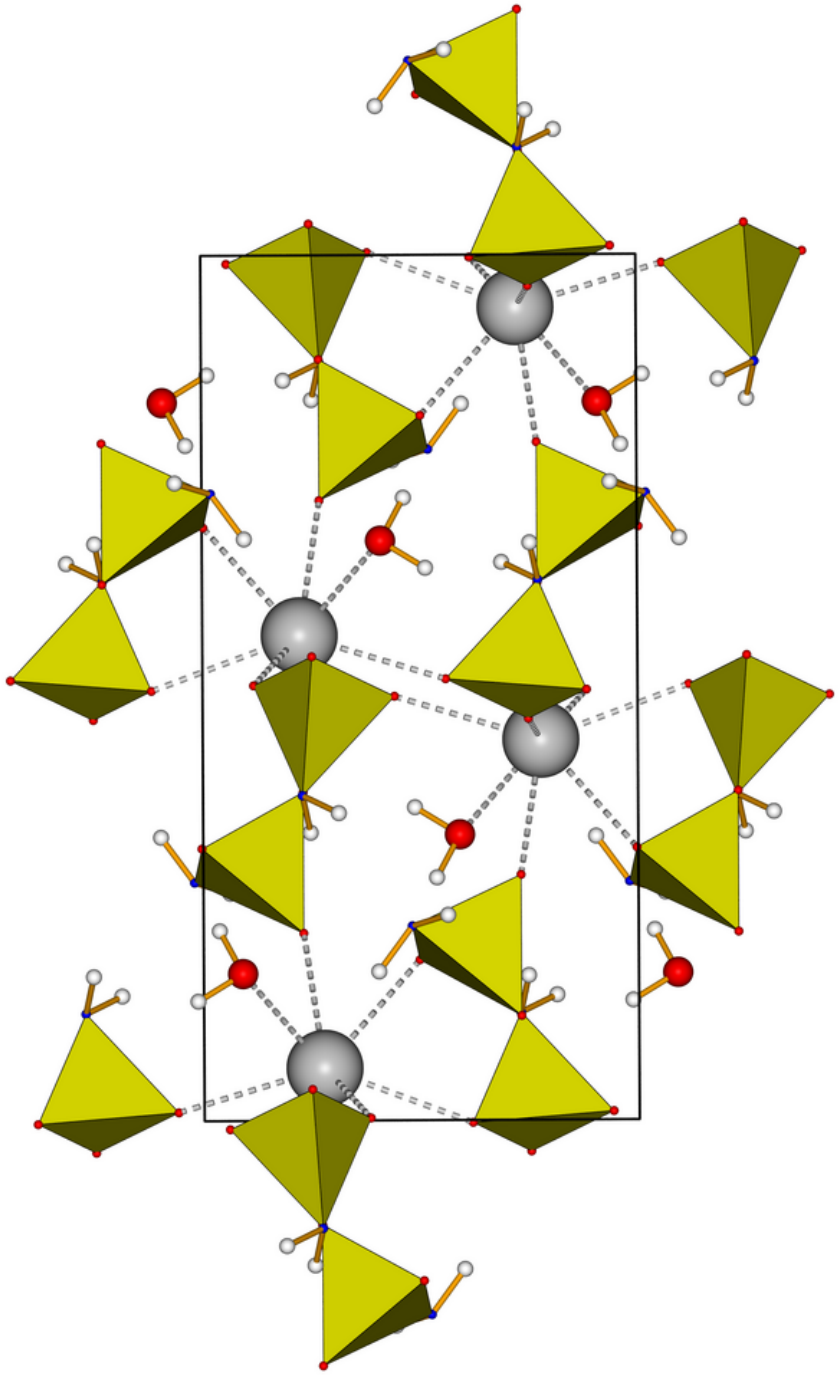

Figure S16: The unit cell of $Sr(NH_2SO_3)_2 \cdot H_2O$ viewed along [0 1 0] (H atoms in white, N atoms in blue, O atoms in red, SO_3N tetrahedra in yellow, Sr atoms in grey, covalent bonds as yellow sticks and coordinate bonds as grey broken lines).

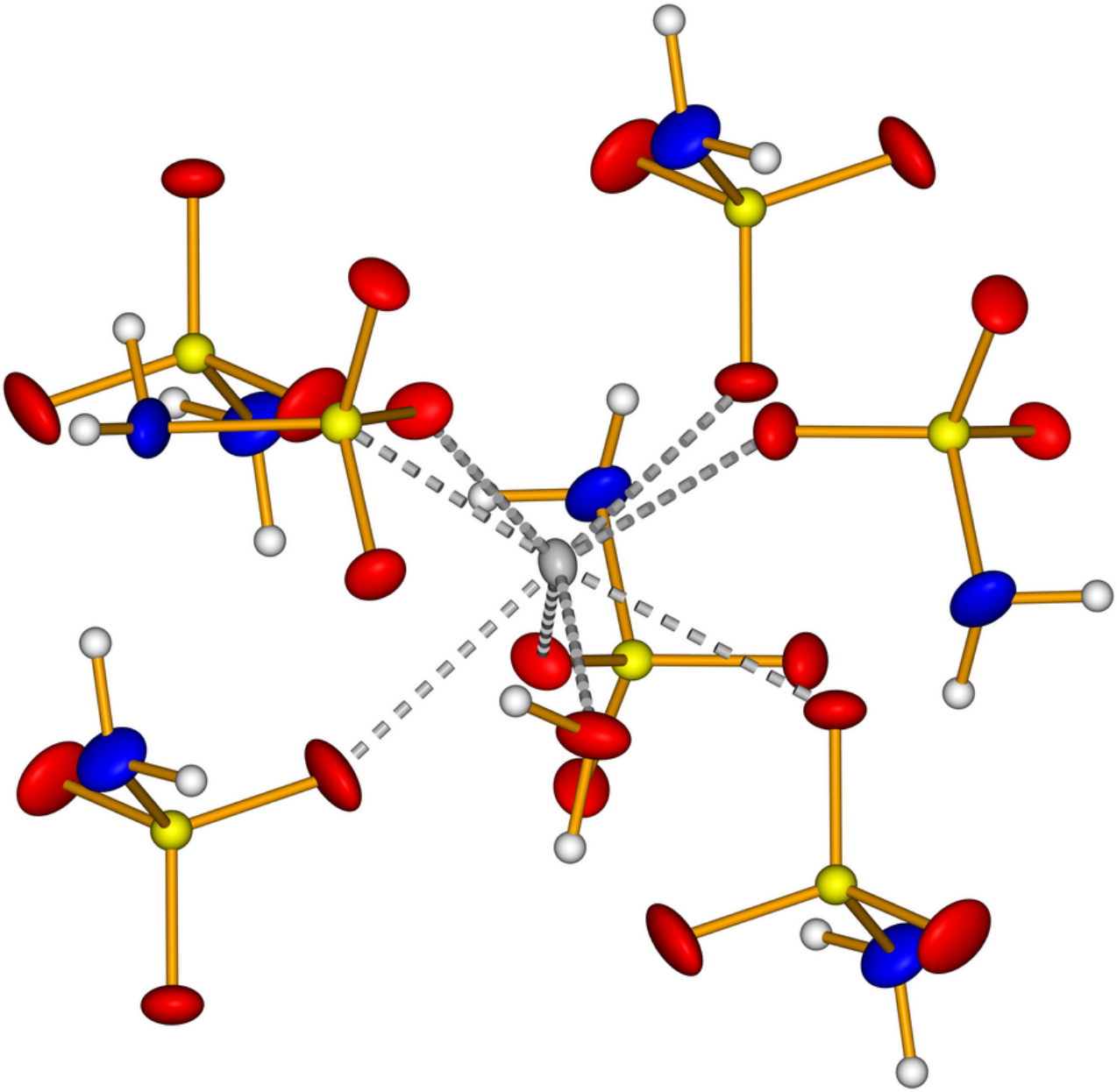

Figure S17: Coordination environment of Sr^{2+} in $Sr(NH_2SO_3)_2 \cdot H_2O$ (H atoms in white, N atoms in blue, O atoms in red, S atoms in yellow, Sr atom in grey, covalent bonds as yellow sticks and coordinate bonds as grey broken lines; displacement ellipsoids for all atoms but hydrogen correspond to 70% probability level)

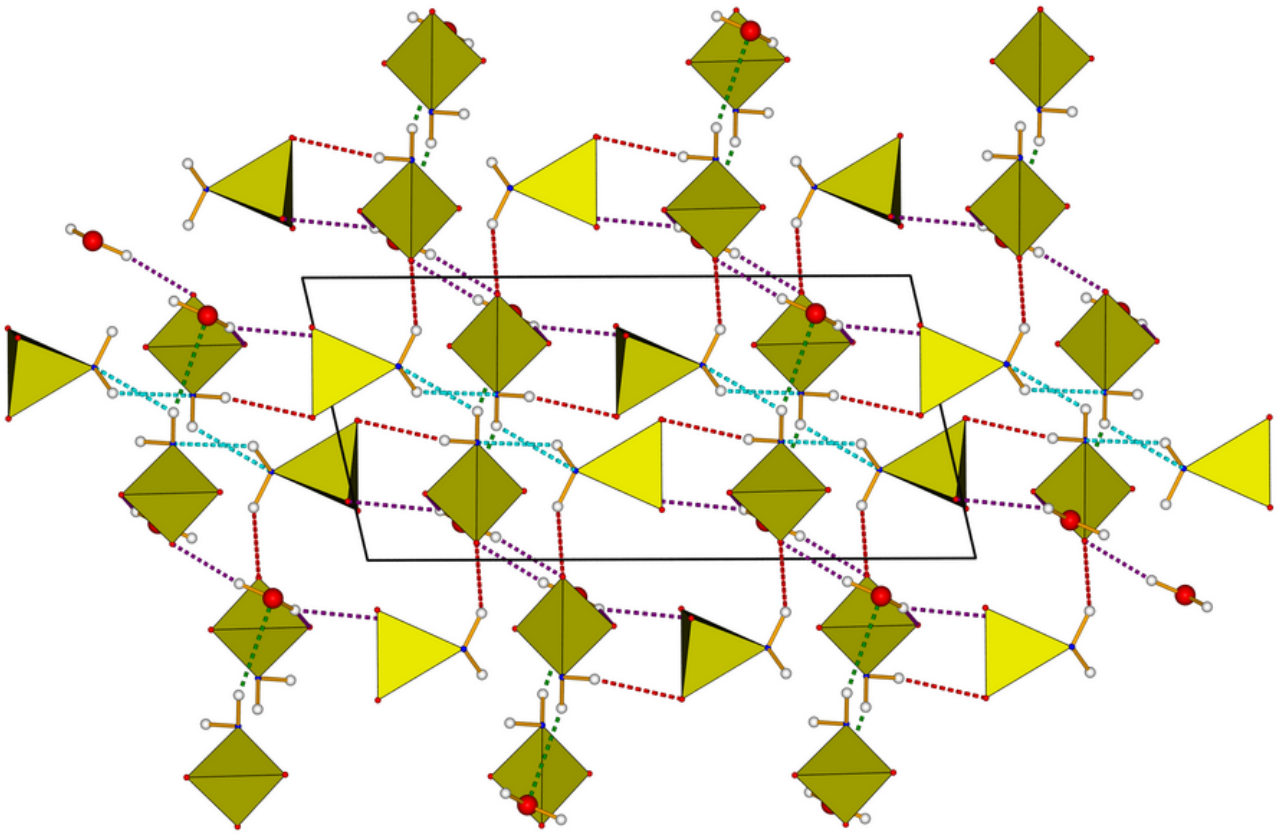

Figure S18: Hydrogen bonding pattern of $Sr(NH_2SO_3)_2 \cdot H_2O$ viewed along [0 1 0] (H atoms in white, N atoms in blue, O atoms in red, SO_3N tetrahedra in yellow). Hydrogen bonds are displayed as broken lines with colour coding as follows: N-H$\cdots$O$_{as}$ in red, N-H$\cdots$O$_w$ in dark green, N-H$\cdots$N in light blue, O-H$\cdots$O$_{as}$ in violett.

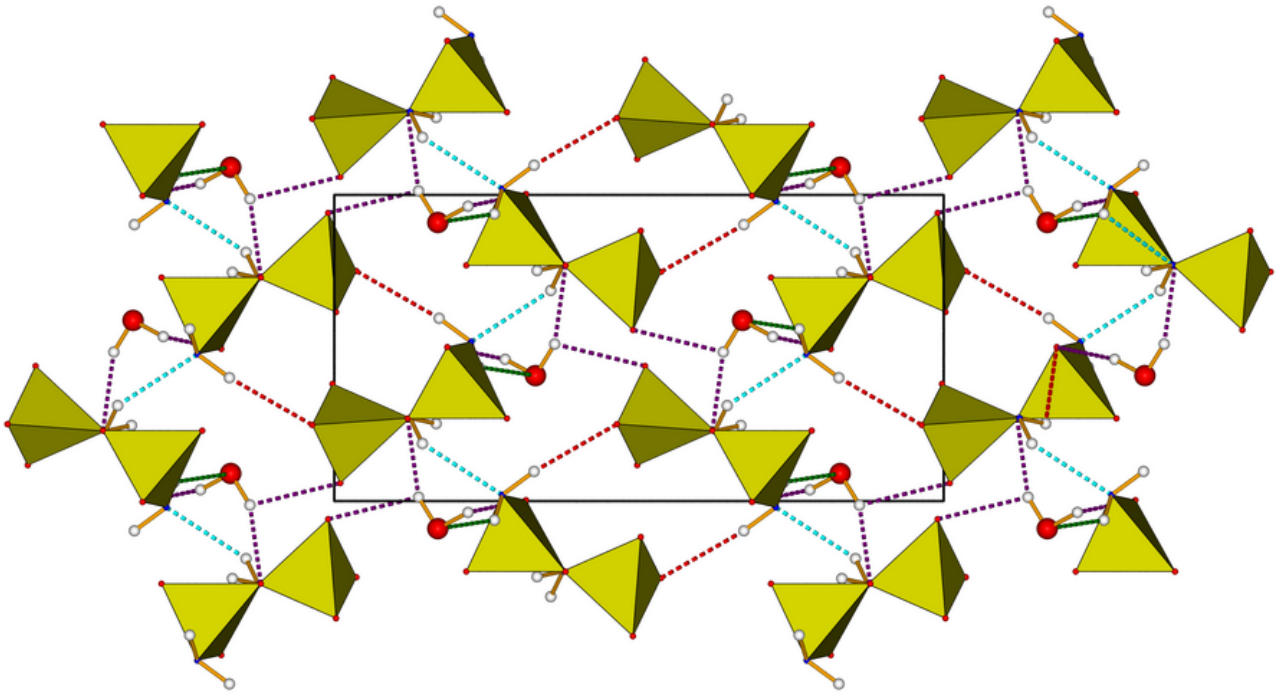

Figure S19: Hydrogen bonding pattern of $Sr(NH_2SO_3)_2 \cdot H_2O$ viewed along [1 0 0] (H atoms in white, N atoms in blue, O atoms in red, SO_3N tetrahedra in yellow). Hydrogen bonds are displayed as broken lines with colour coding as follows: N-H$\cdots$O$_{as}$ in red, N-H$\cdots$O$_w$ in dark green, N-H$\cdots$N in light blue, O-H$\cdots$O$_{as}$ in violett.

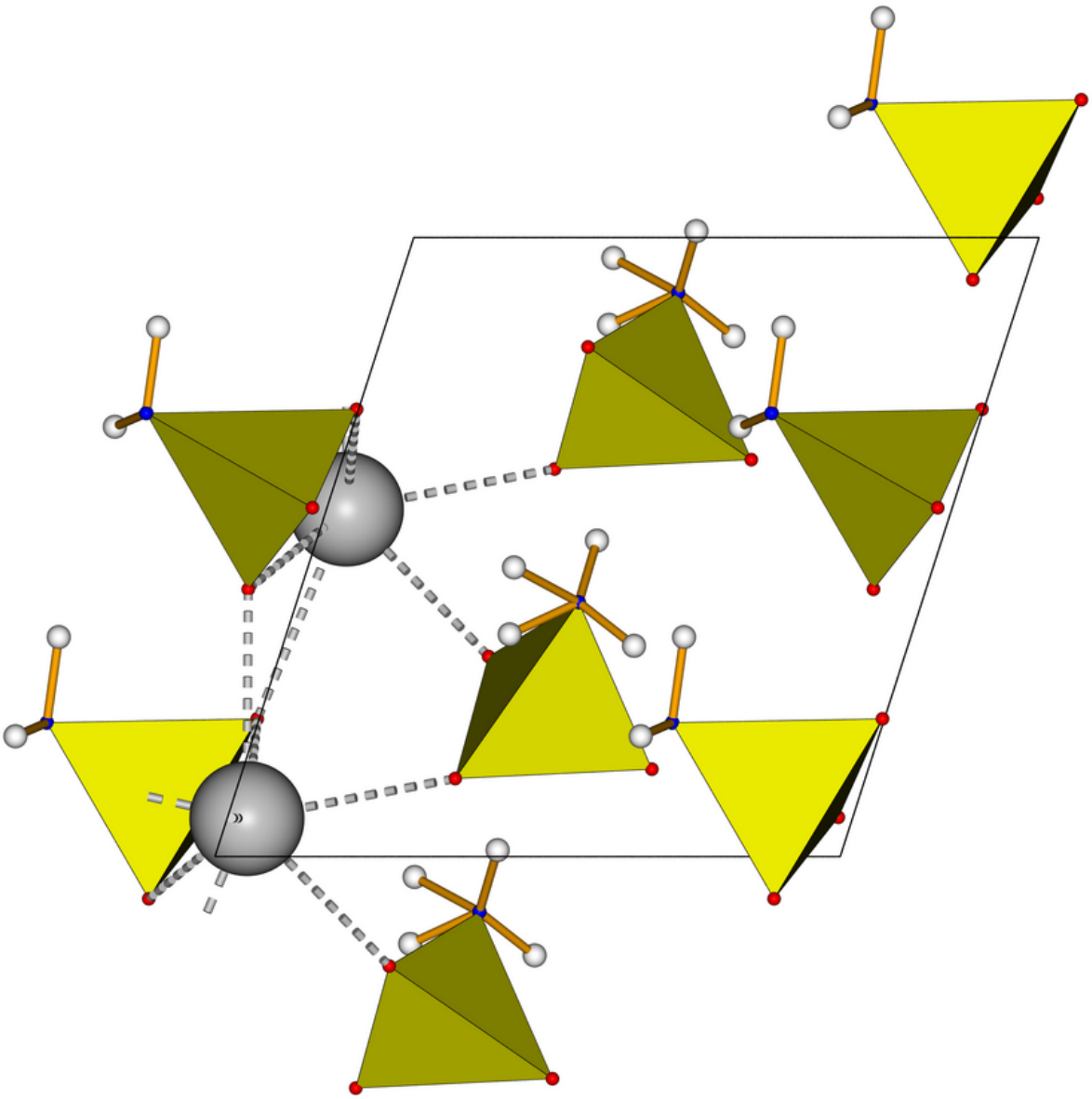

Figure S20: The unit cell of β-Sr(NH_2SO_3)$_2$ viewed along [0 0 1] (H atoms in white, N atoms in blue, O atoms in red, SO_3N tetrahedra in yellow, Sr atoms in grey, covalent bonds as yellow sticks and coordinate bonds as grey broken lines).

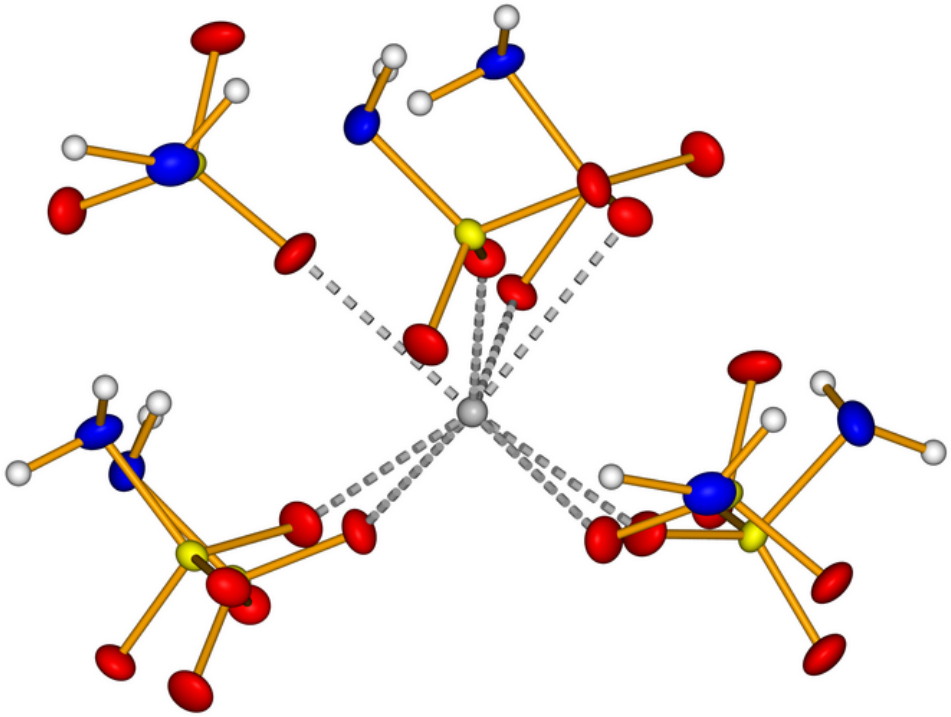

Figure S21: Coordination environment of Sr^{2+} in β-$Sr(NH_2SO_3)$ (H atoms in white, N atoms in blue, O atoms in red, S atoms in yellow, Sr atom in grey, covalent bonds as yellow sticks and coordinate bonds as grey broken lines; displacement ellipsoids for all atoms but hydrogen correspond to 70% probability level)

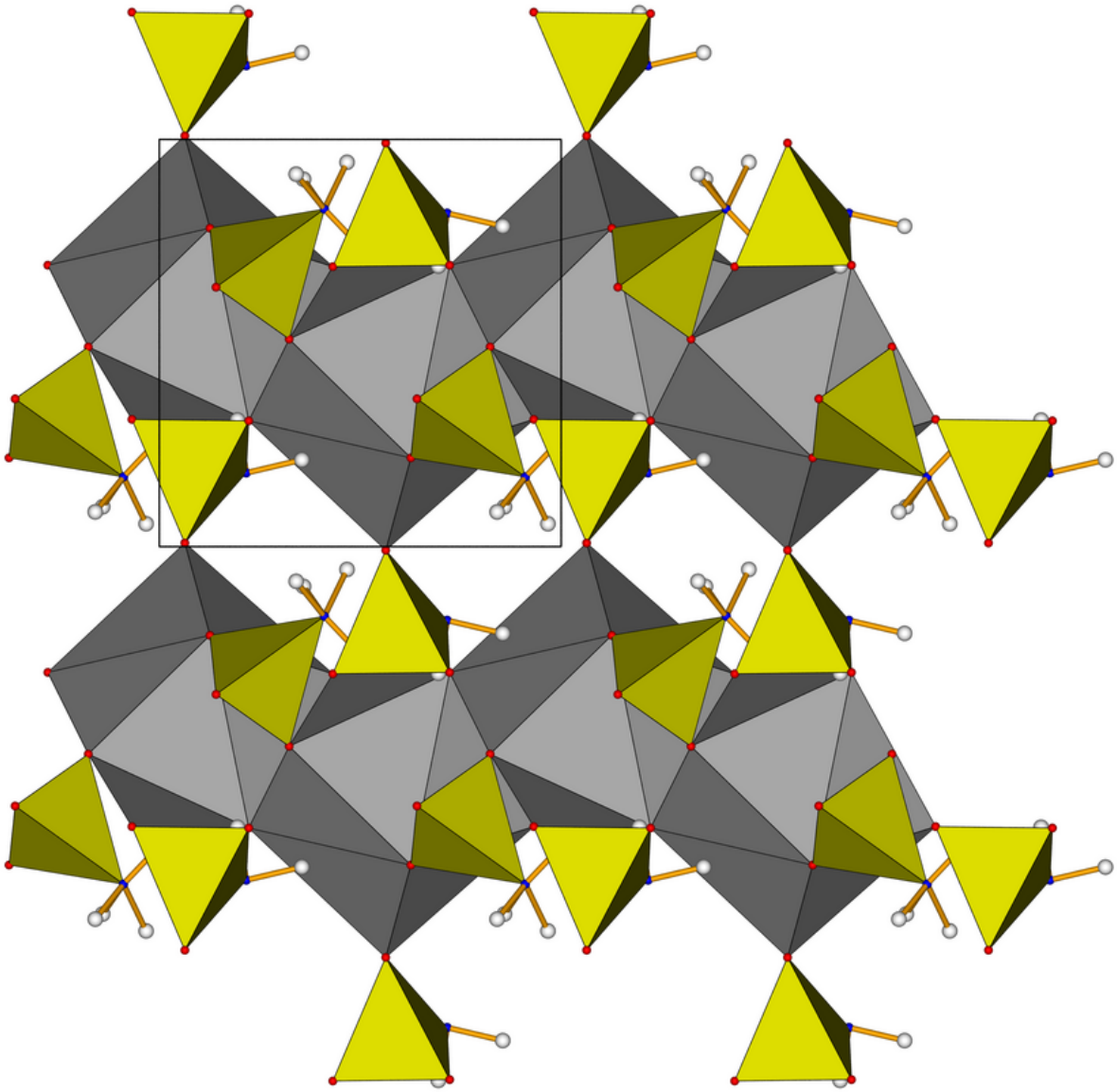

Figure S22: Zigzag chains of SrO_8 antiprisms condensed via edge.png-sharing in β-$Sr(NH_2SO_3)_2$ viewed along [1 0 0] (H atoms in white, N atoms in blue, O atoms in red, SO_3N tetrahedra in yellow, SrO_8 antiprisms in grey and covalent bonds as yellow sticks).

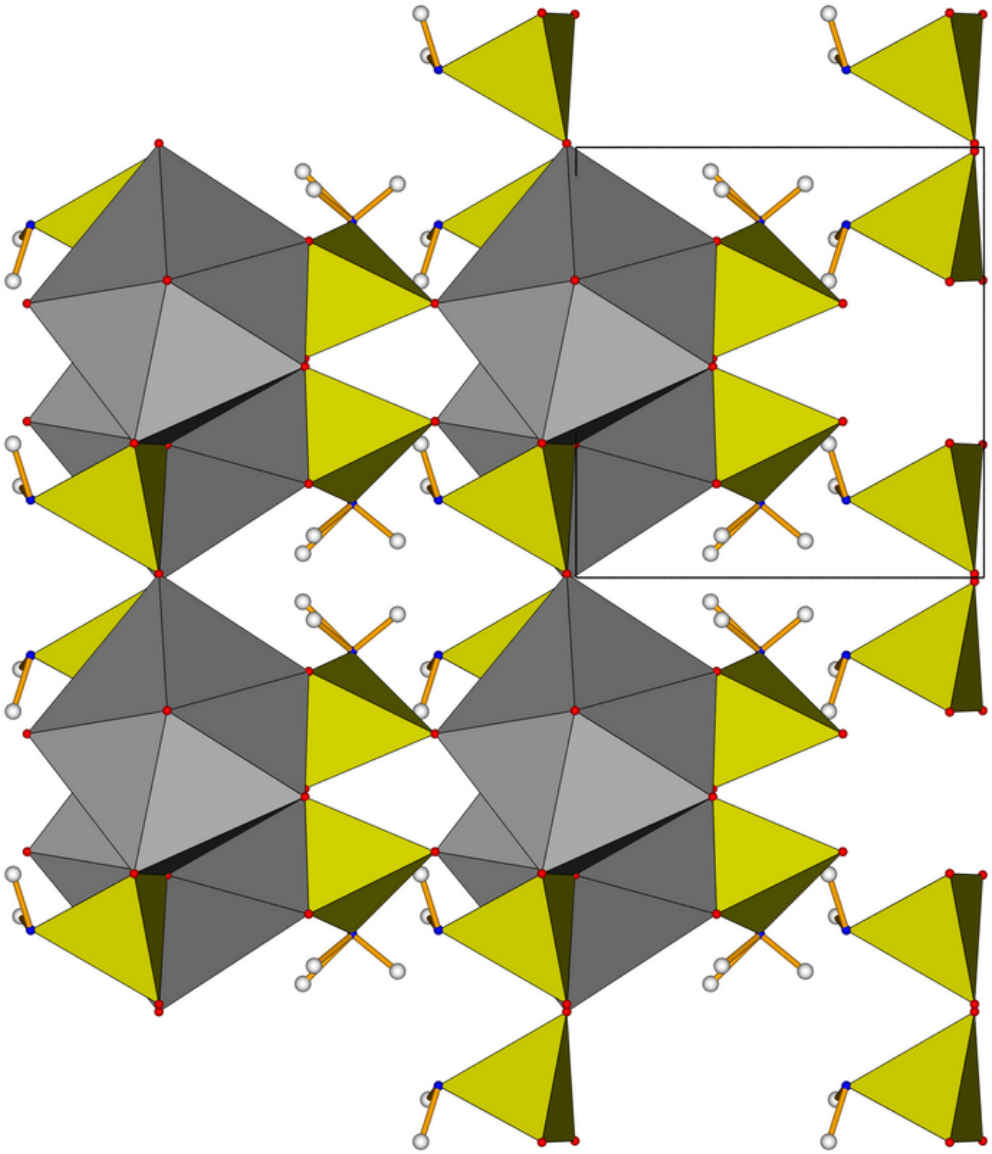

Figure S23: Rod packing of zigzag chains of SrO_8 antiprims condensed via edge.png-sharing in β-$Sr(NH_2SO_3)_2$ viewed along [0 0 1] (H atoms in white, N atoms in blue, O atoms in red, SO_3 antiprisms in yellow, SrO_8N polyhedra in grey and covalent bonds as yellow sticks).

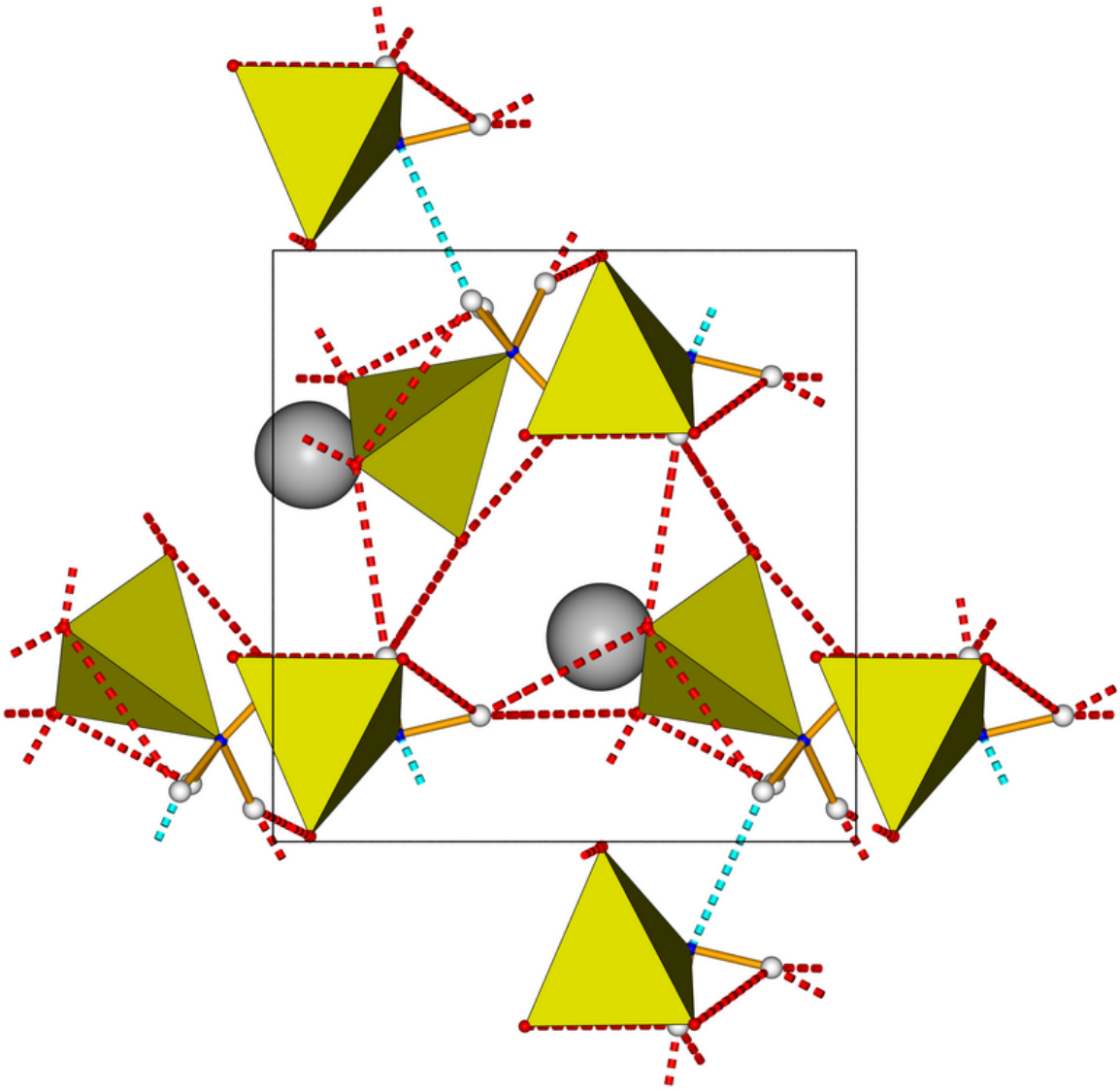

Figure S24: Hydrogen bonding pattern of β-$Sr(NH_2SO_3)_2$ viewed along [0 1 0] (H atoms in white, N atoms in blue, O atoms in red, SO_3N tetrahedra in yellow). Hydrogen bonds are displayed as broken lines with colour coding as follows: N-H$\cdots$$O_{as}$ in red, N-H$\cdots$N in light blue.

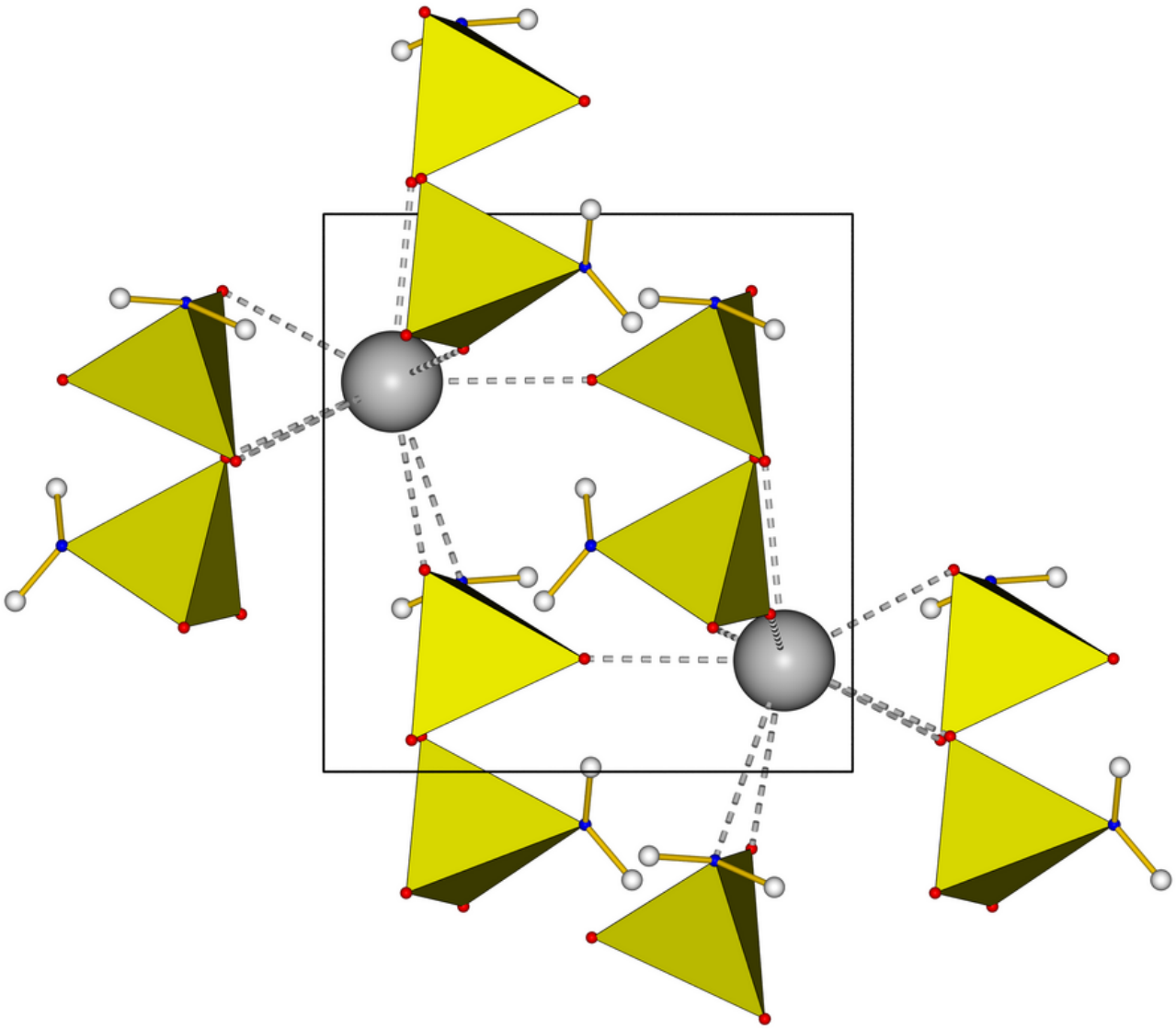

Figure S25: The unit cell of α-$Sr(NH_2SO_3)_2$ viewed along [0 0 1] (H atoms in white, N atoms in blue, O atoms in red, SO_3N tetrahedra in yellow, Sr atoms in grey, covalent bonds as yellow sticks and coordinate bonds as grey broken lines).

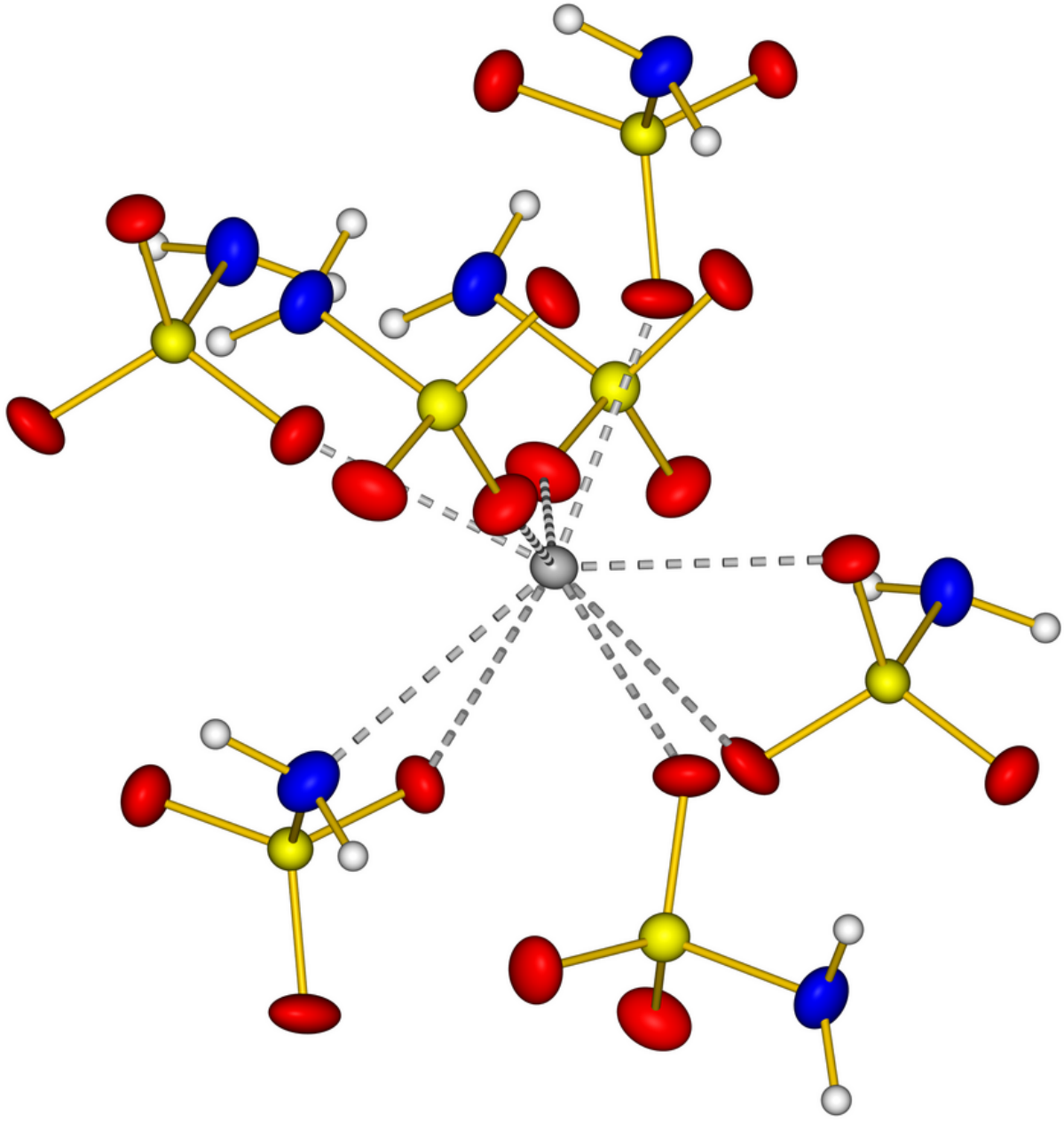

Figure S26: Coordination environment of Sr^{2+} in α-$Sr(NH_2SO_3)_2$ (H atoms in white, N atoms in blue, O atoms in red, S atoms in yellow, Sr atom in grey, covalent bonds as yellow sticks and coordinate bonds as grey broken lines; displacement ellipsoids for all atoms but hydrogen correspond to 70% probability level)

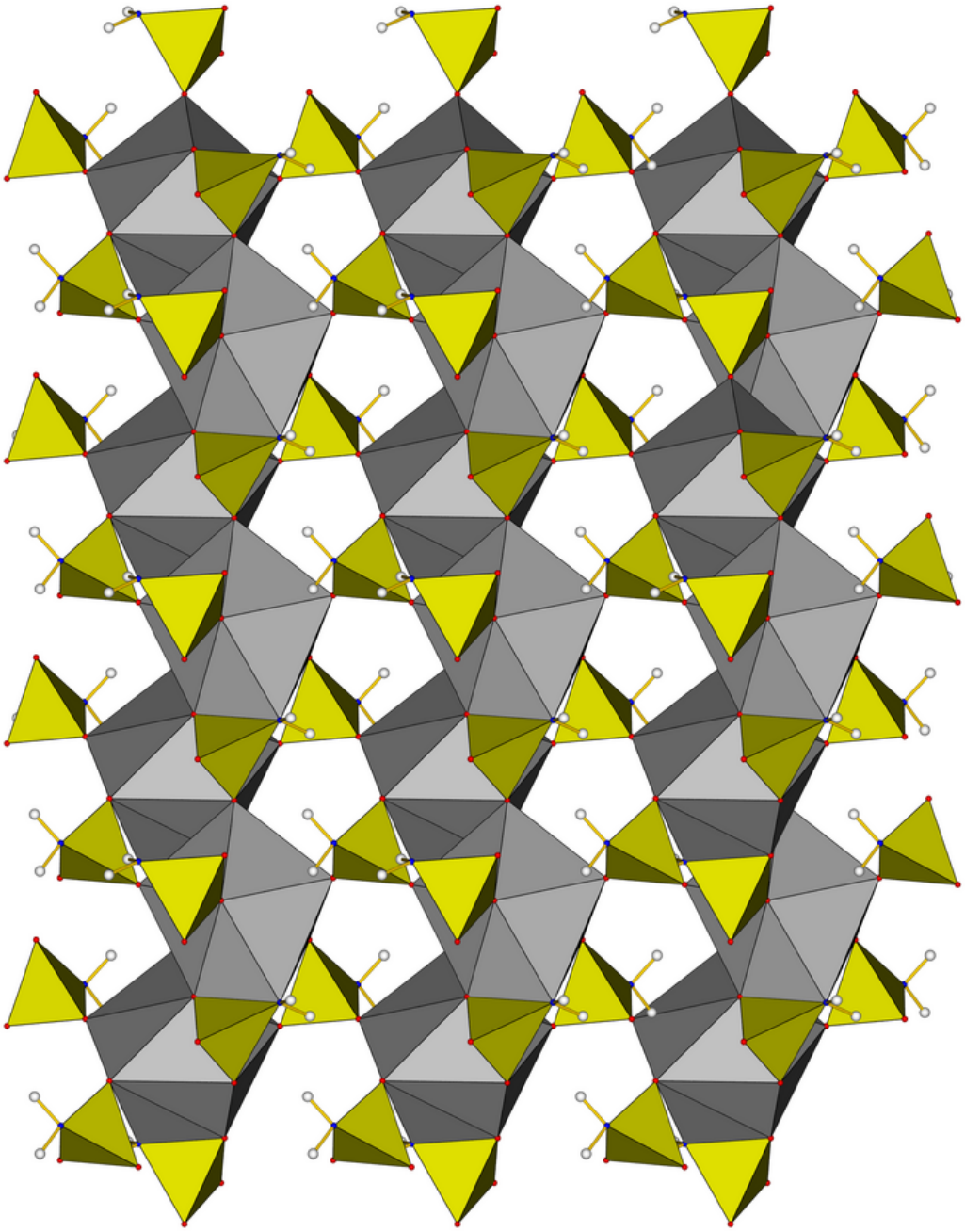

Figure S27: Zigzag chains of SrO_8N polyhedra condensed via edge.png-sharing in α-$Sr(NH_2SO_3)_2$ viewed along [1 0 0] (H atoms in white, N atoms in blue, O atoms in red, SO_3N tetrahedra in yellow, SrO_8N polyhedra in grey and covalent bonds as yellow sticks).

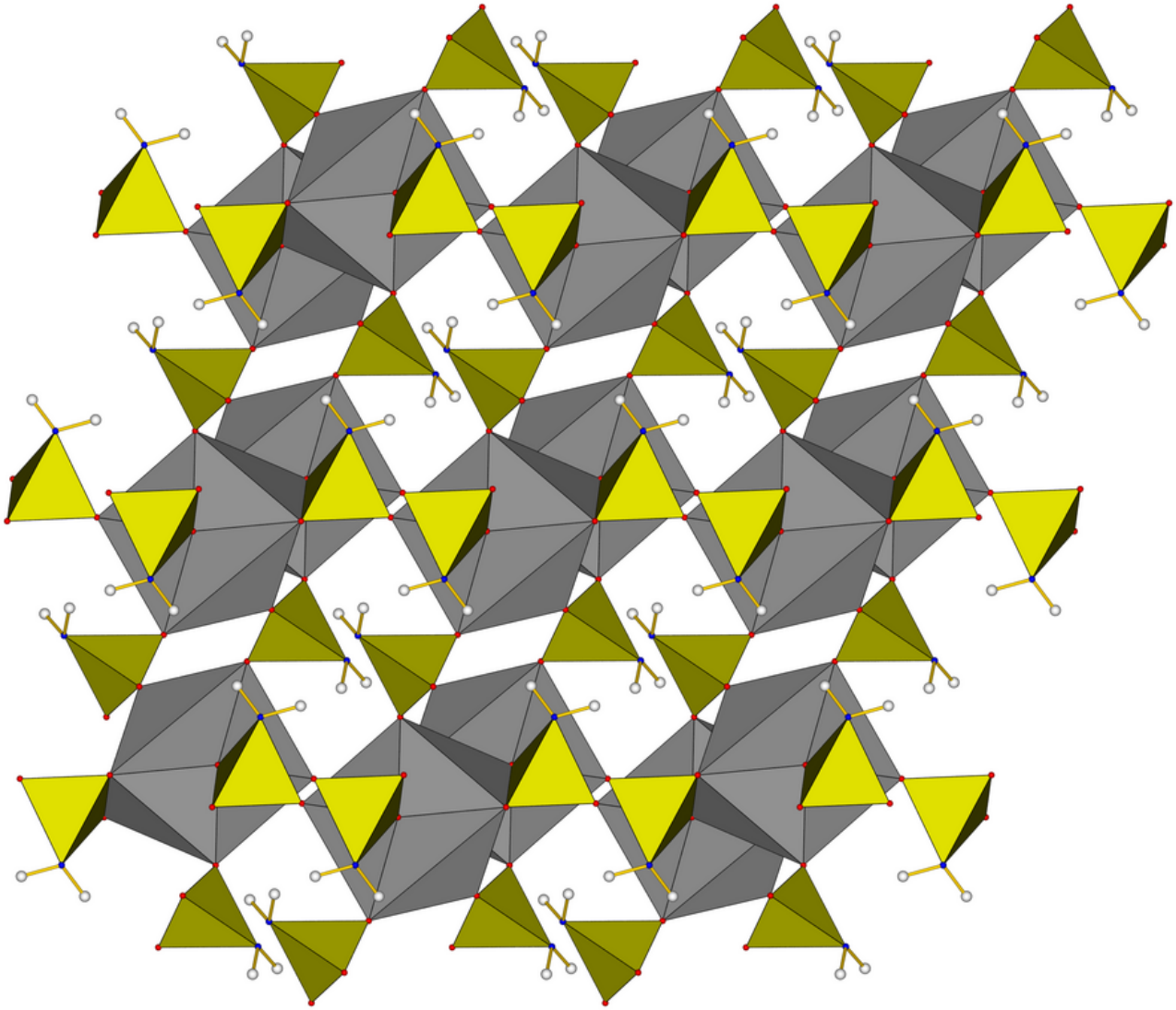

Figure S28: Rod packing of zigzag chains of SrO_8N polyhedra condensed via edge.png-sharing in α-$Sr(NH_2SO_3)_2$ viewed along [0 1 0] (H atoms in white, N atoms in blue, O atoms in red, SO_3N tetrahedra in yellow, SrO_8N polyhedra in grey and covalent bonds as yellow sticks).

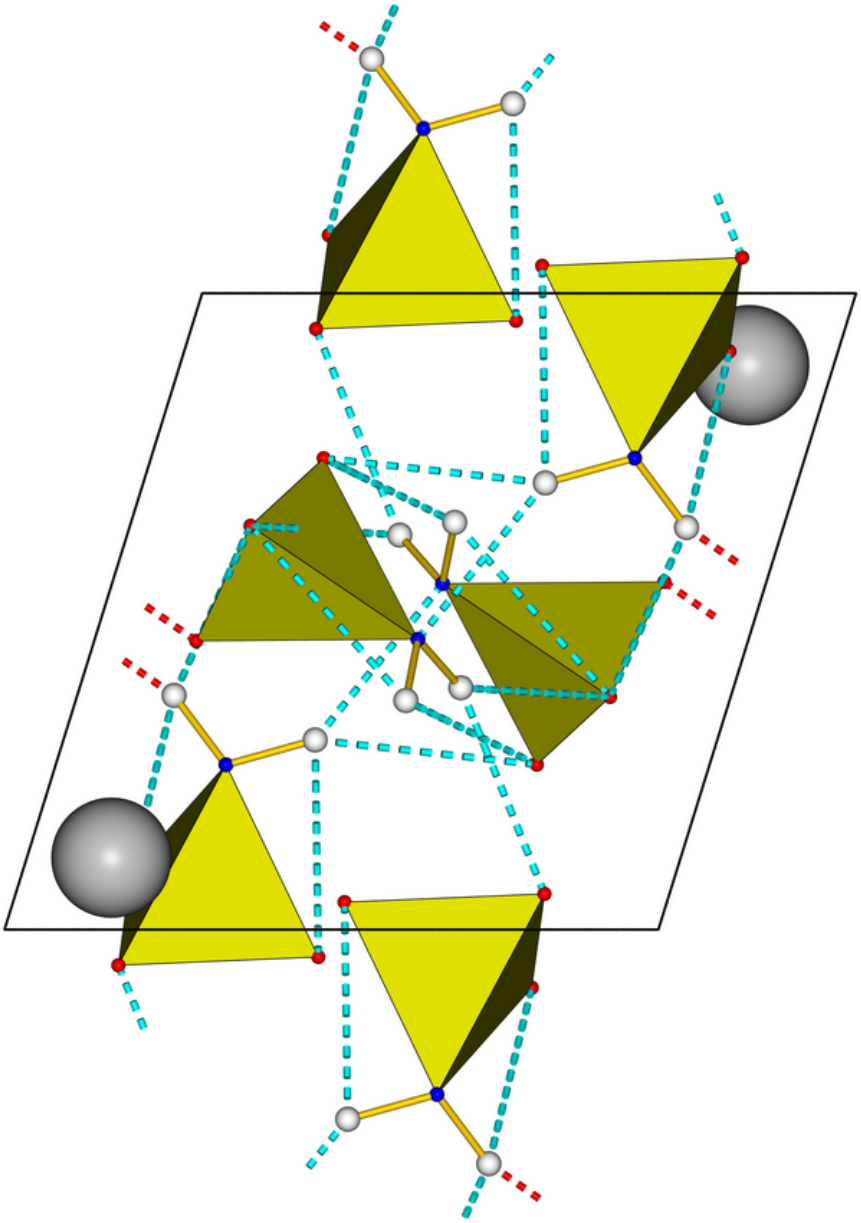

Figure S29: Hydrogen bonding pattern of α-$Sr(NH_2SO_3)_2$ viewed along [0 1 0] (H atoms in white, N atoms in blue, O atoms in red, SO_3N tetrahedra in yellow). Hydrogen bonds are displayed as broken lines with colour coding as follows: N-H$\cdots$$O_{as}$ in red, N-H$\cdots$N in light blue.

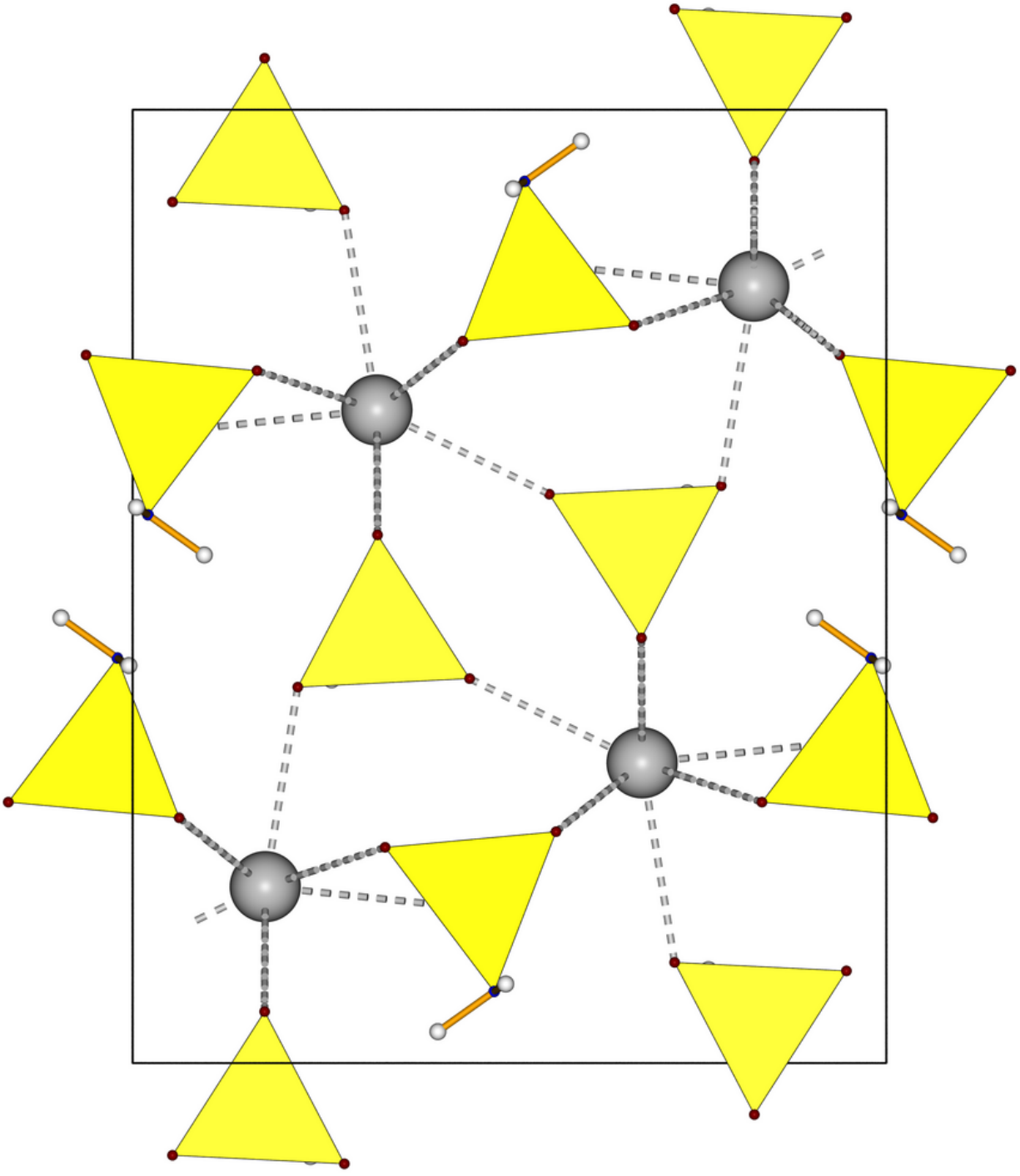

Figure S30: The unit cell of $Ba(NH_2SO_3)_2$ viewed along [0 0 1] (H atoms in white, N atoms in blue, O atoms in red, SO_3N tetrahedra in yellow, Sr atoms in grey, covalent bonds as yellow sticks and coordinate bonds as grey broken lines).

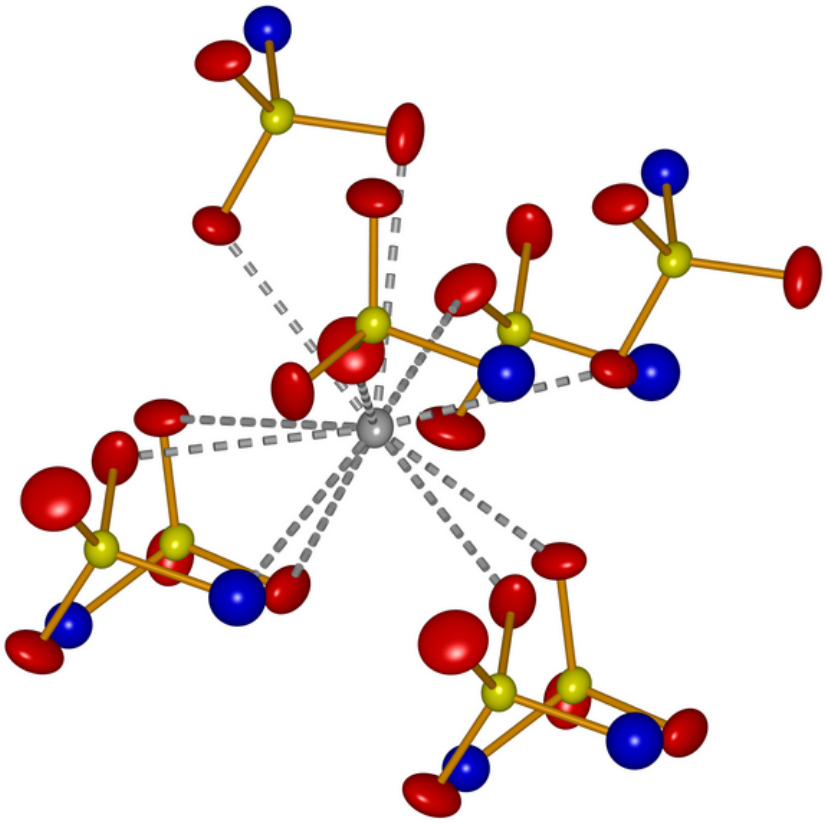

Figure S31: Coordination environment of Ba^{2+} in $Ba(NH_2SO_3)_2$ (H atoms in white, N atoms in blue, O atoms in red, S atoms in yellow, Ba atom in grey, covalent bonds as yellow sticks and coordinate bonds as grey broken lines; displacement ellipsoids for all atoms but hydrogen correspond to 70% probability level)

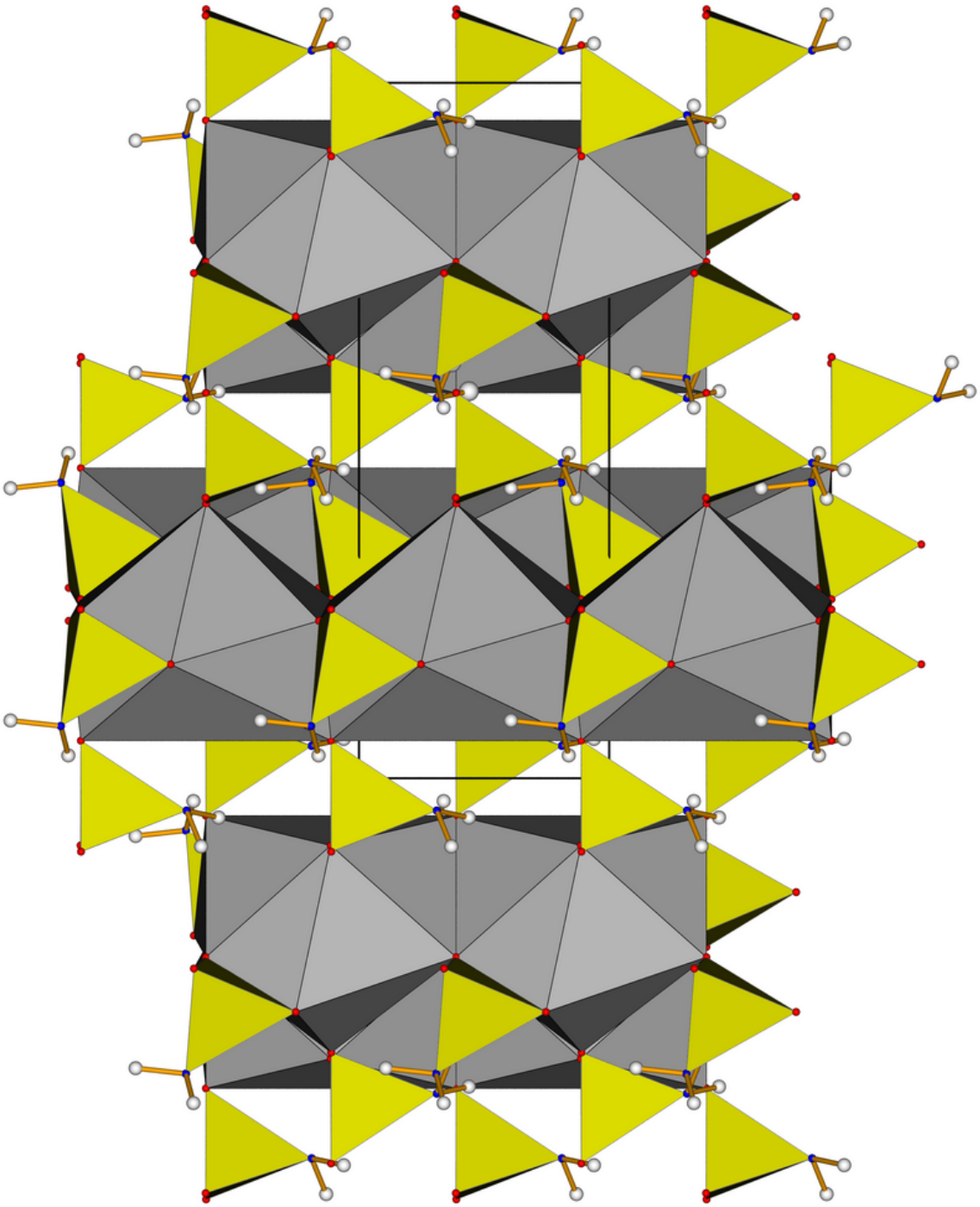

Figure S32: Chains of $BaO_{10}N$ polyhedra condensed via face.png-sharing in $Ba(NH_2SO_3)_2$ viewed along [1 0 0] (H atoms in white, N atoms in blue, O atoms in red, SO_3N tetrahedra in yellow, $BaO_{10}N$ polyhedra in grey and covalent bonds as yellow sticks).

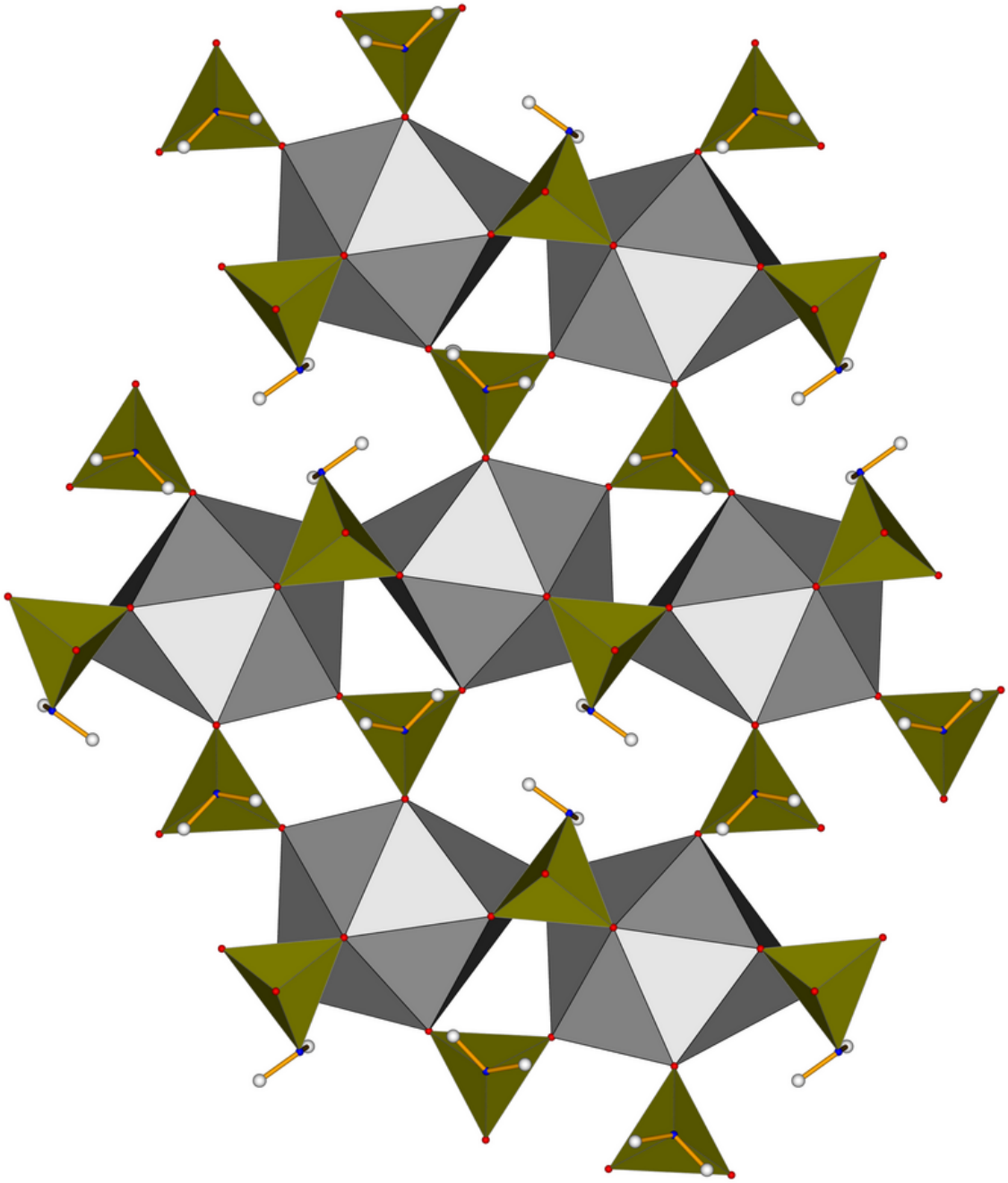

Figure S33: Chains of $BaO_{10}N$ polyhedra condensed via face.png-sharing in $Ba(NH_2SO_3)_2$ viewed along [0 0 1] (H atoms in white, N atoms in blue, O atoms in red, SO_3N tetrahedra in yellow, $BaO_{10}N$ polyhedra in grey and covalent bonds as yellow sticks).

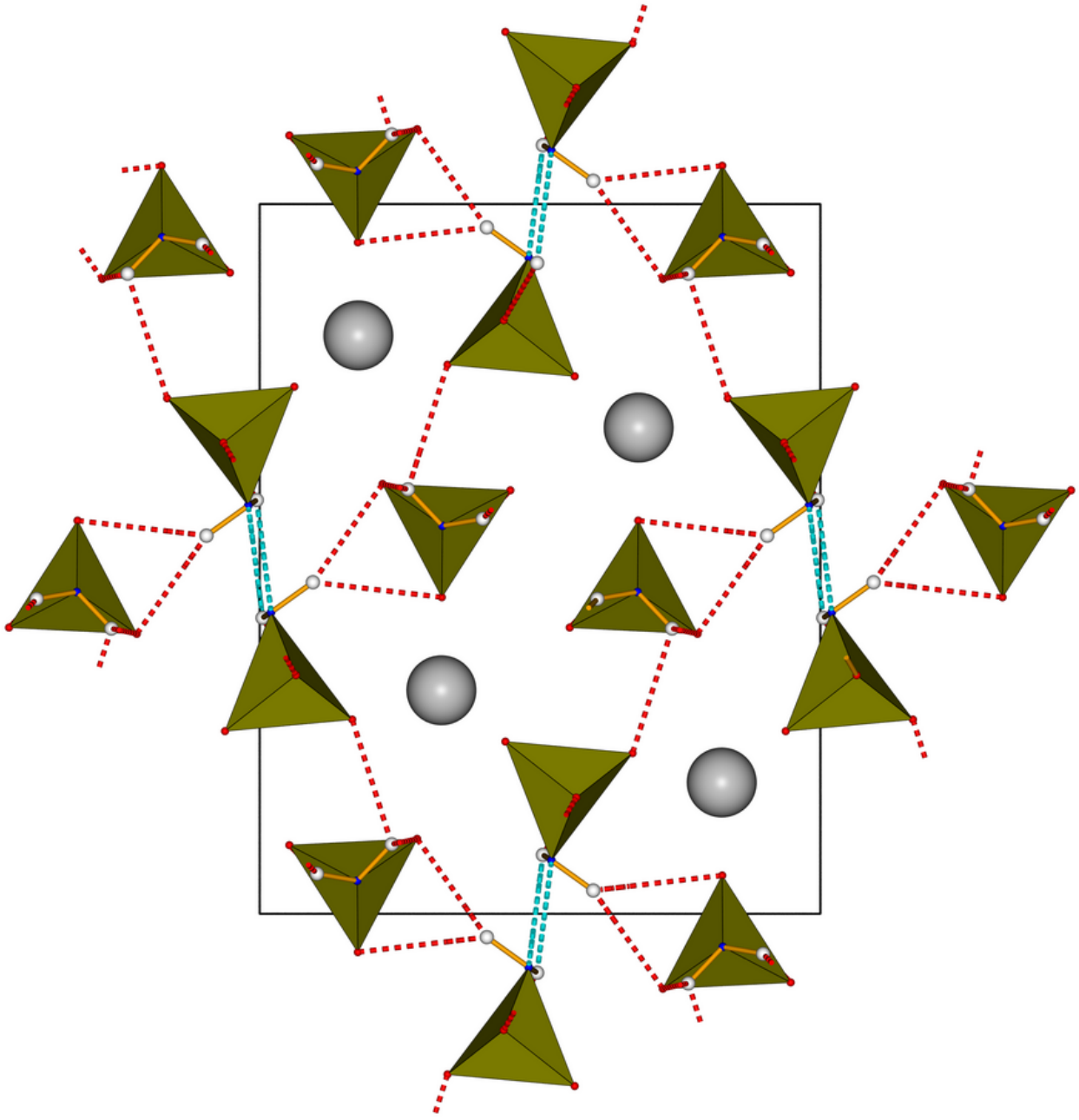

Figure S34: Hydrogen bonding pattern of $Ba(NH_2SO_3)_2$ viewed along [0 0 1] (H atoms in white, N atoms in blue, O atoms in red, Ba atoms in gey and SO_3N tetrahedra in yellow). Hydrogen bonds are displayed as broken lines with colour coding as follows: N-H$\cdots$O$_{as}$ in red, N-H$\cdots$N in light blue.

Table S1: Selected interatomic distances in Å, angles in ° and deviations from ideal tetrahedral symmetry Δ in % (calculated according to the method of Balić-Žunić an Makovicky[1, 2]) for $Mg(NH_2SO_3)_2 \cdot 4\,H_2O$ (1), $Mg(NH_2SO_3)_2 \cdot 3\,H_2O$ (2), $Ca(NH_2SO_3)_2 \cdot 4\,H_2O$ (3), $Ca(NH_2SO_3)_2 \cdot H_2O$ (4), $Sr(NH_2SO_3)_2 \cdot 4\,H_2O$ (5), $Sr(NH_2SO_3)_2 \cdot H_2O$ (6), β-$Sr(NH_2SO_3)_2$ (7), α-$Sr(NH_2SO_3)_2$ (8) and $Ba(NH_2SO_3)_2$ (9), as well as the sum of the corresponding ionic radii $\sum_i r_i$.

	(1)	(2)	(3)	(4)	(5)	(6)	(7)	(8)	(9)
S-O	1.44–1.45	1.44–1.47	1.45–1.46	1.45–1.46	1.45–1.46	1.44–1.46	1.45–1.47	1.45–1.46	1.44–1.46
$\sum_i r_i$=1.46									
S-N	1.65	1.64–1.65	1.63	1.62–1.64	1.63	1.63	1.61–1.63	1.63	1.63
$\sum_i r_i$=1.58									
O.png-s-O	111.2–113.8	110.4–113.9	111.2–112.4	109.8–112.9	111.6–112.4	109.4–113.7	107.0–113.1	109.0–113.6	109.8–113.4
O.png-s-N	104.4–109.7	104.8–109.9	105.2–108.9	104.7-112.3	105.5–108.7	104.9–110.3	104.6–111.0	104.2-111.8	104.3–111.0
Δ (S1/S2)	-0.49	-0.47/-0.55	-0.31	-0.59/-0.45	-0.34	-0.28/-0.44	-0.50/-0.49	-0.41/-0.44	-0.24
M-O/N*	2.04–2.09	2.02–2.10	2.43–2.50	2.23–2.44	2.55–2.60	2.56–2.66	2.53–2.79	2.55–3.04	2.69–3.33
$\sum_i r_i$	2.08	2.08	2.48	2.42	2.62	2.62	2.64	2.67	2.93

* *M*=Mg,Ca,Sr,Ba

Table S2: Interatomic distances d (in Å) and angles $\measuredangle$ (in °) for hydrogen bonds between donor atom D and acceptor atoms A in $Mg(NH_2SO_3)_2 \cdot 4\,H_2O$ (1), $Mg(NH_2SO_3)_2 \cdot 3\,H_2O$ (2), $Ca(NH_2SO_3)_2 \cdot 4\,H_2O$ (3), $Ca(NH_2SO_3)_2 \cdot H_2O$ (4), $Sr(NH_2SO_3)_2 \cdot 4\,H_2O$ (5), $Sr(NH_2SO_3)_2 \cdot H_2O$ (6), β-$Sr(NH_2SO_3)_2$ (7), α-$Sr(NH_2SO_3)_2$ (8) and $Ba(NH_2SO_3)_2$ (9).

D-H	A	d(H-A)	$\measuredangle D$HA	d(D-A)	D-H	A	d(H-A)	$\measuredangle D$HA	d(D-A)
(1)					(6)				
N1-HN11	O2	2.48	150.6	3.36	OW-HW2	O22	1.93	163.8	2.87
N1-HN11	O3	2.43	150.6	3.31	OW-HW2	O22	1.93	163.8	2.87
N1-HN12	O2	2.20	154.7	3.10	OW-HW1	O21	1.95	155.7	2.86
OW1-HW11	OW2	2.01	168.1	2.82	N1-H12	N2	2.31	137.0	3.10
OW1-HW12	O2	1.99	161.9	2.75	OW-HW1	O11	2.33	113.1	2.85
OW2-HW21	O3	2.08	153.2	2.74	N2-H22	O12	2.46	168.8	3.45
OW2-HW22	N1	2.11	159.7	2.90	N1-H11	O22	2.50	119.1	3.11
					N2-H21	OW	2.52	142.5	3.34
					N2-H21	N1	2.53	128.1	3.23
(2)					(7)				
OW2-HW21	O21	1.65	165.6	2.73	N1-H11	O11	1.93	108.7	2.44
OW1-HW12	O12	1.80	171.6	2.74	N1-H12	N2	2.11	150.4	3.01
OW3-HW31	O22	1.81	169.7	2.76	N1-H12	O12	2.41	80.7	2.45
OW2-HW22	O13	1.94	168.3	2.89	N1-H13	O11	2.27	129.4	3.13
OW1-HW11	N1	1.96	160.4	2.89	N1-H14	N2	2.51	110.5	3.03
OW3-HW32	OW1	2.04	161.0	2.97	N1-H14	O13	2.34	89.1	2.54
N1-H12	O12	2.07	164.9	3.02	N2-H21	O12	2.38	162.0	3.34
N1-H11	N2	2.14	178.4	3.10	N2-H21	O11	2.38	133.4	3.15
N2-H22	O21	2.18	152.7	3.06	N2-H21	O21	2.50	80.0	2.53
N2-H21	O22	2.21	146.7	3.06	N2-H22	O12	2.33	156.1	3.26
					N2-H22	O23	2.36	84.1	2.46
					N2-H22	O13	2.38	137.7	3.18
(3)					(8)				
OW1-HW11	O2	1.98	171.2	2.86	N1-H11	O21	2.13	154.5	3.06
OW1-HW12	O2	2.00	169.4	2.90	N1-H12	N2	2.20	144.3	3.06
OW2-HW21	OW1	2.10	167.3	2.96	N2-H22	O23	2.34	149.2	3.23
N1-H12	O1	2.11	159.2	3.05	N2-H22	O13	2.42	122.6	3.06
N1-H11	OW2	2.20	147.8	3.08	N1-H12	O22	2.48	112.2	3.38
N1-H13	N1	2.25	155.5	3.17	N2-H21	O23	2.54	73.0	2.44
					N1-H12	O12	2.55	75.2	2.49
(4)					(9)				
N1-H12	O11	2.10	108.6	3.07	N1-H12	O13	2.14	143.3	2.99
OW-HW2	O12	1.96	158.2	2.89	N2-H22	O22	2.29	142.9	3.13
N2-H22	N1	2.28	153.1	3.19	N1-H11	O23	2.29	161.0	3.23
OW-HW1	O22	2.30	168.1	3.02	N2-H21	O23	2.36	83.5	2.46
N2-H21	O23	2.37	134.5	3.14	N1-H11	O21	2.46	137.9	3.26
OW-HW1	O21	2.42	133.7	3.17	N2-H21	O12	2.47	116.7	3.05
N1-H11	N2	2.61	148.4	3.48	N2-H21	O23	2.55	115.4	3.11
					N1-H12	N1	2.58	118.5	3.17
(5)									
OW2-HW22	O1	2.06	166.5	2.89					
OW2-HW21	O1	2.07	170.4	2.87					
OW1-HW11	O1	2.17	152.8	2.92					
OW1-HW12	OW2	2.22	154.7	2.94					
N1-H11	O3	2.18	153.7	3.09					
N1-H12	OW1	2.22	158.1	3.15					
N1-H13	N1	2.28	164.3	3.24					

Table S3: Crystal data and structure refinement of $Ba(NH_2SO_3)_2$ at T =200 K, 300 K, 400 K and 500 K.

T / K	200	300	400	500
Formula	$H_4BaN_2O_6S_2$	$H_4BaN_2O_6S_2$	$H_4BaN_2O_6S_2$	$H_4BaN_2O_6S_2$
M_r/g·mol^{-1}	329.51	329.51	329.51	329.51
crystal size /mm^3	0.18x0.02x0.01	0.18x0.02x0.01	0.18x0.02x0.01	0.18x0.02x0.01
crystal system	orthorhombic	orthorhombic	orthorhombic	orthorhombic
space group	$Pna2_1$ $Pna2_1$	$Pna2_1$	$Pna2_1$	
a / Å	10.5739(6)	10.5749(8)	10.5788(6)	10.5848(10)
b / Å	13.3639(7)	13.3927(10)	13.4398(7)	13.4915(16)
c / Å	4.8015(3)	4.8168(4)	4.8350(3)	4.8551(6)
V / Å^3	678.49(7)	682.19(9)	687.43(7)	693.33(14)
Z	4	4	4	4
D_{calc} / g·cm^{-1}	3.225	3.208	3.184	3.157
μ(Mo-K$_\alpha$) / cm^{-1}	4.842	6.421	6.372	6.318
F(000) / e	462	616	616	616
hkl range	[-20,14], [-25,24], ±9	[-20,13], [-25,24], ±9	[-20,13], [-25,24], ±9	[-12,18], [-23,23], ±8
$[(\sin\theta)/\lambda]_{max}$ / Å^3	0.96	0.96	0.96	0.88
measured reflections	18546	18652	18938	15615
unique reflections	4956	4979	5007	3975
Flack x	0.056(13)	0.062(11)	0.049(14)	0.055(14)
R_{int} / R_{sigma}	0.074/0.074	0.067/0.067	0.084/0.085	0.76/0.71
refined parameters	113	113	113	113
$R_1(F)$ / $wR_2(F^2)$	0.67/0.75	0.064/0.070	0.097/0.089	0.092/0.071
GoF (F^2)	0.99	0.95	1.00	0.98
$\Delta\rho_{fin}$ / e·Å^{-3} (max./min.)	1.85/-1.83	1.55/-1.85	1.18/-1.44	1.11/-1.27

Table S4: Crystal data and structure refinement of S_4N_4 (10).

Formula	S_4N_4
M_r/g·mol^{-1}	288.55
crystal size /mm^3	0.20x0.05x0.05
crystal system	monoclinic
space group	$P2_1/n$
a / Å	8.6933(5)
b / Å	7.1572(4)
c / Å	8.7826(6)
α / °	90
β / °	92.628(4)
γ / °	90
V / Å^3	545.87(6)
Z	4
T / K	278(2)
D_{calc} / g·cm^{-1}	1.682
μ(Mo-K$_\alpha$) / cm^{-1}	1.213
F(000) / e	276
hkl range	±8, [0,7], [0,9]
$[(\sin\theta)/\lambda]_{max}$ / Å^3	0.52
measured reflections	628
unique reflections	628
BASF	0.34
R_{int} / R_{sigma}	0.132/0.073
refined parameters	74
$R_1(F)$ / $wR_2(F^2)$	0.066/0.106
GoF (F^2)	1.13
$\Delta\rho_{fin}$ (max./min.) / e·Å^{-3}	0.47/-0.37

Table S5: Wavenumbers ν / cm^{-1} of all peaks observed via FT-IR respectively Raman spectroscopy as well as assigned modes with major contributions for the vibrations of $Mg(NH_2SO_3)_2 \cdot 4\,H_2O$ (1), $Mg(NH_2SO_3)_2 \cdot 3\,H_2O$ (2), $Ca(NH_2SO_3)_2 \cdot 4\,H_2O$ (3), $Ca(NH_2SO_3)_2 \cdot H_2O$ (4), $Sr(NH_2SO_3)_2 \cdot H_2O$ (6), β-$Sr(NH_2SO_3)_2$ (7), α-$Sr(NH_2SO_3)_2$ (8) and $Ba(NH_2SO_3)_2$ (9).

mode assignment	FT-IR	(1)	(2)	(3)	(4)	(6)	(7)	(9)	Raman	(4)	(7)	(9)
H_2O as. str.			3487	3570	3590	3498				3580		
H_2O s. str.		3404	3390	3500	3521	3464				3526		
NH_2 as. str.		3293	3305	3309	3340	3373	3367	3348		3340	3369	3350
			3282			3356	3342				3345	
NH_2 s. str.		3226	3240	3248	3251	3286	3251	3277		3241	3254	3277
			3074			3267	3188				3182	3277
							3099			3098		
H_2O bend.		1665	1645	1620	1620	1633				1614		
				1614								
NH_2 bend.		1535	1574	1554	1572	1550	1568	1558			1570	1556
			1531				1441	1470				
			1294									
SO_3 as. str.		1211	1226	1255	1245	1257	1252	1250		1288	1245	
SO_3 s. str.			1198	1232	1209	1236	1230	1200		1203	1228	1207
		1198	1209	1226								
NH_2 as. rock.		1140	1157	1161	1184	1163	1187	1160			1139	1168
			1142	1130		1126	1141	1108				1115
SO_3 s. str.		1058	1182	1049	1107	1101	1080	1059		1088	1081	1060
			1068		1072	1053	1049	1045			1056	1053
NH_2 s. wag.		956	954	887	904	910	916	916		920	916	920
							883	885			883	
								856				
S-N str.		792	814	800	789	785	725	743		777		763
		700	706	663	750	741	705					
						650						
SO_3 as. def.		576	575	584	600	606	596	594		590	595	595
		552	550	540	561	584	577	575		576	567	576
						557	566	552		567	567	557
						546	550			556	551	
SO_3 s. def.		490	480		486	457	469		473	469	468	
		445	445		446	434	413	430			412	428
SO_3 as. rock.		410	416			405		405		396		407
SO_3 s. rock.		402								356	397	391
S-N tors.										300	312	
ext.										176	173	153

Table S6: Crystal data and structure refinement of $Mg(NH_2SO_3)_2 \cdot 4\,H_2O$ (1, CSD–2118236), $Mg(NH_2SO_3)_2 \cdot 3\,H_2O$ (2, CSD–2118237), $Ca(NH_2SO_3)_2 \cdot 4\,H_2O$ (3, CSD–2118238), $Ca(NH_2SO_3)_2 \cdot H_2O$ (4, CSD–2118239), $Sr(NH_2SO_3)_2 \cdot 4\,H_2O$ (5, CSD–2118240), $Sr(NH_2SO_3)_2 \cdot H_2O$ (6, CSD–2118241), β-$Sr(NH_2SO_3)_2$ (7, CSD–2118242), α-$Sr(NH_2SO_3)_2$ (8, CSD–2118243) and $Ba(NH_2SO_3)_2$ (9, CSD–2118244).

	(1)	(2)	(3)	(4)	(5)	(6)	(7)	(8)	(9)
Formula	$H_{12}MgN_2O_{10}S_2$	$H_{10}MgN_2O_9S_2$	$H_{12}CaN_2O_{10}S_2$	$H_6CaN_2O_7S_2$	$H_{12}N_2O_{10}S_2Sr$	$H_6N_2O_7S_2Sr$	$H_4N_2O_6S_2Sr$	$H_4N_2O_6S_2Sr$	$H_4BaN_2O_6S_2$
M_r/g·mol^{-1}	288.55	252.51	304.32	250.27	351.86	297.79	279.79	279.79	329.51
crystal size /mm^3	0.20x0.05x0.05	0.14x0.13x0.09	0.25×0.10×0.05	0.09x0.08x0.06	0.25×0.10×0.05	0.36x0.16x0.11	0.20x0.04x0.04	0.15x0.08x0.03	0.18x0.02x0.01
crystal system	monoclinic	triclinic	monoclinic	orthorhombic	monoclinic	monoclinic	monoclinic	monoclinic	orthorhombic
space group	$P2_1/c$	$P\bar{1}$	$C2/c$	$P2_12_12_1$	$C2/c$	$P2_1/c$	Pc	$P2_1$	$Pna2_1$
a / Å	6.1147(3)	5.2305(5)	11.6250(4)	7.960(2)	11.9293(8)	7.0842(3)	7.0050(2)	7.0047(3)	10.5749(8)
b / Å	5.2369(3)	8.0012(9)	7.7639(3)	8.143(2)	7.8827(5)	7.2765(3)	7.0430(2)	7.0574(3)	13.3927(10)
c / Å	15.3002(8)	10.9903(14)	11.6238(4)	11.995(2)	11.8664(8)	14.8525(6)	7.2915(2)	7.1430(3)	4.8168(4)
α / °	90	95.057(7)	90	90	90	90	90	90	90
β / °	91.574(2)	96.011(5)	98.957(2)	90	99.593(3)	102.8013(15)	107.7870(10)	107.246(3)	90
γ / °	90	92.464(5)	90	90	90	90	90	90	90
V / Å^3	489.76(4)	455.00(9)	1036.32(6)	777.5(3)	1100.25(13)	746.59(5)	342.539(17)	337.24(3)	682.19(9)
Z	2	2	4	4	4	4	2	2	4
T / K	288(2)	298(2)	266(2)	298(2)	297(2)	250(2)	297(2)	296(2)	283
D_{calc} / g·cm^{-1}	1.957	1.843	1.950	2.138	2.124	2.649	2.713	2.755	3.208
μ(Mo-K$_\alpha$) / cm^{-1}	0.654	0.674	1.052	1.350	5.321	7.787	8.467	8.600	6.421
F(000) / e	300	260	632	512	704	584	272	272	616
hkl range	±9, ±7 ±23	±8, ±13 ±18	±15, ±10 ±15	±12, ±12 ±18	[-14,13], [0,9] [0,14]	±11, ±11 ±24	±18, ±18 ±19	±8, ±8 ±8	[-20,13], [-25,24] ±9
$[(\sin\theta)/\lambda]_{max}$ / Å^3	0.76	0.85	0.68	0.76	0.59	0.82	1.31	0.60	0.96
measured reflections	13322	86846	28865	18016	1713	79259	145939	8517	18652
unique reflections	1758	4627	1386	2823	979	3466	12344	1255	4979
Flack x					0.03(2)		0.035(5)		0.062(11)
BASF					0.03(2)			0.43(12)	
R_{int} / R_{sigma}	0.049/0.033	0.062/0.024	0.10/0.03	0.056/0.038	0.082/0.015	0.067/0.022	0.057/0.038	0.082/0.042	0.067/0.067
refined parameters	89	157	91	127	97	128	119	113	113
$R_1(F)$ / $wR_2(F^2)$	0.048/0.089	0.048/0.085	0.052/0.070	0.044/0.083	0.019/0.041	0.033/0.055	0.05/0.110	0.032/0.049	0.064/0.070
GoF (F^2)	1.07	1.09	1.11	1.12	1.15	1.09	1.09	1.05	0.95
$\Delta\rho_{fin}$ / e·Å^{-3} (max./min.)	0.41/-0.48	0.51/-0.46	0.29/-0.45	0.71/-0.42	0.23/-0.30	0.78/-0.55	1.76/-1.49	0.40/-0.32	1.55/-1.85

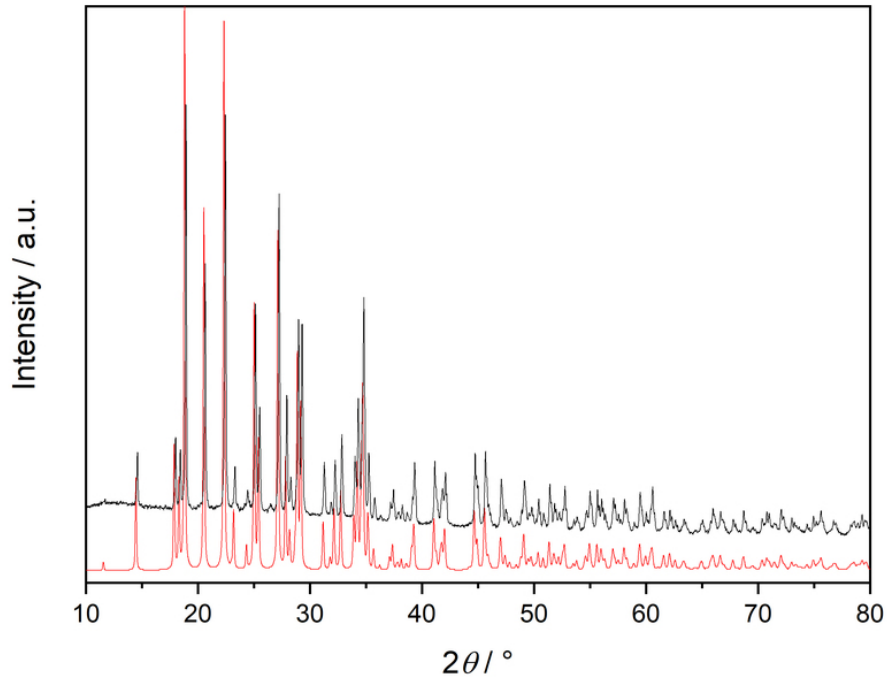

Figure S35: X-ray powder diffraction pattern of $Mg(NH_2SO_3)_2 \cdot 4\,H_2O$ shown in black compared with a calculated pattern based on single-crystal data shown in red.

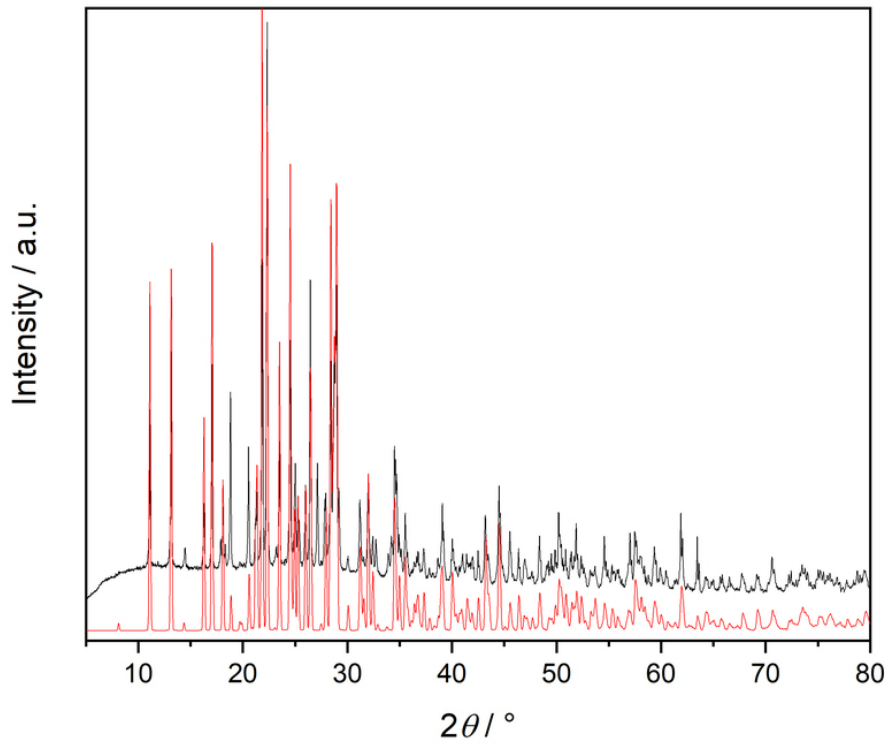

Figure S36: X-ray powder diffraction pattern of $Mg(NH_2SO_3)_2 \cdot 3\,H_2O$ shown in black compared with a calculated pattern based on single-crystal data shown in red.

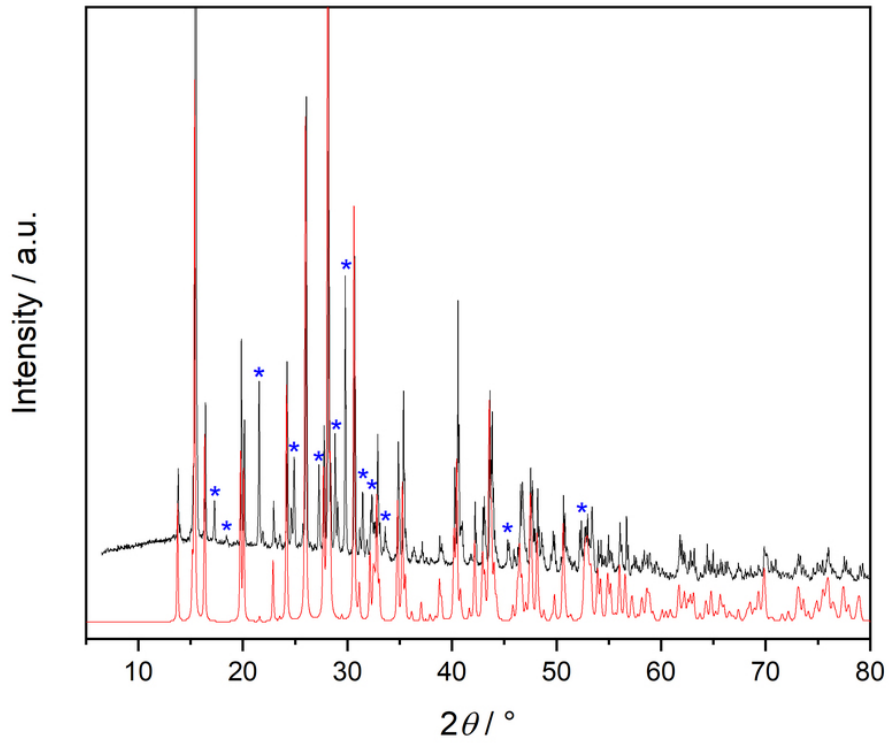

Figure S37: X-ray powder diffraction pattern of $Ca(NH_2SO_3)_2 \cdot 4\,H_2O$ shown in black compared with a calculated pattern based on single-crystal data shown in red. Reflections belonging to $Ca(NH_2SO_3)_2 \cdot H_2O$ are marked with $*$.

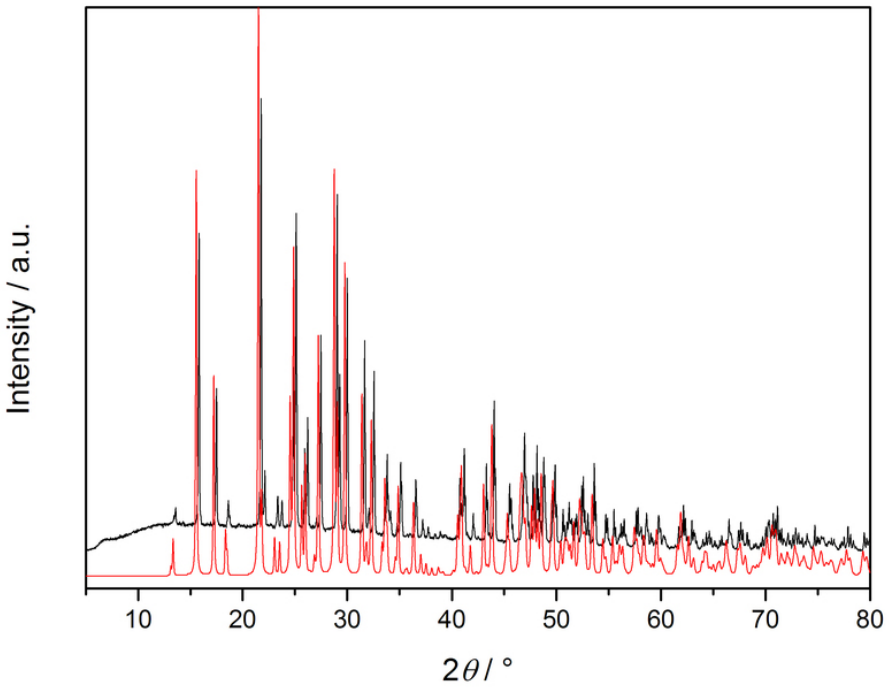

Figure S38: X-ray powder diffraction pattern of $Ca(NH_2SO_3)_2 \cdot H_2O$ shown in black compared with a calculated pattern based on single-crystal data shown in red.

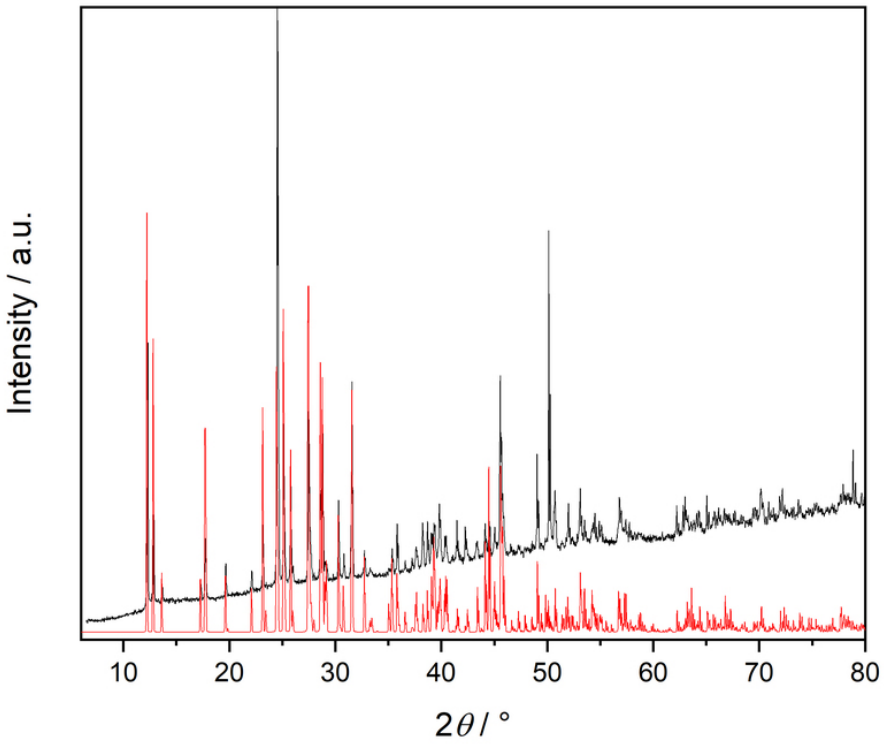

Figure S39: X-ray powder diffraction pattern of $Sr(NH_2SO_3)_2 \cdot H_2O$ shown in black compared with a calculated pattern based on single-crystal data shown in red.

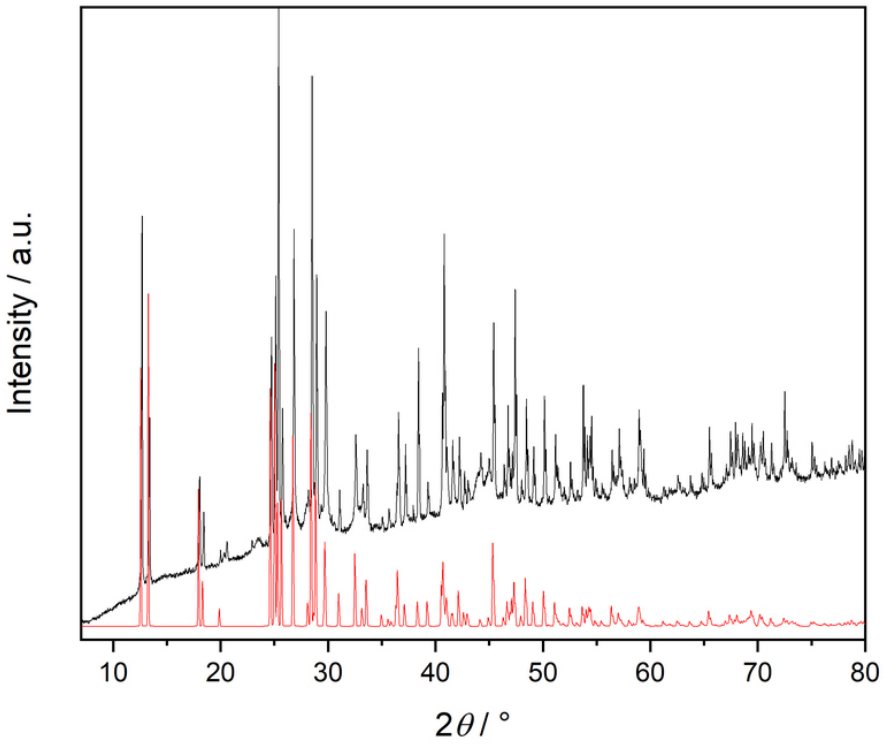

Figure S40: X-ray powder diffraction pattern of β-$Sr(NH_2SO_3)_2$ shown in black compared with a calculated pattern based on single-crystal data shown in red.

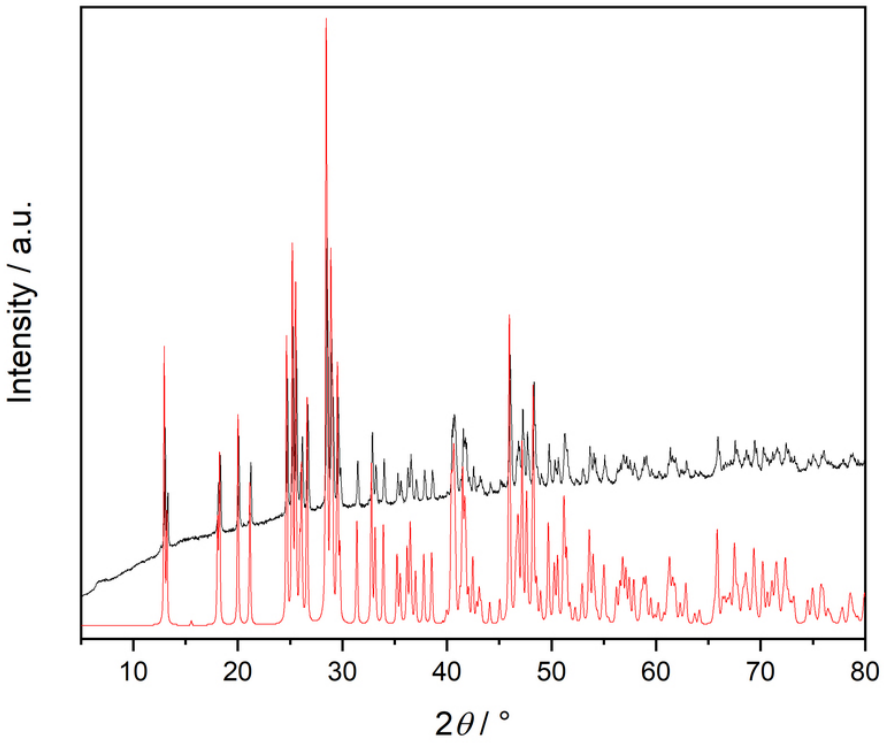

Figure S41: X-ray powder diffraction pattern of α-$Sr(NH_2SO_3)_2$ shown in black compared with a calculated pattern based on single-crystal data shown in red.

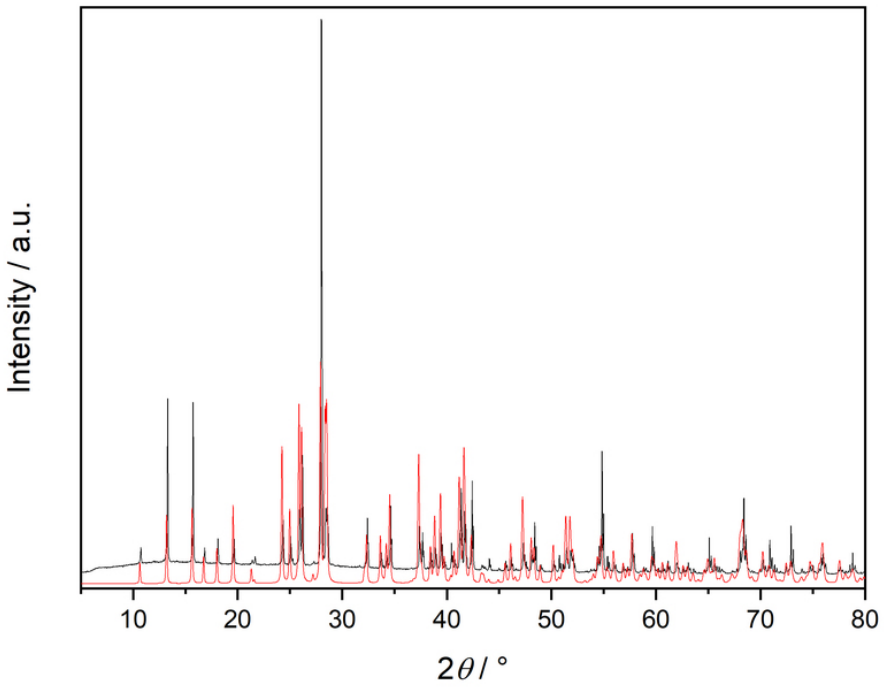

Figure S42: X-ray powder diffraction pattern of $Ba(NH_2SO_3)_2$ shown in black compared with a calculated pattern based on single-crystal data shown in red.

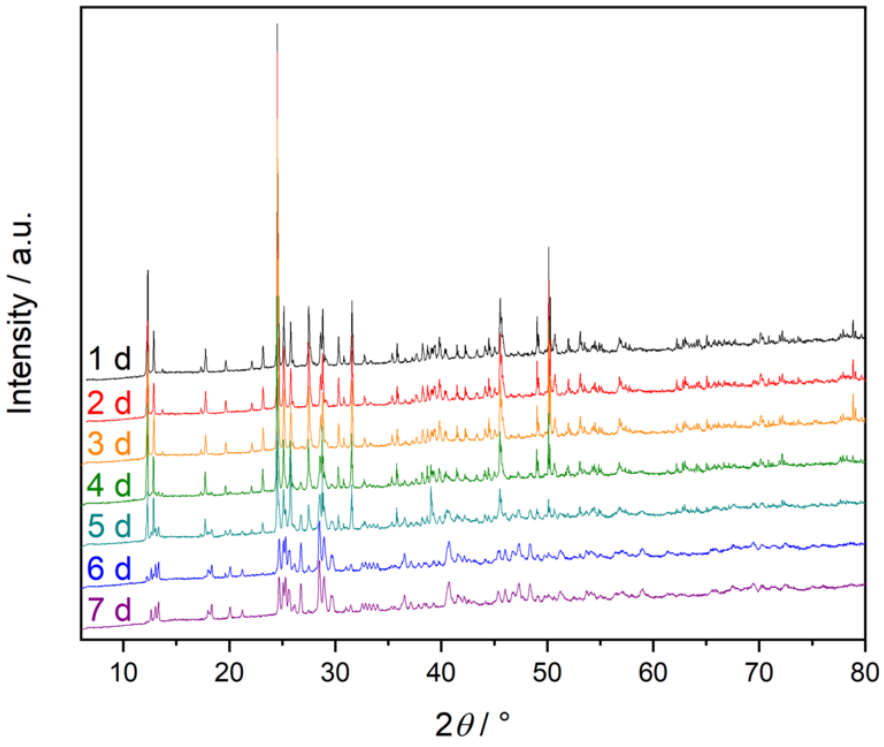

Figure S43: X-ray powder diffraction pattern of a finely ground samle of $Sr(NH_2SO_3)_2 \cdot H_2O$ aged over the course of six days on air.

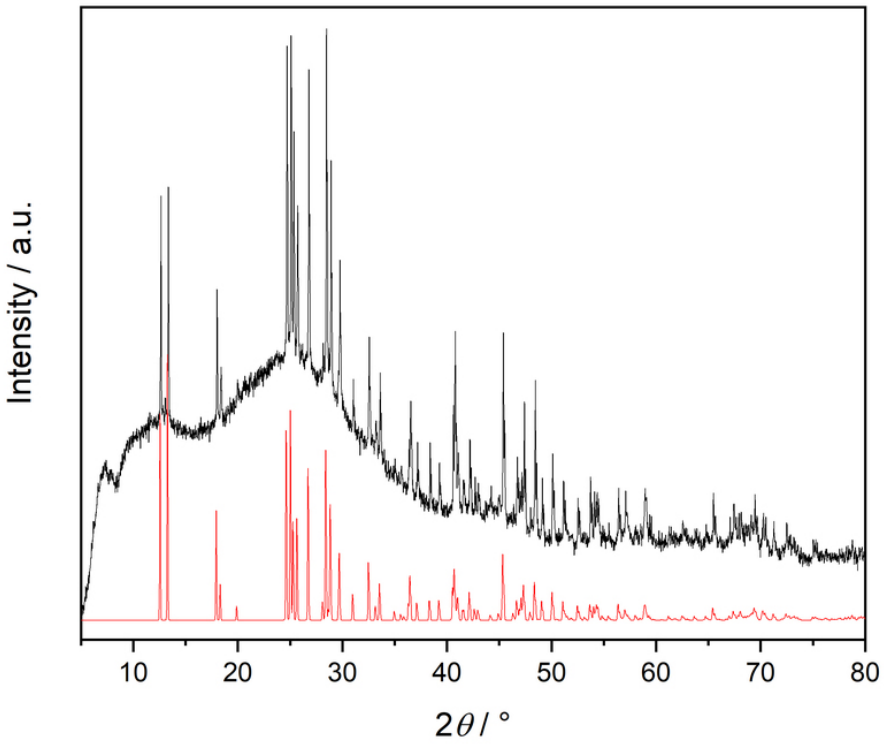

Figure S44: X-ray powder diffraction pattern of a sample of β-$Sr(NH_2SO_3)_2$ heated to 220 °C shown in black compared with a calculated pattern based on single-crystal data shown in red.

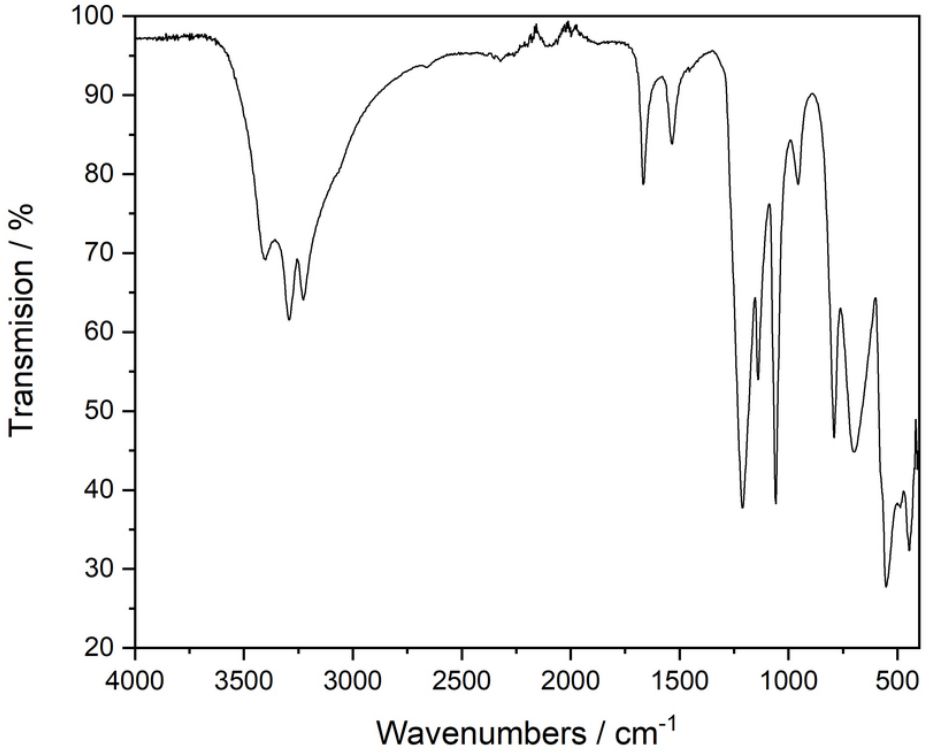

Figure S45: FT-IR spectrum of $Mg(NH_2SO_3)_2 \cdot 4\,H_2O$.

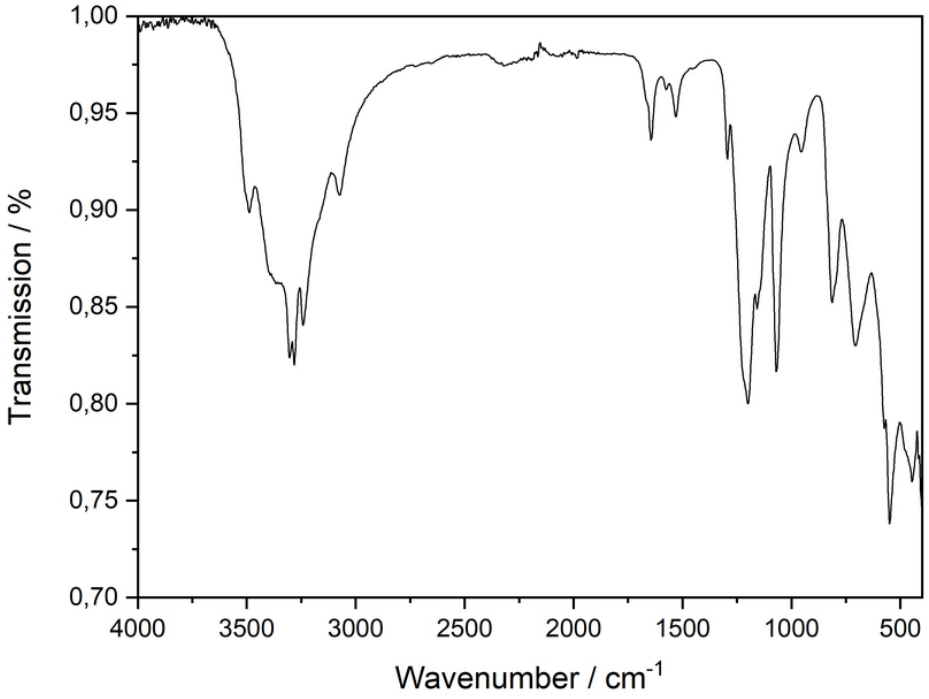

Figure S46: FT-IR spectrum of $Mg(NH_2SO_3)_2 \cdot 3\,H_2O$.

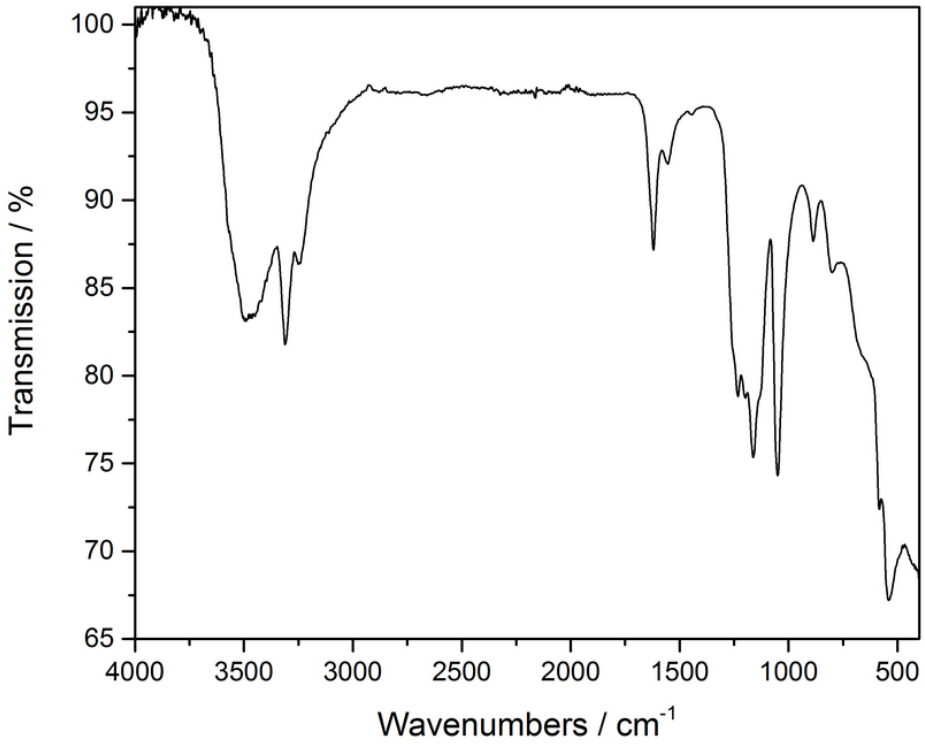

Figure S47: FT-IR spectrum of $Ca(NH_2SO_3)_2 \cdot 4\,H_2O$.

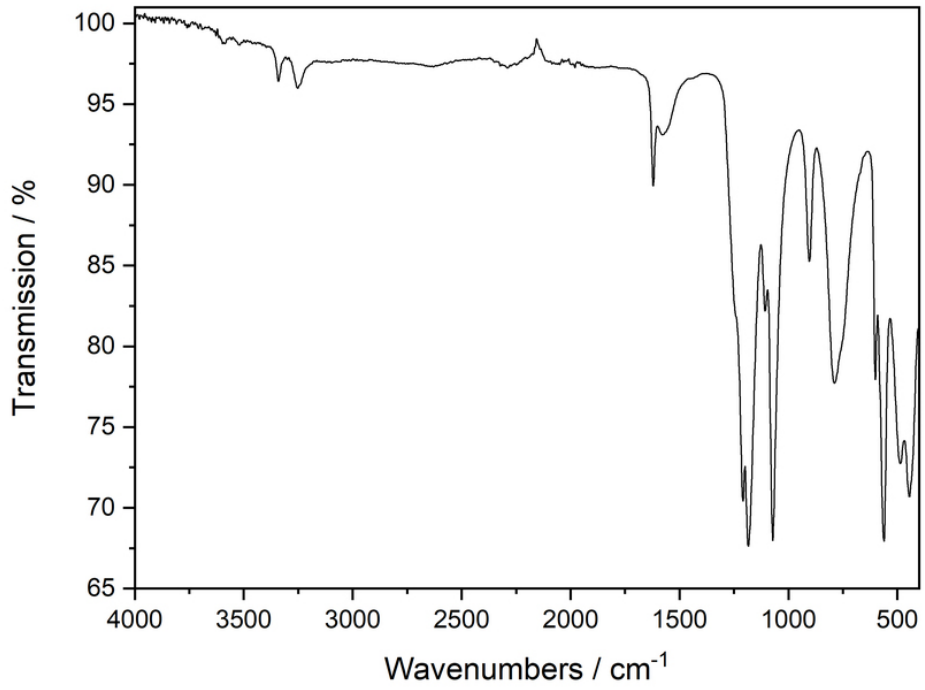

Figure S48: FT-IR spectrum of $Ca(NH_2SO_3)_2 \cdot H_2O$.

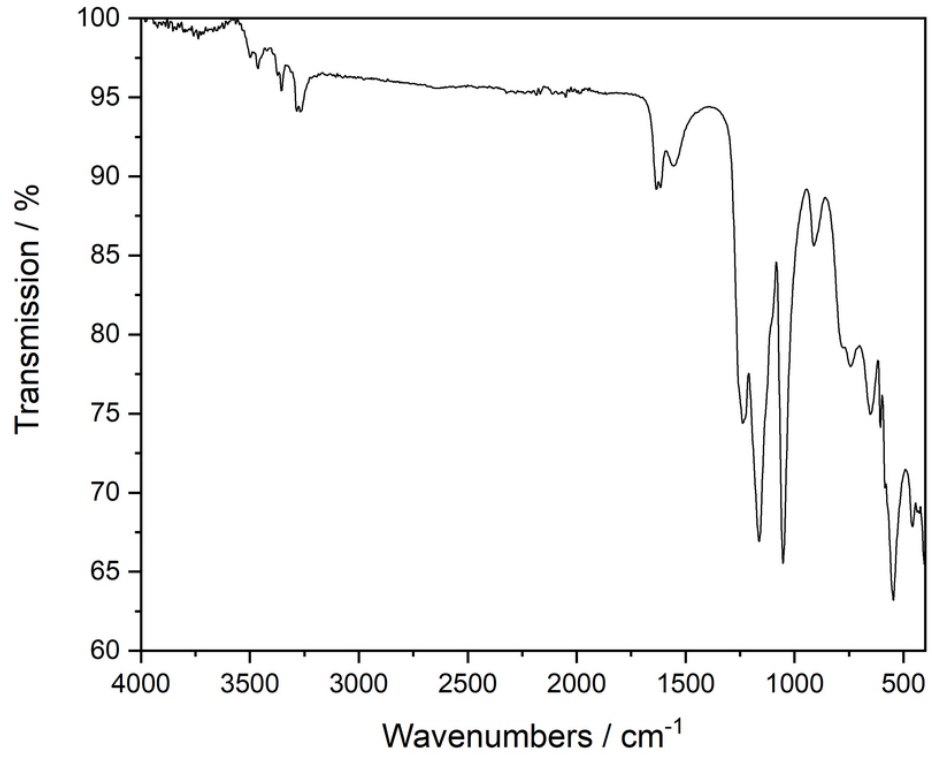

Figure S49: FT-IR spectrum of $Sr(NH_2SO_3)_2 \cdot H_2O$.

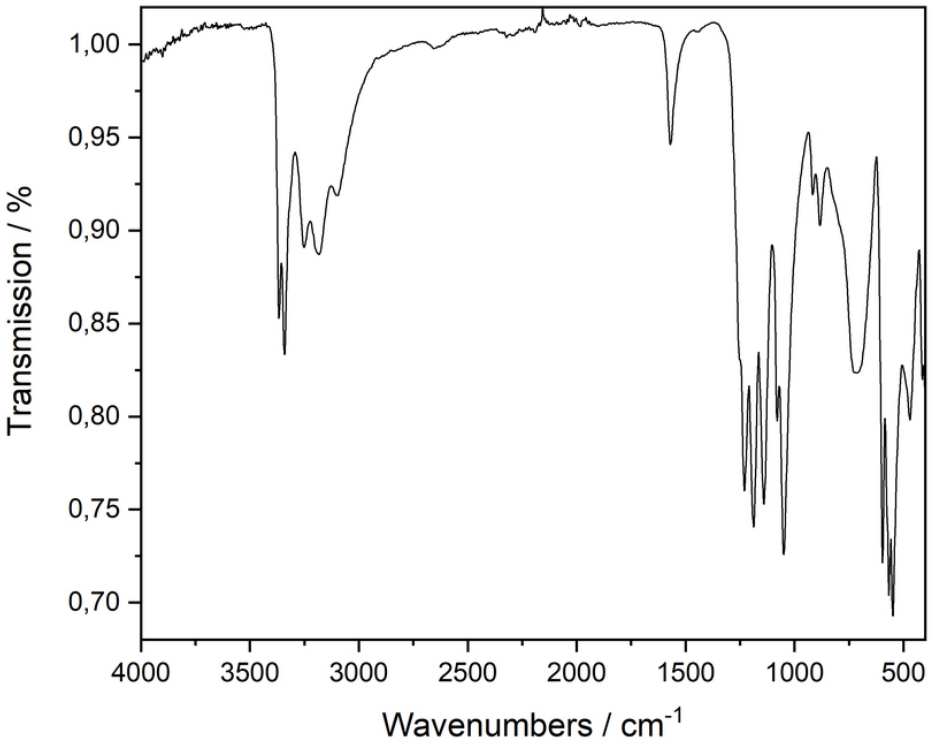

Figure S50: FT-IR spectrum of β-$Sr(NH_2SO_3)_2$.

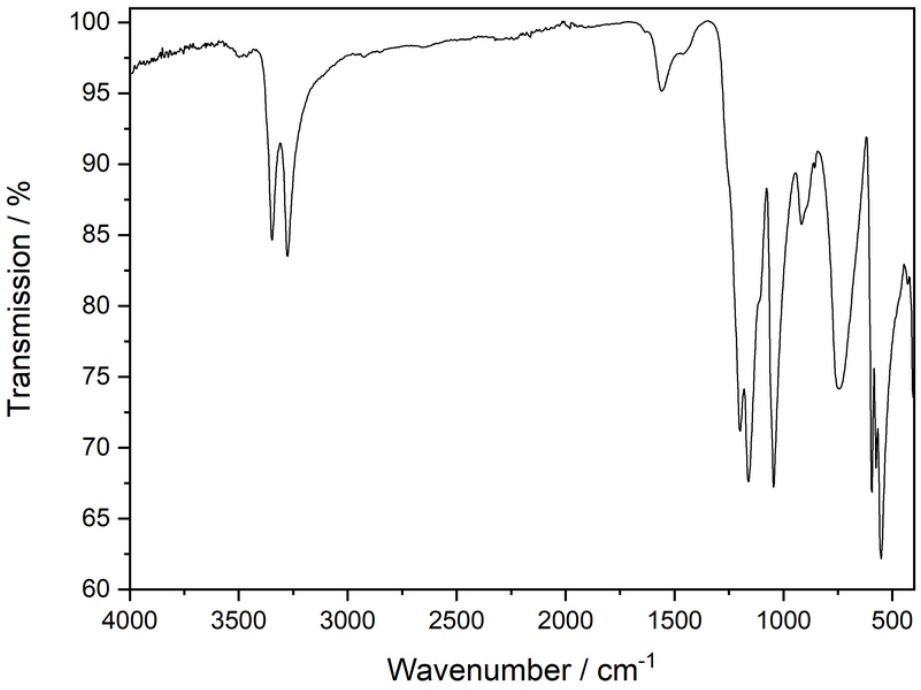

Figure S51: FT-IR spectrum of $Ba(NH_2SO_3)_2$.

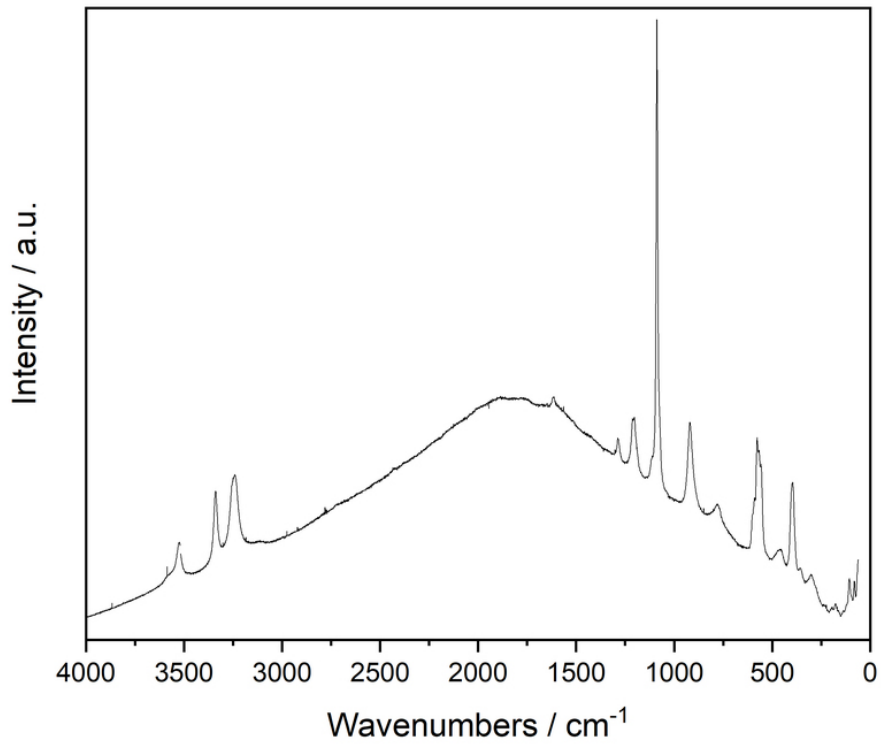

Figure S52: Raman spectrum of $Ca(NH_2SO_3)_2 \cdot H_2O$.

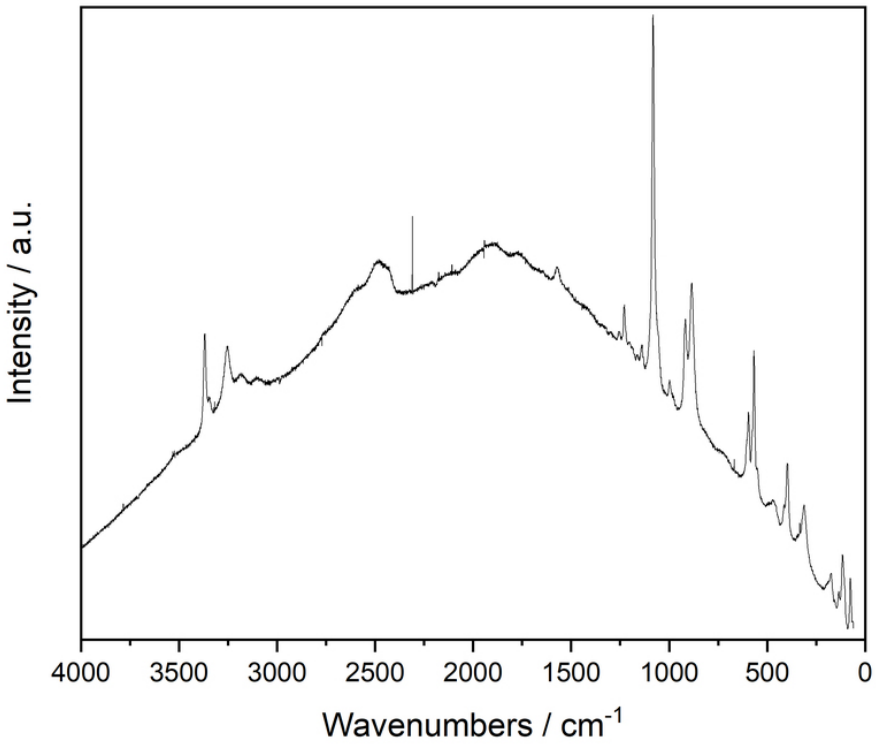

Figure S53: Raman spectrum of $Sr(NH_2SO_3)_2 \cdot H_2O$.

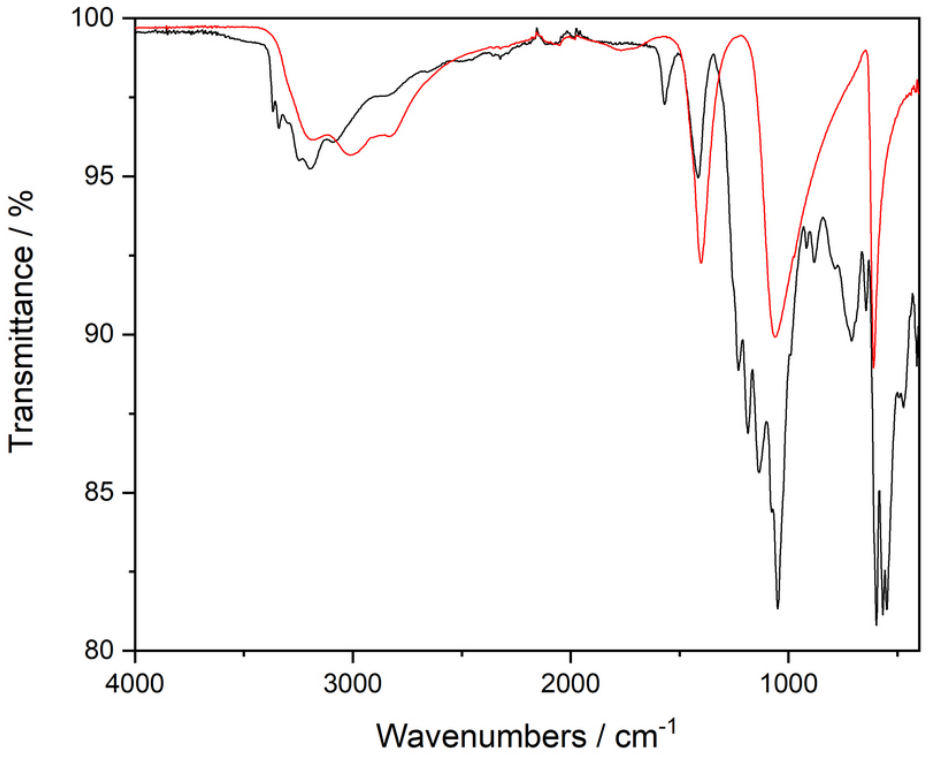

Figure S54: FT-IR spectrum of a sample of β-$Sr(NH_2SO_3)_2$ heated to 220 °C (black line) compared with a FT-IR spectrum of $(NH_4)_2SO_4$ (red line).

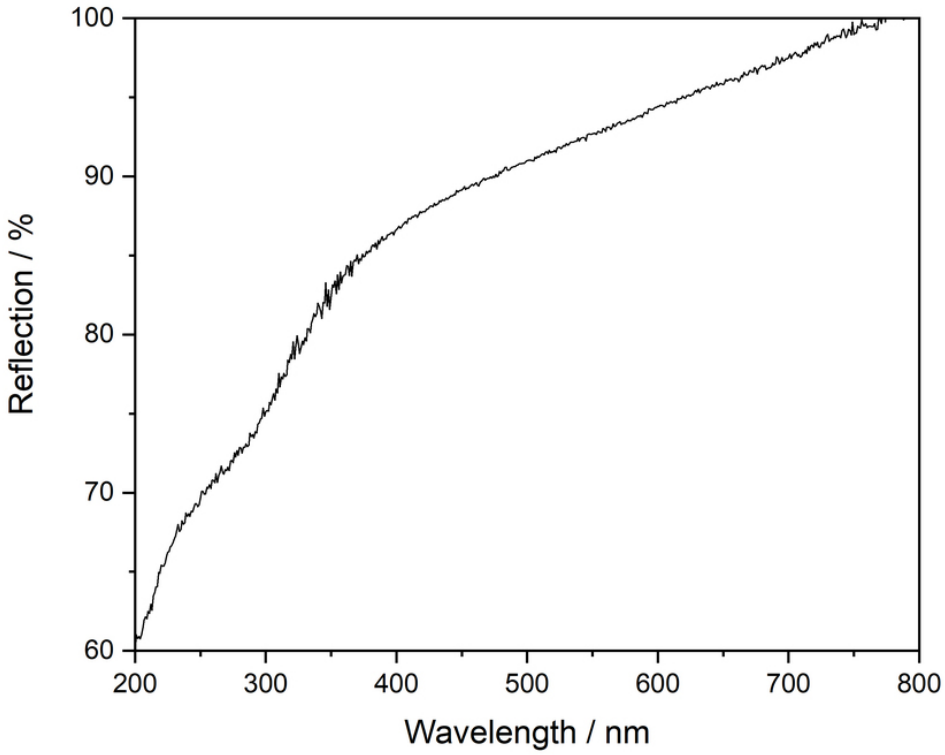

Figure S55: UV-Vis spectrum of $Mg(NH_2SO_3)_2 \cdot 3\,H_2O$.

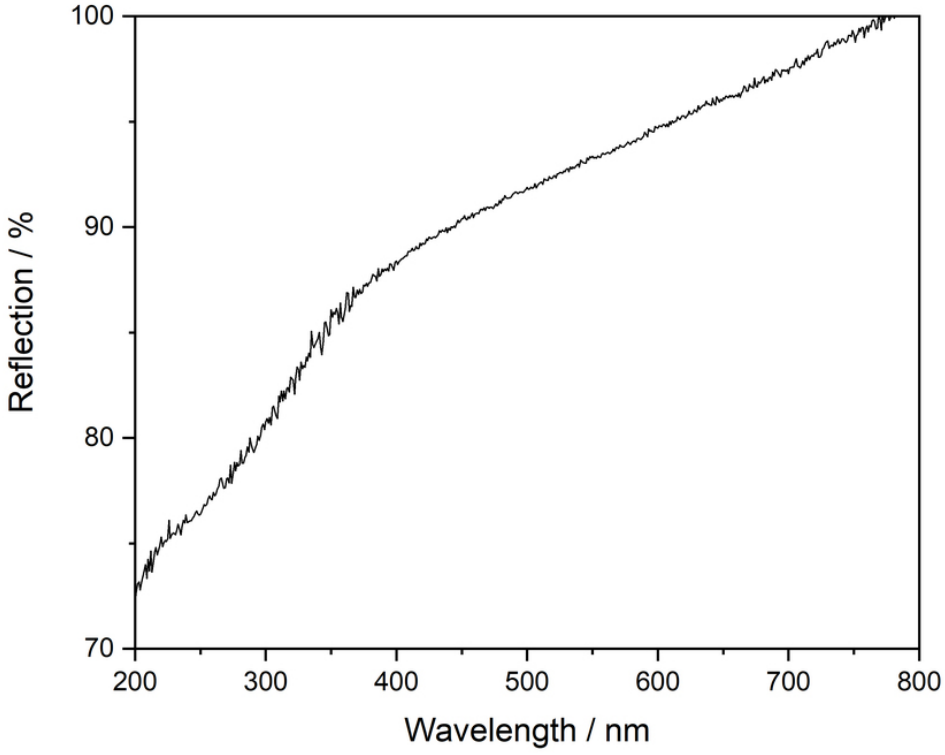

Figure S56: UV-Vis spectrum of $Ca(NH_2SO_3)_2 \cdot H_2O$.

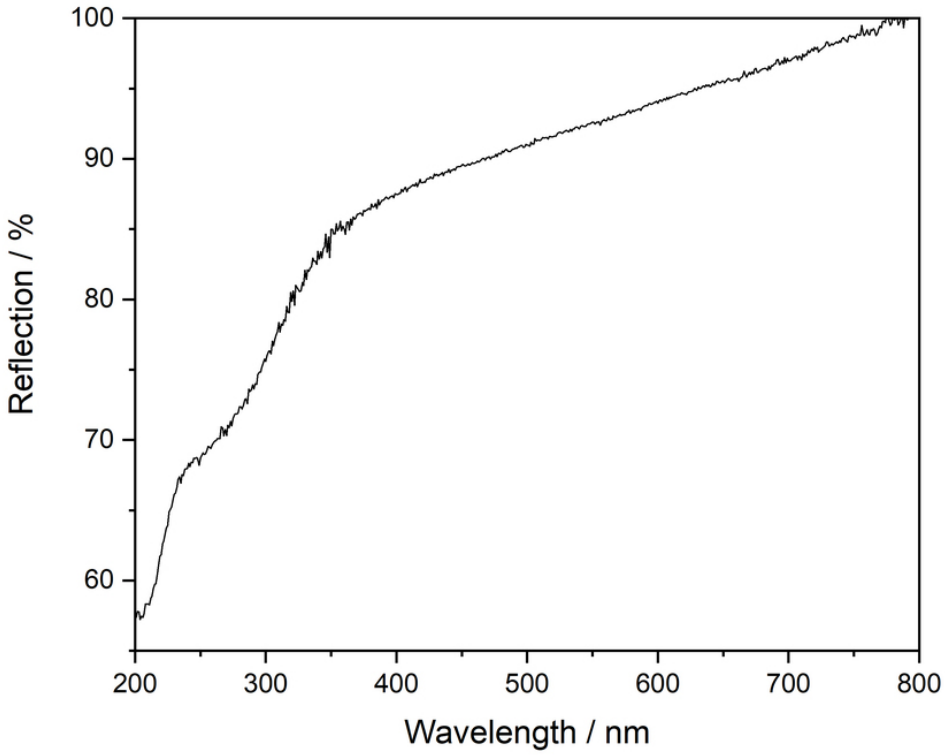

Figure S57: UV-Vis spectrum of $Sr(NH_2SO_3)_2 \cdot H_2O$.

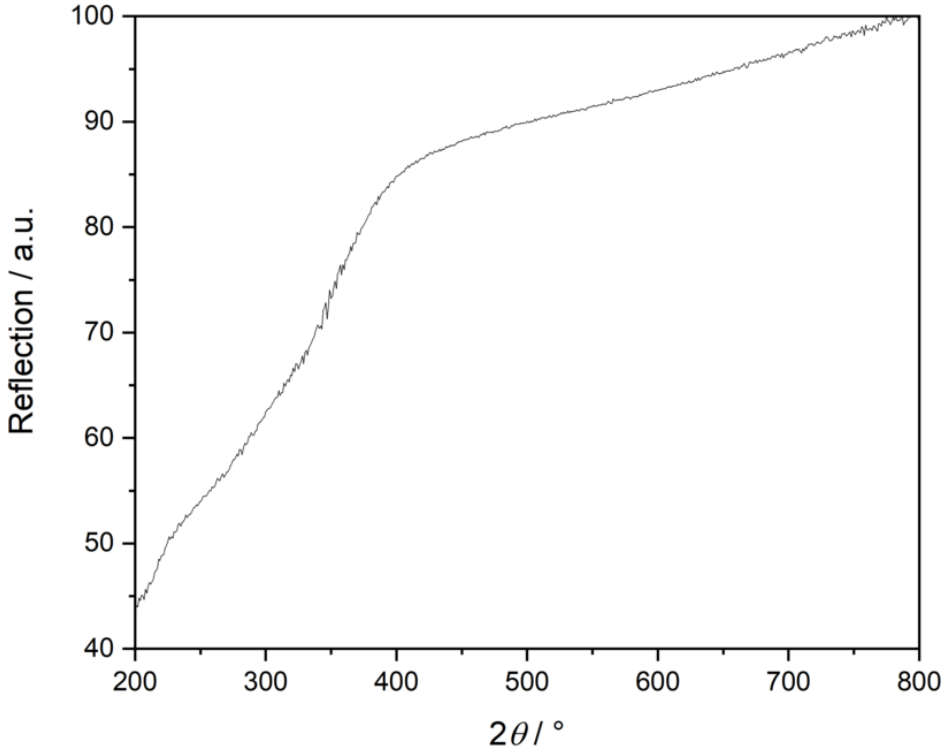

Figure S58: UV-Vis spectrum of β-$Sr(NH_2SO_3)_2$.

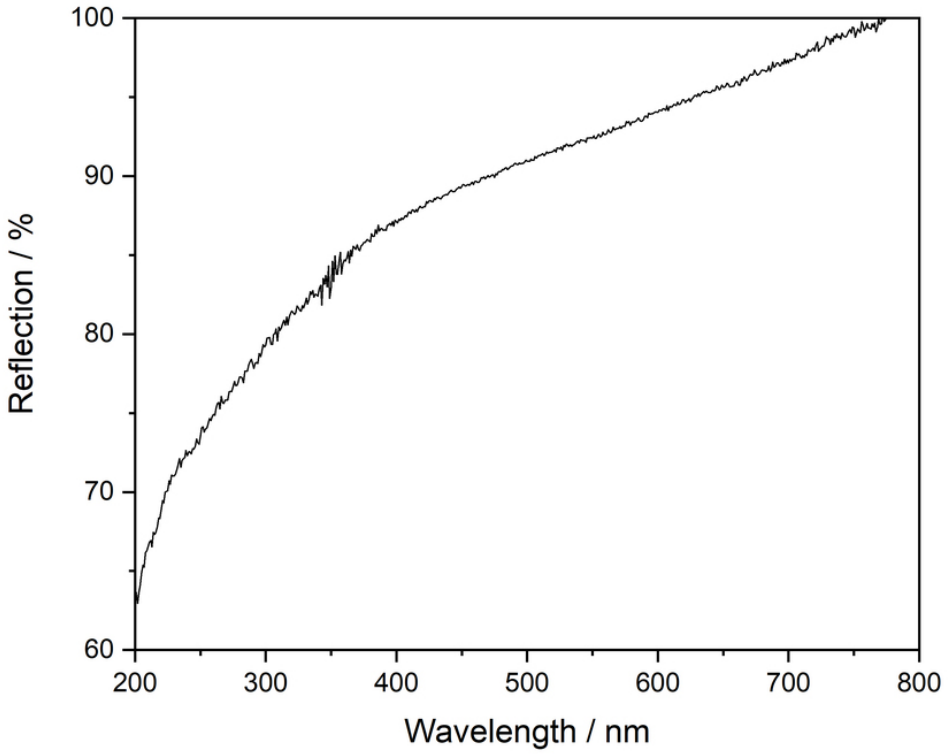

Figure S59: UV-Vis spectrum of $Ba(NH_2SO_3)_2$.

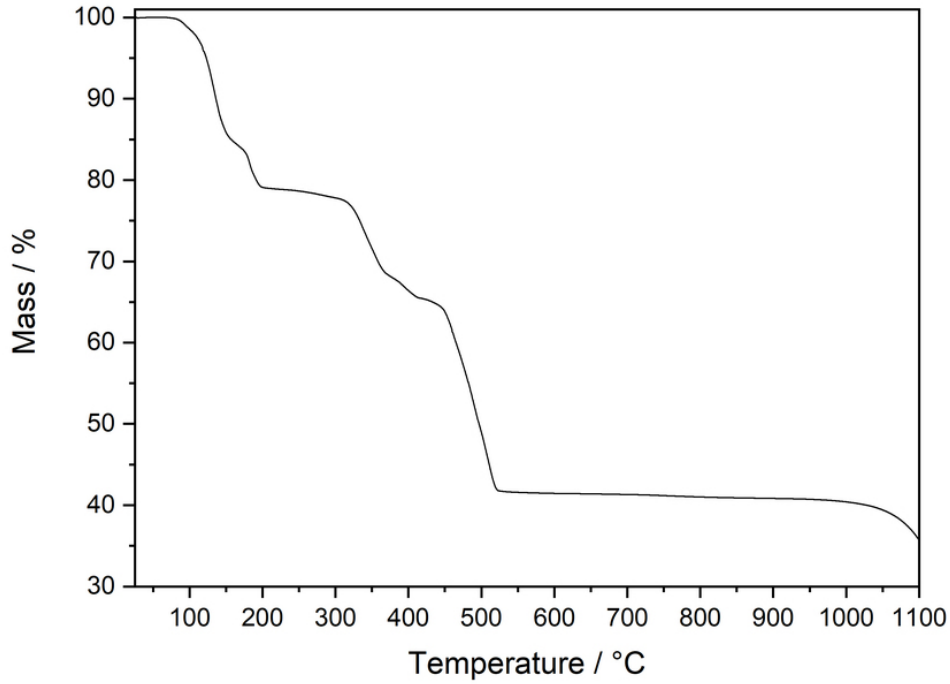

Figure S60: TG curve of $Mg(NH_2SO_3)_2 \cdot 4\,H_2O$.

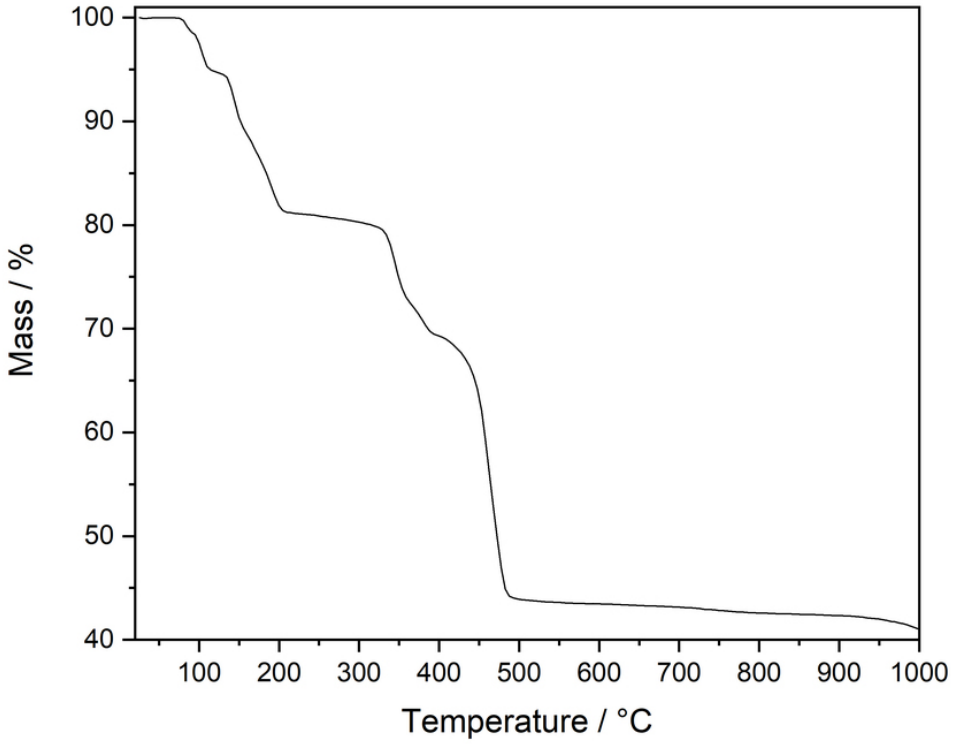

Figure S61: TG curve of $Mg(NH_2SO_3)_2 \cdot 3\,H_2O$.

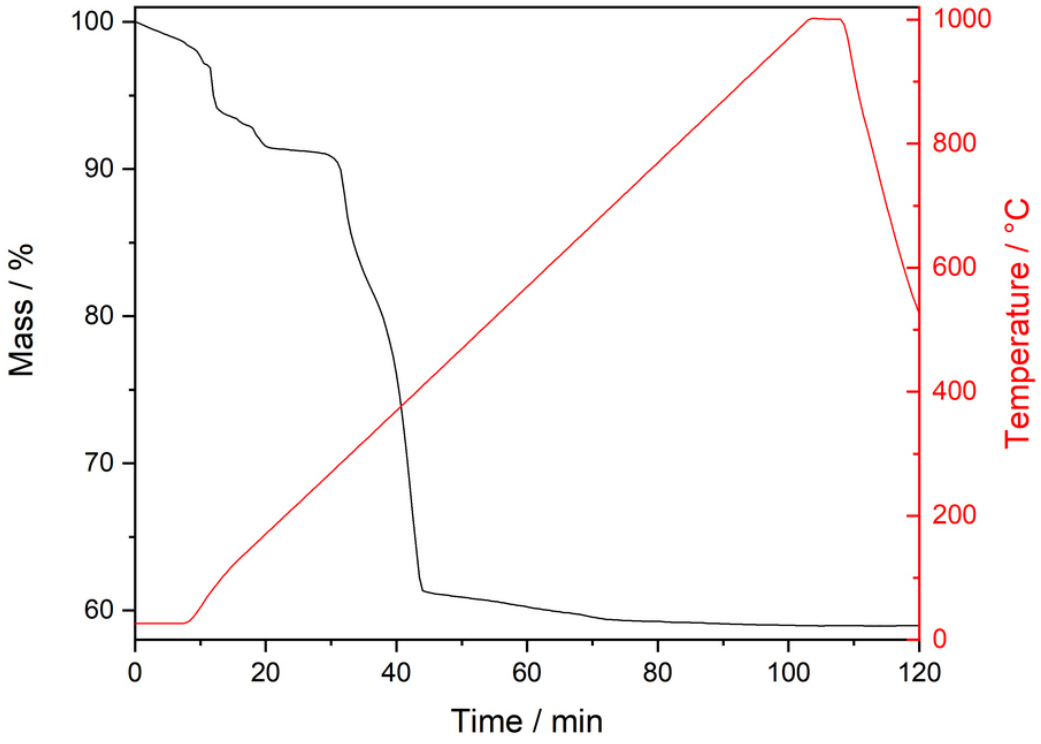

Figure S62: TG curve of $Ca(NH_2SO_3)_2 \cdot 4\,H_2O$.

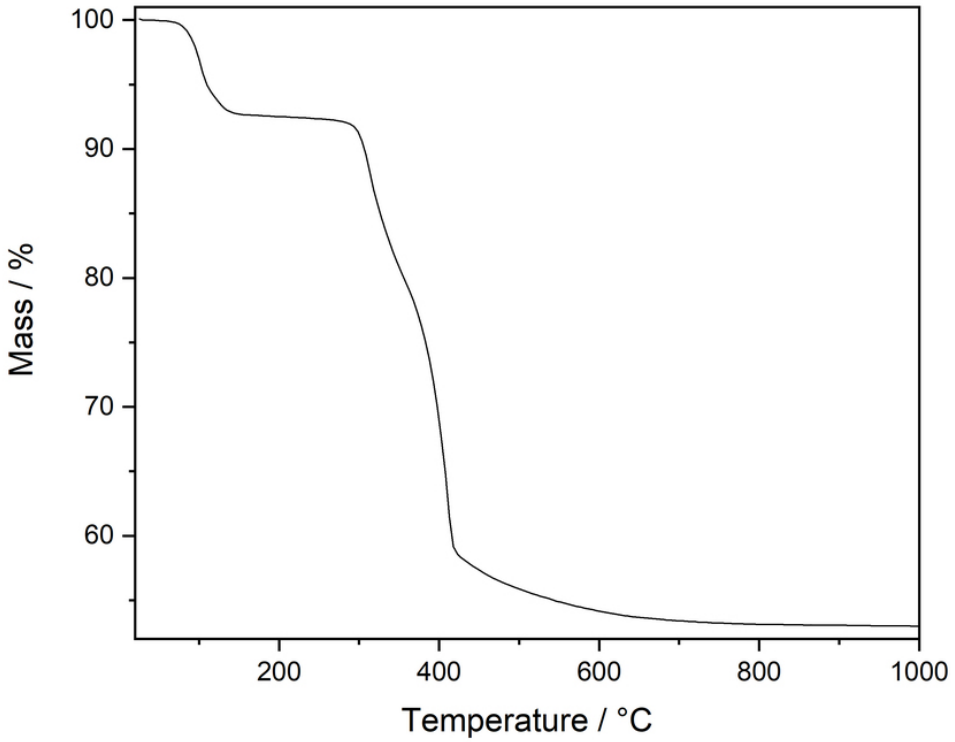

Figure S63: TG curve of $Ca(NH_2SO_3)_2 \cdot H_2O$.

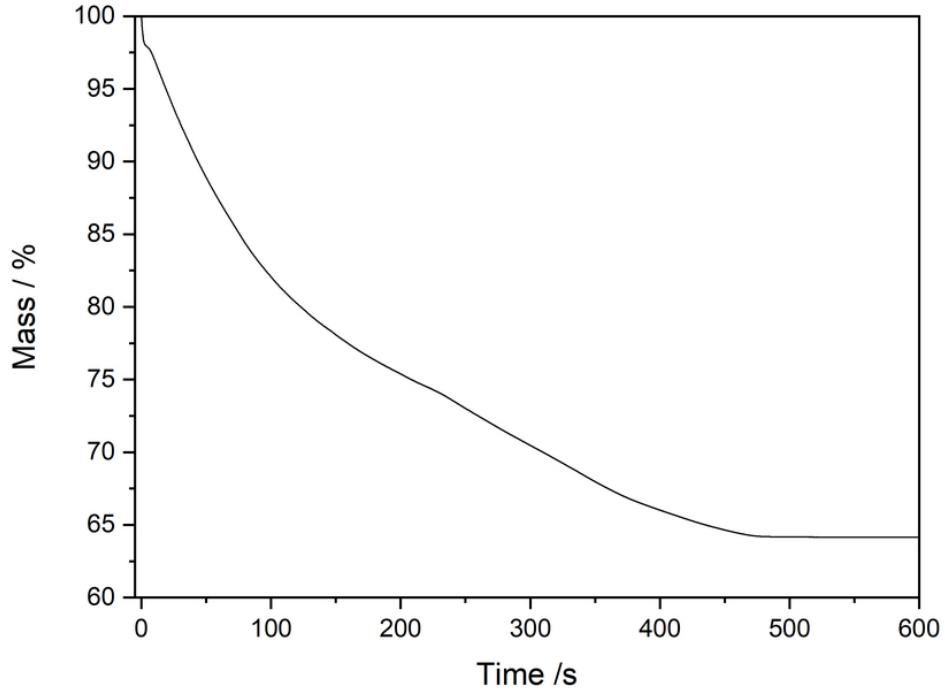

Figure S64: Room temperature isothermal thermogram of a single-crystal of $Sr(NH_2SO_3)_2 \cdot 4\,H_2O$.

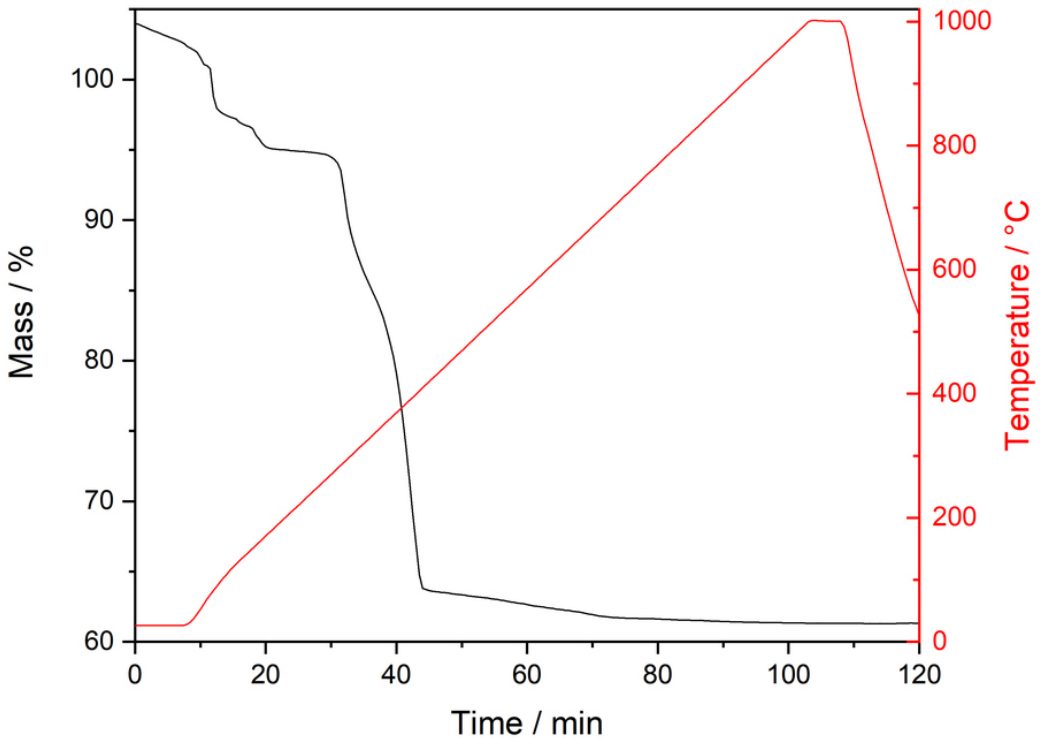

Figure S65: TG curve of $Sr(NH_2SO_3)_2 \cdot H_2O$.

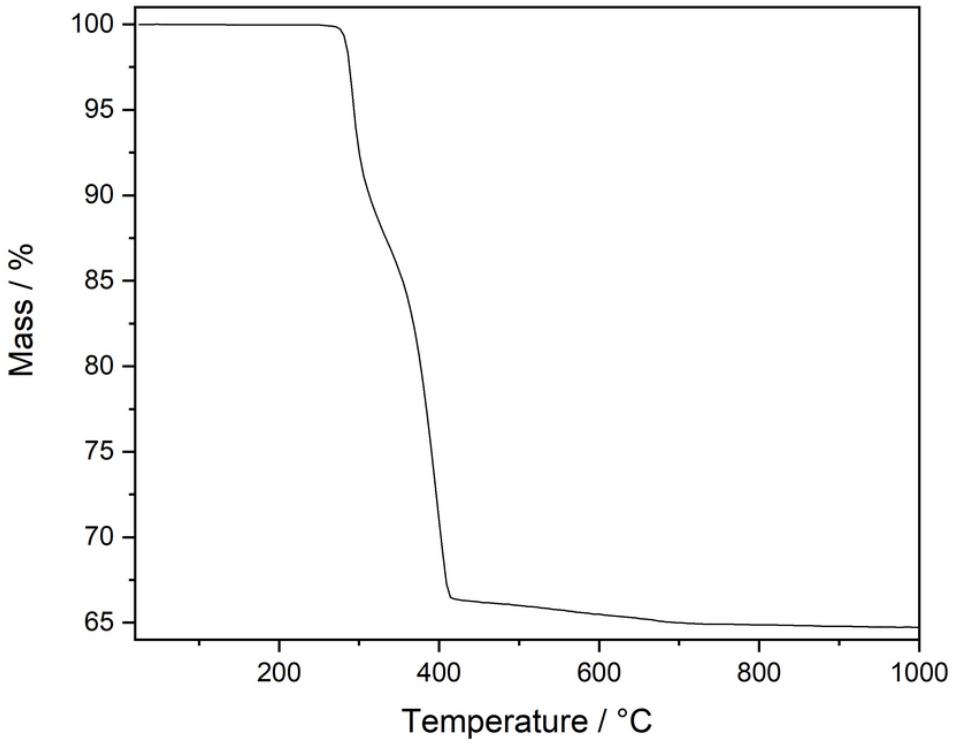

Figure S66: TG curve of $Sr(NH_2SO_3)_2$.

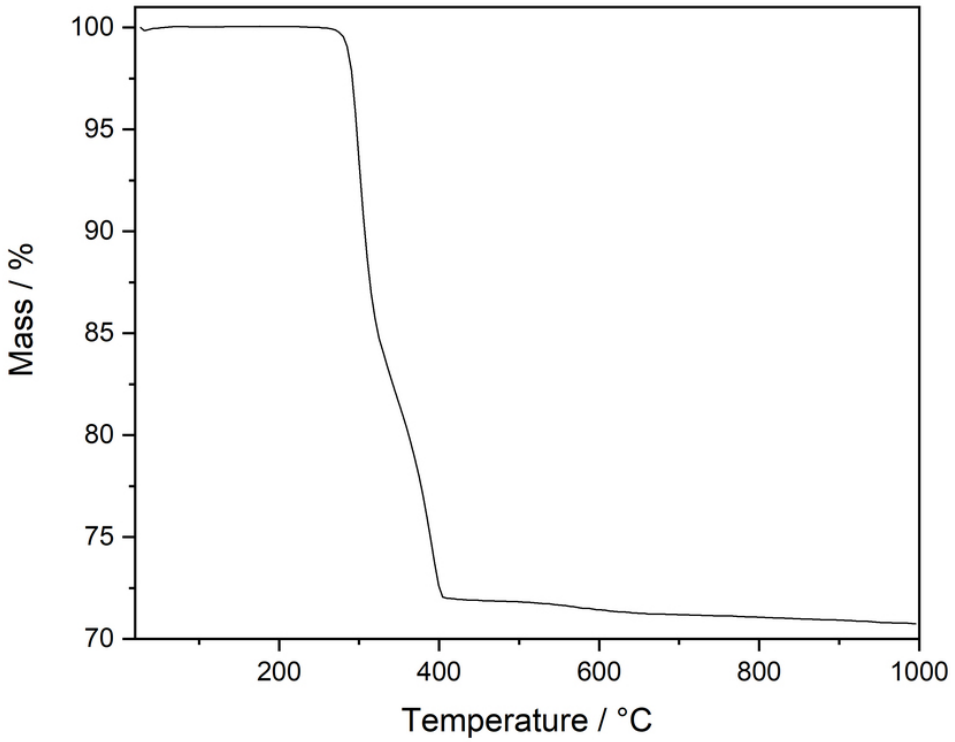

Figure S67: TG curve of $Ba(NH_2SO_3)_2$.

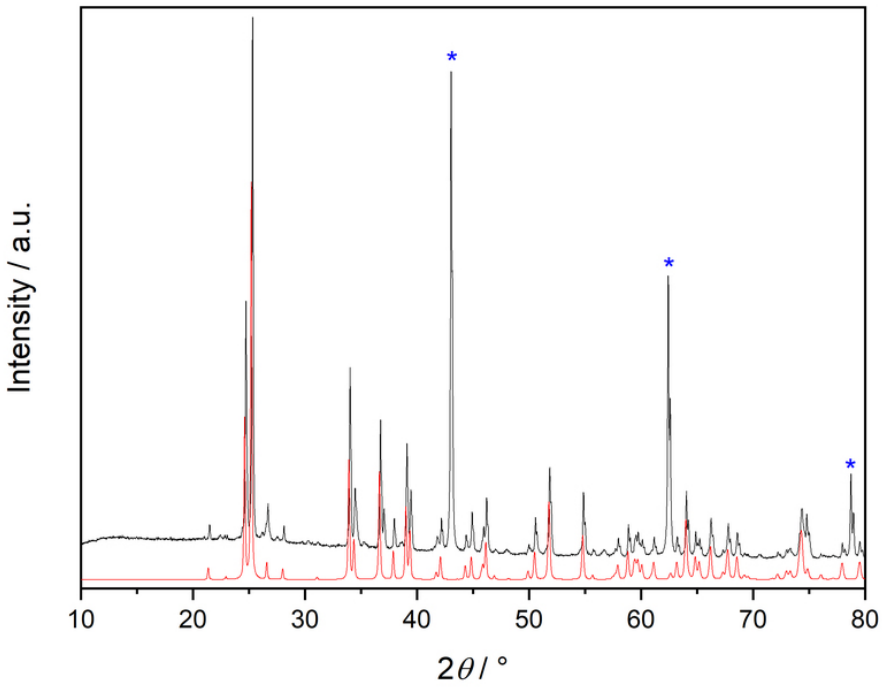

Figure S68: X-ray powder diffraction pattern of the pyrolysis residue of $Mg(NH_2SO_3)_2 \cdot 4\,H_2O$ after TGA shown in black compared with a calculated pattern of β-$MgSO_4$ based on single-crystal data[3] shown in red. Reflections belonging to α-$MgSO_4$[4] are marked with a blue asterisk.

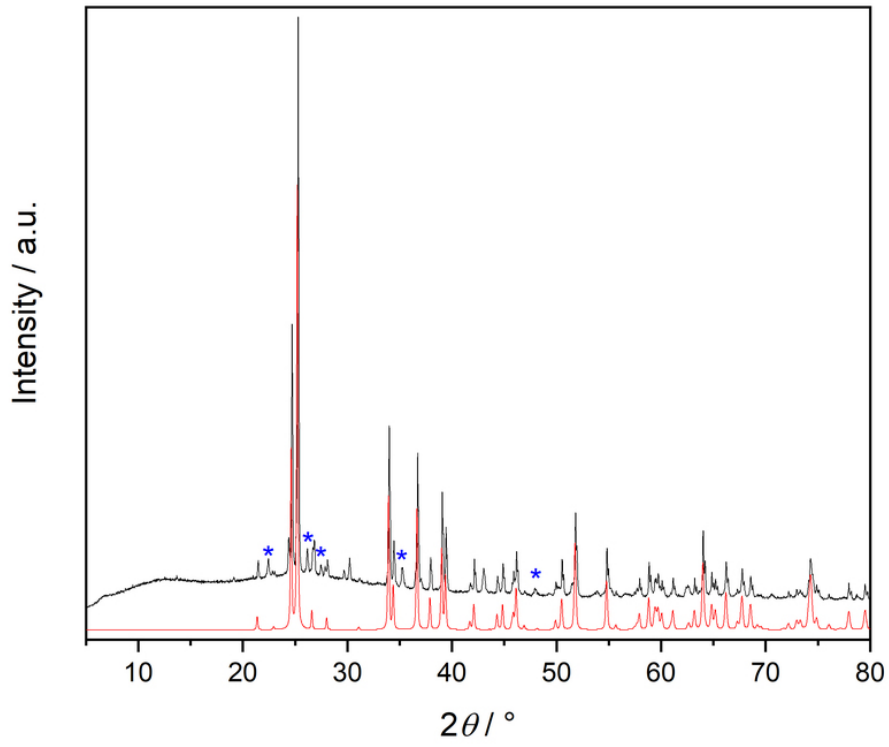

Figure S69: X-ray powder diffraction pattern of the pyrolysis residue of $Mg(NH_2SO_3)_2 \cdot 3\,H_2O$ after TGA shown in black compared with a calculated pattern of β-$MgSO_4$ based on single-crystal data[3] shown in red. Reflections belonging to α-$MgSO_4$[4] are marked with a blue asterisk.

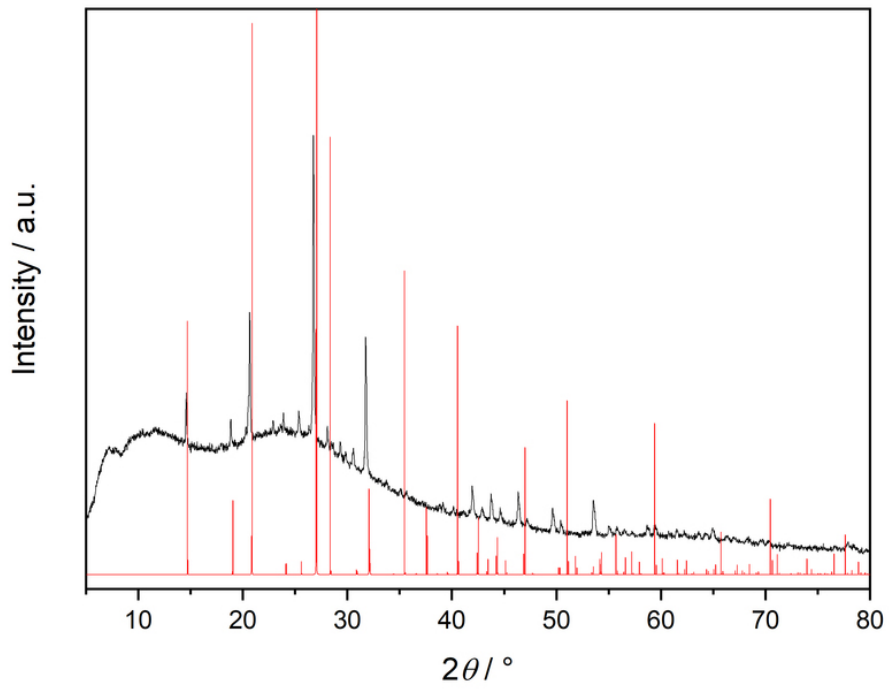

Figure S70: X-ray powder diffraction pattern of the decompostion product of $Ca(NH_2SO_3)_2 \cdot 4\,H_2O$ heated to 300 °C shown in black compared with a calculated pattern of synthetic calciolangbeinite $K_2Ca_2(SO_4)_3$ based on single-crystal data[5] shown in red.

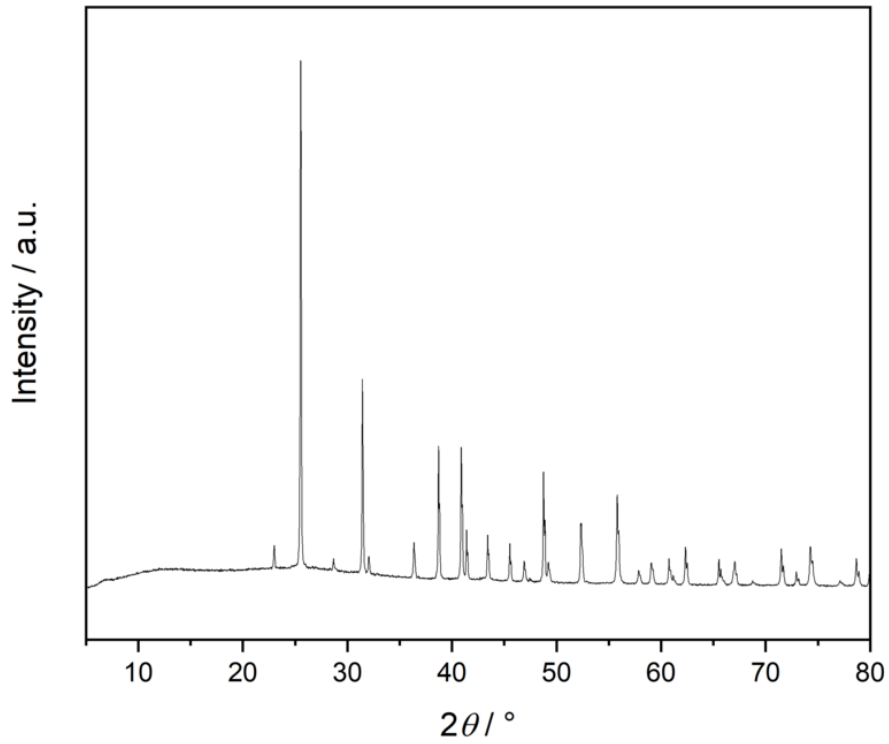

Figure S71: X-ray powder diffraction pattern of the decompostion product of $Ca(NH_2SO_3)_2 \cdot H_2O$ after TGA shown in black compared with a calculated pattern of synthetic anhydrite $CaSO_4$ based on single-crystal data[6] shown in red.

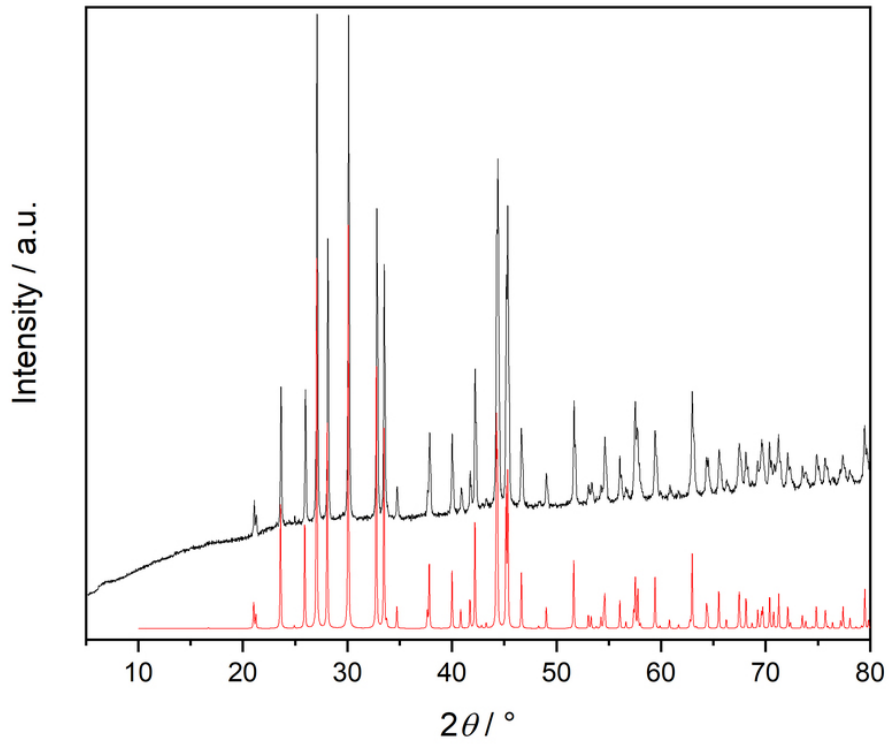

Figure S72: X-ray powder diffraction pattern of the pyrolysis residue of $Sr(NH_2SO_3)_2 \cdot H_2O$ after TGA shown in black compared with a calculated pattern of synthetic celestine $SrSO_4$ based on single-crystal data[7] shown in red.

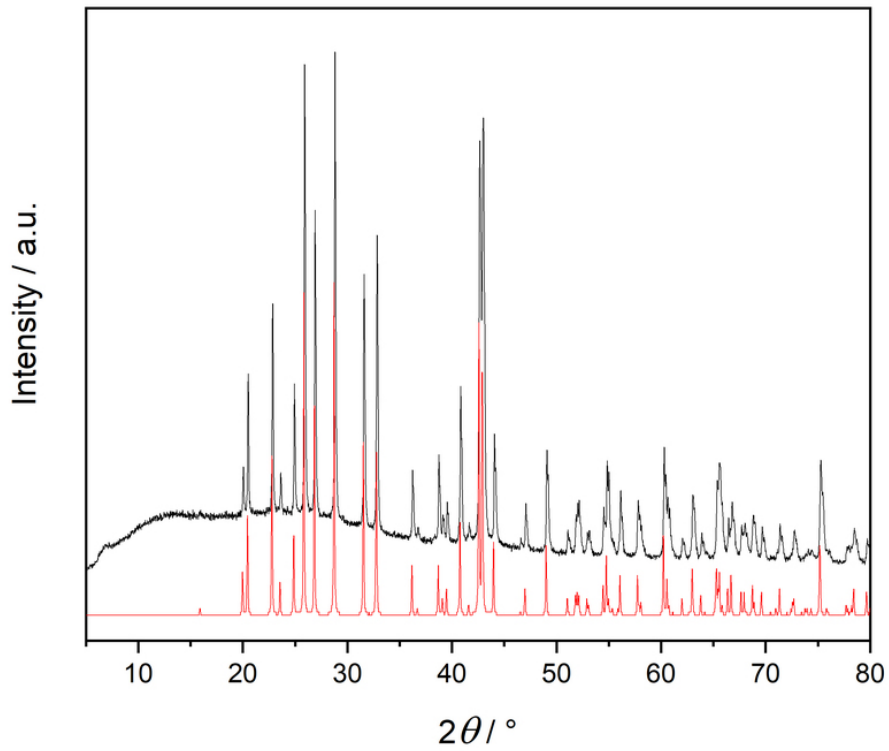

Figure S73: X-ray powder diffraction pattern of the pyrolysis residue of $Ba(NH_2SO_3)_2$ after TGA shown in black compared with a calculated pattern of synthetic barite $BaSO_4$ based on single-crystal data[8] shown in red.

Figure S74: Photograph of $Sr(NH_2SO_3)_2 \cdot 4\,H_2O$ as synthesised inside a 100 ml beaker (50 mm in diameter).

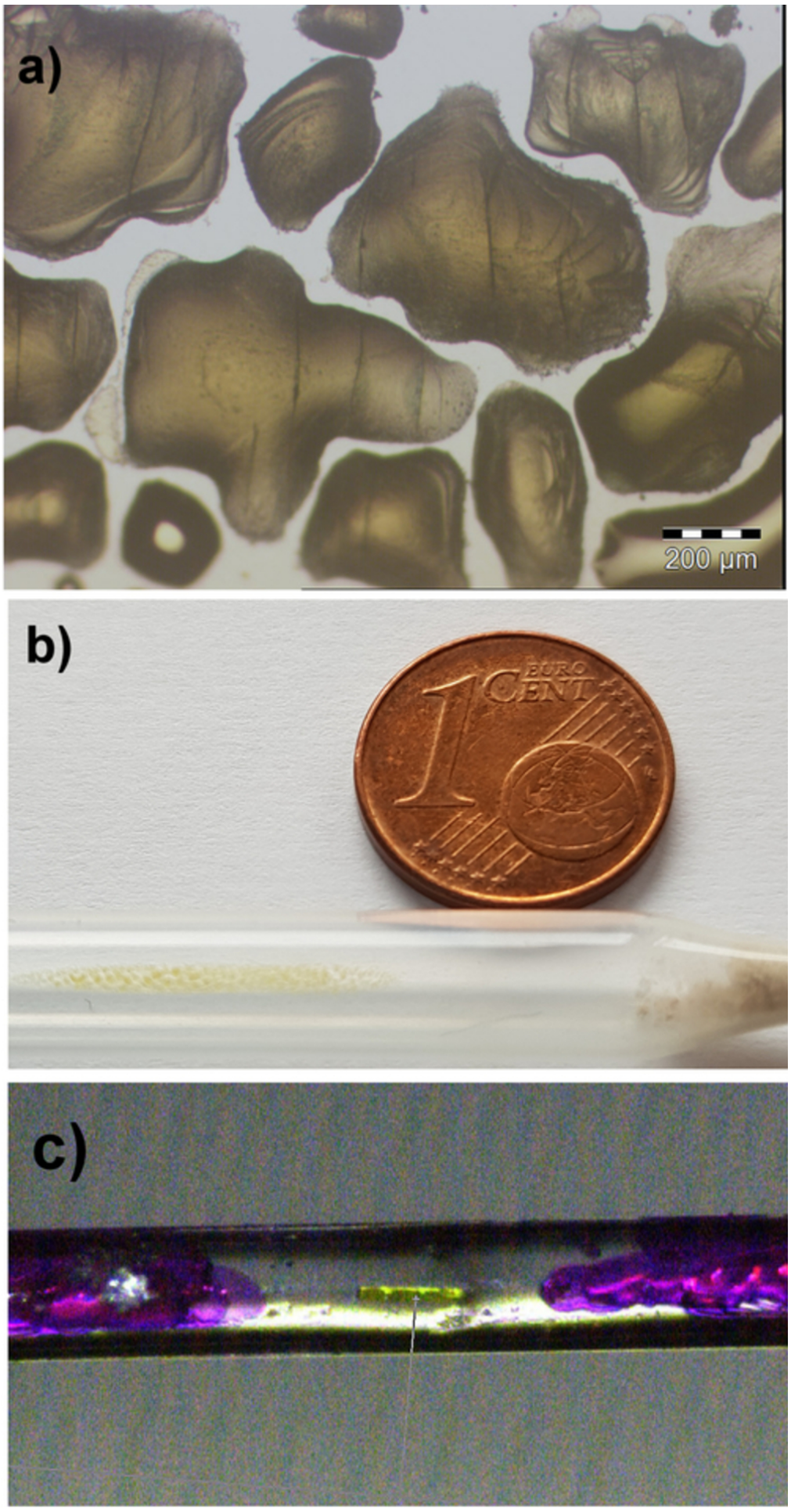

Figure S75: a) Light microscopy image of S_4N_4 crystallised on the wall of an ampoule. b) Photograph of the ampoule with yellow S_4N_4 crystallised on the wall of an ampoule over $SrSO_4$ on the bottom. c) Specimen selected for single-crystal XRD study in Lindemann-glass capillary (0.3 mm diameter).

References

[1] T. Balić-Žunić and E. Makovicky. Determination of the centroid or 'the best centre' of a coordinationpolyhedron. *Acta Crystallogr., Sect. B: Struct. Sci.*, 52:78 – 81, 1996.

[2] E. Makovicky and Balić-Žunić. New measure of distortion for coordination polyhedra. *Acta Crystallogr., Sect. B: Struct. Sci.*, 54:766–773, 1998.

[3] M. Weil. The high-temperature modification of magnesium sulfate (β-mgso4) from single-crystal data. *Acta Crystallogr., Sect. E: Crystallogr. Commun.*, 63:i172, 2007.

[4] P. J. Rentzeperis and C. T. Soldatos. The crystal structure of the anhydrous magnesium sulphate. *Acta Crystallogr.*, 11:686–688, 1958.

[5] D. Speer and E. Salje. Phase transitions in langbeinites i: Crystal chemistry and structures of k-double sulfates of the langbeinite type $m_2^{++}k_2(so_4)_3$, m = mg, ni, co, zn, ca. *Phys. Chem. Minerals*, 13:17–24, 1986.

[6] H. Morikawa, I. Minato, T. Tomita, and S. Iwai. Anhydrite: a refinement. *Acta Crystallogr., Sect. B: Struct. Crystallogr. Cryst. Chem.*, 31(8):2164–2165, 1975.

[7] S.D. Jacobsen, J.R. Smyth, R.J. Swope, and R.T. Downs. Rigid-body character of the so_4 groups in celestine, anglesite and barite. *Can. Mineral.*, pages 1053–1060, 1998.

[8] R. J. Hill. A further refinement of the barite structure. *Can. Miner.*, 15:522–526, 1977.